

DATA-DRIVEN SIMULATION OF SUSTAINABLE RESIDENTIAL HVAC SYSTEMS IN FAIRBANKS, AK

by

Joshua Young

A Thesis Submitted in Partial Fulfillment of the Requirements

for the Degree of

Master of Science

In

Mechanical Engineering

University of Alaska Fairbanks

May 2025

APPROVED:

Dr. Sunwoo Kim, Committee Chair

Dr. Daisy Huang, Committee Member

Dr. Rorik Peterson, Committee Member

Dr. Rorik Peterson, Chair

Department of Mechanical Engineering

Dr. William Schnabel, Dean

College of Engineering and Mines

Dr. Emeline Jones, Interim Director

Graduate School



© Copyright by Joshua Young

All rights reserved.

## **Abstract**

Residential heating comes at extremely high costs and with harmful air pollution in many Alaskan communities. In Fairbanks, the issue of air pollution has received special attention in recent years, specifically due to the high concentration of small particulate matter resulting from residential space heating. This thesis aims to address energy insecurity and air pollution in Fairbanks by proposing an improved residential HVAC system. A computer simulation was developed to model the operations of several different HVAC configurations for comparison with standard heating oil boiler and portable air conditioner systems. This Python model provided a means of simulating one year of heating and cooling using TMY3 weather data, performance data from commercially available HVAC equipment, and historic energy pricing. The proposed HVAC system integrated a hybrid source heat pump with thermal storage, radiative sky cooling, and solar evacuated tube heating technology. Other tested systems included single and dual air source heat pumps, and water source heat pumps integrated with thermal storage, radiative sky cooling, and solar evacuated tube heating technology. Each of the tested systems were fitted with a backup boiler to meet the heating requirement in Fairbanks at the ASHRAE design temperature. A boiler and portable AC unit were also simulated in operation as a baseline for comparison to the tested systems. Each tested system was found to greatly reduce the operational cost, heating oil consumption, and associated  $CO_2$  and  $PM_{2.5}$  emissions compared to the baseline system. The proposed hybrid source heat pump system saw the greatest of these operational benefits, demonstrating operational cost savings of 19.12% and heating oil consumption reduction of 43.1% as compared to the heating oil boiler and portable AC unit. A benefit-cost analysis revealed that while each tested system showed operational benefits from the baseline, the increased maintenance costs associated with these complex systems outweighed the operational benefits. Furthermore, the capital costs were found to increase substantially with system complexity, creating a barrier to entry for users. While each tested system was found to lower operational costs and increase social benefit by reducing  $CO_2$  and  $PM_{2.5}$  emissions, the disproportionate capital and maintenance costs of these systems resulted in economic nonviability. This research highlighted the need for sustainable HVAC solutions for residential homes in Fairbanks. While these results showcased a

modern-day application of the developed model in Fairbanks, the key contribution of this thesis was the development of a powerful, adaptable model which can simulate the operation of a variety of HVAC systems in different locations. The structure of the model allows the user to simply upload new location specific data to perform a one-year HVAC simulation in any location where this data is available. While this thesis uses a sample Fairbanks home in simulation, the simulated building's construction geometry and material properties are easily adaptable, allowing the user to fully specify the desired building for analysis. Similarly, the selected HVAC equipment is easily adaptable, allowing the user to specify performance data for commercially available equipment, or even test new technology in a variety of locations and building applications. This adaptability allows the model to be applied for both residential and commercial buildings and used to simulate HVAC operations across a variety of locations for cost analysis, research and development.

## **Acknowledgments**

I want to thank Dr. Sunwoo Kim for his excellent advice throughout this research project. His guidance and expertise in the field helped me to achieve success in my research. I would also like to thank my advisory committee members Drs. Daisy Huang and Rorik Peterson for their review and feedback throughout the research process. I want to thank the University of Alaska Fairbanks Department of Mechanical Engineering for its continued support to see this research through. I'd also like to thank Charles Hnilicka for collaborating with me to perform a case study analysis using his own home, and Sam Thornton for providing useful product data and industry insight.

## Table of Contents

Copyright.....	iii
Abstract.....	iv
Acknowledgments.....	vi
Table of Contents.....	vii
List of Figures .....	xii
List of Tables .....	xiv
Abbreviations .....	xv
Chapter 1: Introduction .....	1
1.1 Significance .....	1
1.2 Introduction to Principles .....	2
1.2.1 Radiative Sky Cooling .....	2
1.2.2 Solar Evacuated Tube Heating .....	5
1.2.3 Hybrid Source Heat Pumps .....	7
1.3 Literature Review .....	9
1.3.1 Hybrid Heat Pumps and Solar Thermal Collectors for Heating .....	9
1.3.2 Thermal Energy Storage Integration.....	10
1.3.3 Hybrid Systems for Cooling with Radiative Sky Cooling (RSC).....	10
1.3.4 Intelligent Control and Optimization in Hybrid Systems .....	11
1.3.5 Research Gaps and Relevance to High-Latitude Communities .....	11
1.4 Purpose .....	12
Chapter 2: Steady State Analysis .....	14
2.1 Overview .....	14
2.2 Methodology.....	15

2.2.1 Input Data .....	15
2.2.2 Ventilation.....	17
2.2.3 Solar Irradiance .....	20
2.2.4 Simplified Conductive Heat Loss.....	21
2.2.5 Home Energy Balance .....	22
2.2.6 RSC Panel and Solar Evacuated Tube Collector Energy Balance .....	24
2.3 Validation/Verification.....	32
2.3.1 Home Heat Loss Modeling .....	32
2.3.2 Spectral Solar Irradiance Data Modeling .....	33
2.3.3 RSC Energy Balance.....	37
2.3.4 Solar Irradiance .....	38
2.4 Results – Cost-Optimized Model .....	41
2.5 Discussion – Cost-Optimized Model .....	42
2.6 Results – Emissions-Optimized Model.....	47
2.7 Discussion – Emissions-Optimized Model .....	48
Chapter 3: Controls Study .....	51
3.1 Overview .....	51
3.2 Deadband Controls .....	52
3.2.1 Methodology.....	52
3.2.2 Results.....	56
3.2.3 Discussion.....	58
3.3 Variable Load Distribution Controls.....	62
3.3.1 Methodology.....	62
3.3.2 Results.....	63

3.3.3 Discussion.....	65
Chapter 4: System Selection and Optimization Study .....	67
4.1 Overview .....	67
4.2 System Selection .....	67
4.2.1 Methodology.....	67
4.2.2 Results – Cost-Optimized Model .....	74
4.2.3 Results – Emissions-Optimized Model.....	77
4.2.4 Discussion.....	78
4.3 System Optimization.....	81
4.3.1 Methodology.....	81
4.3.2 Results and Discussion .....	81
Chapter 5: System Configuration Study.....	89
5.1 Overview .....	89
5.2 Methodology.....	89
5.2.1 Heating System Configuration .....	89
5.2.2 AC System Configuration .....	90
5.3 Results.....	92
5.3.1 Boiler - Heating .....	92
5.3.2 LG Portable Unit - Air Conditioning .....	94
5.3.3 HSHP and Backup Boiler - Heating.....	94
5.3.4 HSHP - Air Conditioning .....	96
5.3.5 ASHP and Backup Boiler - Heating.....	96
5.3.6 ASHP - Air Conditioning.....	99
5.3.7 WSHP and Backup Boiler - Heating.....	99

5.3.8 WSHP - Air Conditioning .....	101
5.3.9 Dual ASHPs and Backup Boiler - Heating .....	101
5.3.10 Dual ASHPs - Air Conditioning.....	103
5.3.11 Comparative Heating and Cooling .....	103
5.4 Discussion.....	105
Chapter 6: Benefit-Cost Analysis.....	107
6.1 Overview .....	107
6.2 Methodology.....	108
6.3 Results .....	116
6.4 Discussion.....	117
Chapter 7: Conclusion .....	120
7.1 Limitations and Model Improvements .....	122
Nomenclature .....	126
References .....	145

## List of Figures

Figure 1.1: RSC Energy Balance [8] .....	3
Figure 1.2: Solar Evacuated Tube Heater [15] .....	6
Figure 1.3: Proposed HSHP System.....	13
Figure 2.1: Steady State Energy Balance .....	15
Figure 2.2: Plane Wall .....	23
Figure 2.3: WSHP Control Logic .....	28
Figure 2.4: ASHP Control Logic.....	29
Figure 2.5: Boiler Control Logic.....	30
Figure 2.6: AM1.5 Reference Spectra from NREL [48].....	34
Figure 2.7: Spectral Solar Irradiance at Noon on Summer Solstice .....	35
Figure 2.8: Spectral Solar Irradiance at Noon on May 1st.....	36
Figure 2.9: Spectral Solar Irradiance at 8pm on Summer Solstice .....	37
Figure 2.10: Tilted Surface Irradiance (TI).....	39
Figure 2.11: Vertical Surface Irradiance (VI) .....	40
Figure 2.12: Horizontal Surface Irradiance (HI) .....	40
Figure 2.13: HVAC System Usage (Steady State, Cost-Optimized) .....	41
Figure 2.14: Boiler Usage (Steady State, Cost-Optimized) .....	44
Figure 2.15: WSHP Usage (Steady State, Cost-Optimized) .....	45
Figure 2.16: ASHP Usage (Steady State, Cost-Optimized) .....	45
Figure 2.17: Thermal Tank Versus Ambient Temperature (Steady State, Cost-Optimized).....	47
Figure 2.18: HVAC System Usage (V1 Emissions-Optimized) .....	47
Figure 2.19: Boiler Usage (Steady State, Emissions-Optimized).....	49
Figure 2.20: Thermal Tank Versus Ambient Temperature (Steady State).....	49
Figure 3.1: Transient Energy Balance.....	53
Figure 3.2: HVAC System Usage (Deadband Controls, Cost-Optimized) .....	57
Figure 3.3: ASHP Usage (Deadband Controls, Cost-Optimized) .....	59
Figure 3.4: WSHP Usage (Deadband Controls, Cost-Optimized) .....	59
Figure 3.5: Boiler Usage (Deadband Controls, Cost-Optimized) .....	60

Figure 3.6: Thermal Tank Versus Ambient Temperature (Deadband Controls).....	61
Figure 3.7: Inside Air Temperature Versus Time (Deadband Controls, Cost-Optimized).....	62
Figure 3.8: HVAC System Usage (Variable Load Distribution, Cost-Optimized) .....	64
Figure 3.9: Inside Air Temperature Versus Time (Variable Load Distribution, Cost-Optimized)..	65
Figure 4.1: Weil-McLain Boiler and GO-2 Becket Oil Burner from Supply House [51], [50] .....	69
Figure 4.2: ASHP Model 050ZA/BE Performance Data .....	70
Figure 4.3: ASHP 050ZA/BE and Buffer Tank from Arctic Heat Pumps [44] .....	71
Figure 4.4: Bosch WSHP Model CE061 [54] .....	72
Figure 4.5: Bosch WSHP Model CE061 Performance Data .....	73
Figure 4.6: HVAC System Usage (System Selection, Cost-Optimized).....	75
Figure 4.7: Inside Air Temperature (System Selection, Cost-Optimized) .....	76
Figure 4.8: Thermal Tank Versus Ambient Temperature (System Selection, Cost-Optimized) ...	77
Figure 4.9: HVAC System Usage (System Selection, Emissions-Optimized) .....	78
Figure 4.10: RSC Panel Size Cost Optimization .....	82
Figure 4.11: Solar Collector Size Optimization.....	84
Figure 4.12: Thermal Tank Size Optimization .....	85
Figure 4.13: Thermal Tank .....	85
Figure 4.14: HVAC System Usage (System Optimization, Cost-Optimized Model) .....	87
Figure 4.15: Thermal Tank Versus Ambient Temperature (System Optimization) .....	87
Figure 5.1: Selected AC Unit (model LP0821GSSM) from LG [57] .....	92
Figure 5.2: HVAC System Usage (Boiler Only).....	93
Figure 5.3: Thermal Tank Versus Ambient Temperature (Boiler Only) .....	94
Figure 5.4: HVAC System Usage (HSHP and Backup Boiler) .....	95
Figure 5.5: Thermal Tank Versus Ambient Temperature (HSHP and Backup Boiler) .....	96
Figure 5.6: HVAC System Usage (ASHP and Backup Boiler).....	98
Figure 5.7: Thermal Tank Versus Ambient Temperature (ASHP and Backup Boiler) .....	99
Figure 5.8: HVAC System Usage (WSHP and Backup Boiler) .....	100
Figure 5.9: Thermal Tank Versus Ambient Temperature (WSHP and Backup Boiler).....	101
Figure 5.10: HVAC System Usage (2 ASHPs and Backup Boiler) .....	102

Figure 5.11: Thermal Tank Versus Ambient Temperature (2 ASHPs and Backup Boiler)..... 103

## List of Tables

Table 2.1: HVAC System Performance (Steady State, Cost-Optimized) .....	42
Table 2.2: HVAC System Performance (Steady State, Emissions-Optimized) .....	48
Table 3.1: HVAC System Performance (Deadband Controls, Cost-Optimized) .....	57
Table 3.2: HVAC System Performance (Variable Load Distribution Controls).....	64
Table 4.1: HVAC System Performance (System Selection, Cost-Optimized) .....	75
Table 4.2: HVAC System Performance (System Selection, Emissions-Optimized) .....	77
Table 4.3: RSC Panel Size Cost Optimization .....	82
Table 4.4: Solar Collector Panel Size Optimization .....	83
Table 4.5: Thermal Tank Size Optimization .....	84
Table 4.6: HVAC System Performance (System Optimization, Cost-Optimized Model) .....	86
Table 5.1: HVAC System Performance (Boiler Only).....	93
Table 5.2: HVAC System Performance (HSHP and Backup Boiler).....	95
Table 5.3: HVAC System Performance (ASHP and Backup Boiler).....	97
Table 5.4: HVAC System Performance (WSHP and Backup Boiler) .....	100
Table 5.5: HVAC System Performance (2 ASHPs and Backup Boiler) .....	101
Table 5.6: Summary of Results for Each Heating System Configuration .....	104
Table 5.7: Summary of Results for Each Cooling System Configuration .....	104
Table 6.1: Equipment and Installation Costs .....	110
Table 6.2: Annual Maintenance Costs .....	111
Table 6.3: Boiler and LG AC Unit System Capital Costs .....	112
Table 6.4: Single ASHP System Capital Costs .....	112
Table 6.5: Dual ASHP System Capital Costs .....	113
Table 6.6: WSHP System Capital Costs .....	114
Table 6.7: HSHP System Capital Costs .....	115
Table 6.8: Annual Cost Comparison of Systems .....	117
Table 6.9: 15-Year Project Cost Comparison of Systems.....	117
Table 6.10: Relative Cost Compared to a Standard Boiler and Portable AC unit System .....	118

## **Abbreviations**

AC	Air Conditioning
ASHP	Air Source Heat Pump
COP	Coefficient of Performance
EER	Energy Efficiency Ratio
EM	Electromagnetic
EPA	Environmental Protection Agency
FNSB	Fairbanks North Star Borough
GHI	Global Horizontal Irradiance
HSHP	Hybrid Source Heat Pump
HVAC	Heating Ventilation and Air Conditioning
NAAQ	National Ambient Air Quality
O&M	Operations and Maintenance
PM <sub>2.5</sub>	Particulate Matter (2.5 microns or smaller)
RSC	Radiative Sky Cooling
SSI	Spectral Solar Irradiance
WSHP	Water Source Heat Pump

## Chapter 1: Introduction

### 1.1 Significance

Many Alaskan communities are remotely located and are often not interconnected with infrastructure such as roads or an electric grid. Additionally, many of these rural communities are in high latitude regions which experience extremely cold temperatures for significant portions of the year. Due to these extreme temperatures and a lack of shared infrastructure, many Alaskan communities are extremely reliant on fossil fuels such as heating oil and diesel for heat and power. With reliance on these fossil fuels come logistical challenges, especially for communities which lack the transportation infrastructure to efficiently and reliably deliver fuel. The cost of such logistical challenges is typically passed onto the consumer, resulting in high costs of heating, especially in rural Alaskan communities.

Along with energy insecurity, dependence on fossil fuels for heating can create serious environmental concerns especially during winter months. In Fairbanks, heating oil boilers and heaters are the industry standard for residential space heating. However, the use of residential heating oil creates  $PM_{2.5}$  air pollution in Fairbanks due to the emission of primary sulfate [1]. Research from the State of Alaska indicates that in 2006-2008, the EPA deemed Fairbanks in violation of National Ambient Air Quality standards for  $PM_{2.5}$  concentration [2]. During these years, sampling produced a design value of  $41 \frac{\mu g}{m^3}$  for Fairbanks, which is 17.14% over the NAAQ standard of  $35 \frac{\mu g}{m^3}$  [2]. In an attempt to meet federal Clean Air Act standards, the Fairbanks North Star Borough (FNSB) banned No. 2 heating oil in 2022 for all residents of the FNSB  $PM_{2.5}$  non-attainment area [3]. In this area, No. 1 heating oil is now sold in place of No. 2 heating oil, due to its 56% lower sulfur content [4]. Sulfate particles are known to be roughly .7 microns or less in diameter, falling into a dangerous classification of  $PM_{2.5}$  – particulate matter which is smaller than 2.5 microns [1]. Sulfate accounts for 15 – 33% of the total  $PM_{2.5}$  in Fairbanks and is known to stem directly from heating oil boilers [1]. This makes heating oil the second largest  $PM_{2.5}$  contributor in Fairbanks, with the largest being smoke from wood stove space heating [1].  $PM_{2.5}$  is the most concerning pollutant which contributes to the serious air quality issues in Fairbanks. The unique environment created by Fairbanks' geography and climate cause a large

inversion layer to form over the much of the Fairbanks North Star Borough in the wintertime. This inversion causes frigid air to puddle in the sump-like city, trapping pollutants and impeding air dispersion.  $PM_{2.5}$  causes respiratory and heart conditions to those who are regularly exposed to it, and the FNSB has continuously remained in violation of Clean Air Act standards which aim to regulate exposure to  $PM_{2.5}$  [5], [6].

From energy insecurity to extreme air pollution, dependence on fossil fuels for space heating causes serious issues in many high latitude communities. These issues highlight a serious need for long-term arctic heating solutions, especially in Fairbanks, which was found to be the most polluted city in the US in 2018, based on year-round particle pollution [7]. Due to the air quality crisis and community size, Fairbanks has been chosen as the focus of this study. Fairbanks embodies some of the most critical challenges of addressing the issue of sustainable heating and cooling, with its extreme winter temperatures and lack of community wide heating alternatives such as district steam or natural gas. A sustainable HVAC solution for Fairbanks could address both environmental and cost of living concerns. Electrification of space heating is a strategy to provide a more sustainable solution as compared to fossil fuel systems. Although the Fairbanks electric grid is largely powered from diesel plants, it also integrates cleaner renewable energy such as hydroelectric, wind, and solar power. This electricity has lower associated  $CO_2$  and  $PM_{2.5}$  emissions, making it a better potential alternative than fossil fuels for space heating. There is a great need and opportunity for sustainable, economically viable HVAC technology in many Alaskan communities, of which Fairbanks tops the list.

## **1.2 Introduction to Principles**

### **1.2.1 Radiative Sky Cooling**

Radiative sky cooling (RSC) is a natural, passive cooling process that harnesses the thermal radiation emitted by a surface to the coldness of outer space. This phenomenon is based on the fundamental principle of radiative heat transfer, where surfaces at terrestrial temperatures emit infrared radiation within the atmospheric transparency window (8–14  $\mu m$  wavelength) [8]. When this radiation escapes into space, which acts as a near-perfect heat sink with an effective temperature of approximately 3K, the surface undergoing radiative sky

cooling can achieve cooling below ambient air temperatures without requiring external energy input [9].

The effectiveness of RSC relies on several physical principles. Thermal radiation is emitted by all surfaces according to their temperature, and surfaces designed for RSC are optimized to maximize their emissivity within the atmospheric transparency window while minimizing absorption of solar radiation in the visible spectrum [9], [10]. The atmospheric transparency window plays a critical role, as it allows infrared radiation to pass through the atmosphere unimpeded. Greenhouse gases, such as water vapor and carbon dioxide, outside this spectral range can absorb and re-radiate heat, which reduces the efficiency of RSC [11]. The net cooling power of an RSC system is determined by the balance between the surface's emitted radiation and incoming heat from the atmosphere and surrounding environment, and optimized systems are designed to enhance this differential [10]. A visual description of an RSC panel's surface energy balance is shown in Figure 1.1, taken from [8].

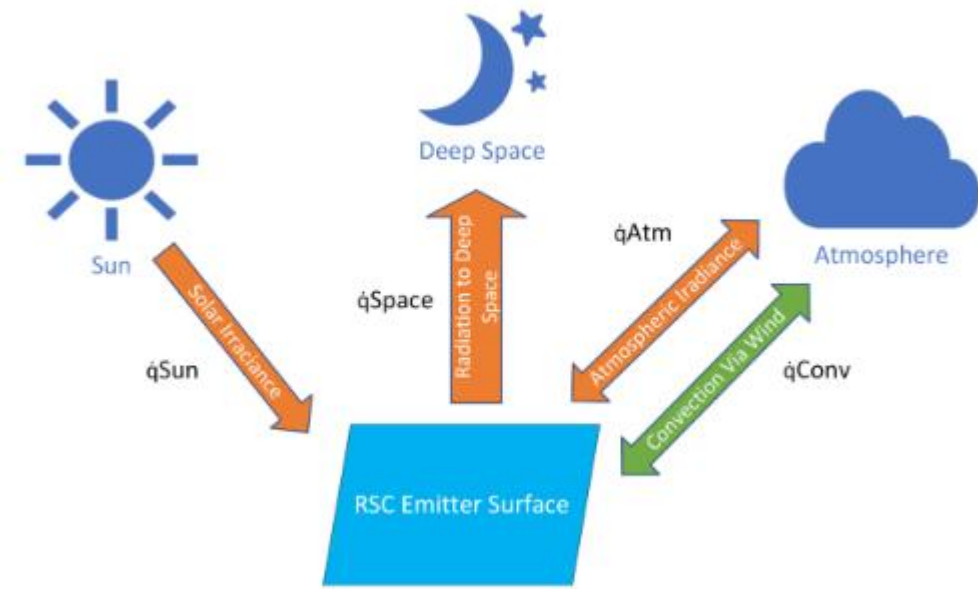


Figure 1.1: RSC Energy Balance [8]

Advancements in material science have significantly improved the efficiency of RSC systems. Selective emitters, such as dielectric-metal composites and photonic structures, are engineered to enhance emissivity in the atmospheric window while reflecting solar radiation

[11]. Research by [9] introduced a photonic structure capable of achieving sub-ambient cooling under direct sunlight, demonstrating a cooling power of approximately  $40 \text{ W/m}^2$ . More recent advancements in nanophotonics and metamaterials have enabled daytime radiative cooling and have increased the cooling power of RSC systems to exceed  $100 \text{ W/m}^2$  in ideal conditions [11]. However, even more recent advancements in thermal management systems for RSC using asymmetrically sized heat source for thermal concentration have achieved over  $2000 \text{ W/m}^2$  at night, and up to  $1000 \text{ W/m}^2$  under direct sunlight [11]. These advancements enable cost-effective and scalable deployment of RSC panels for residential and industrial applications.

Radiative sky cooling has diverse applications. In building cooling, RSC panels reduce reliance on active air conditioning systems, lowering energy consumption and associated costs [12]. When integrated with thermal storage systems, RSC can store cooling energy during the night for use during the day. This approach is particularly effective in climates with significant daily temperature variations [11]. Additionally, RSC is increasingly being integrated with hybrid heat pump and air conditioning systems to enhance overall efficiency. By cooling a thermal reservoir or directly reducing condenser temperatures, RSC can substantially reduce electricity demand during peak cooling periods [10].

Despite its promise, RSC systems face challenges that must be addressed for widespread adoption. Atmospheric conditions, such as high humidity and cloud cover, can reduce the transparency of the atmospheric window, diminishing cooling performance [9], [11]. Effective integration of RSC panels into existing buildings and systems requires careful engineering and design to maximize performance [10]. Additionally, the cost of advanced materials and manufacturing processes can be a barrier to entry, though ongoing research aims to reduce these costs and improve economic viability.

Radiative sky cooling offers a sustainable, low-energy solution to the growing demand for cooling in residential, commercial, and industrial sectors. As material technologies advance and integration strategies improve, RSC has the potential to play a significant role in global energy transitions. In high-latitude regions, where heating dominates energy demand, RSC presents opportunities for seasonal cooling and hybrid system optimization. This thesis explores

the integration of RSC with hybrid source heat pumps and thermal energy storage to assess its potential for improving cooling efficiency in Fairbanks, Alaska.

### **1.2.2 Solar Evacuated Tube Heating**

Solar evacuated tube heating systems are an efficient method of capturing solar thermal energy for residential, commercial, and industrial heating applications. These systems leverage the principles of solar energy absorption and thermal insulation to deliver reliable and high-performance heat generation, even in cold or cloudy conditions.

Evacuated tube collectors consist of a series of glass tubes, each containing an absorber plate or a heat pipe. The space between the inner absorber and the outer glass tube is evacuated to create a vacuum, which serves as a thermal insulator. This vacuum significantly reduces heat loss through conduction and convection, allowing the system to maintain high thermal efficiency even in low ambient temperatures [13], [14]. The absorber plate, coated with a selective material, maximizes solar energy absorption while minimizing thermal radiation losses [14]. A visual description of the technology is shown in Figure 1.2, taken from [15].

A key advantage of solar evacuated tube systems is their ability to perform efficiently under diffuse solar radiation. Unlike flat-plate collectors, which rely heavily on direct sunlight, evacuated tube systems can harness indirect solar energy, making them effective in overcast conditions [16]. Research by [17] indicates that evacuated tube collectors achieve 132.6% increases in daily efficiency compared to typical flat plate collectors.

Another critical feature of evacuated tube systems is their modular design. Individual tubes can be replaced or adjusted without disrupting the entire system, providing flexibility and ease of maintenance. Furthermore, the cylindrical geometry of the tubes enables optimal solar tracking throughout the day, ensuring consistent energy capture without requiring active tracking mechanisms [14].

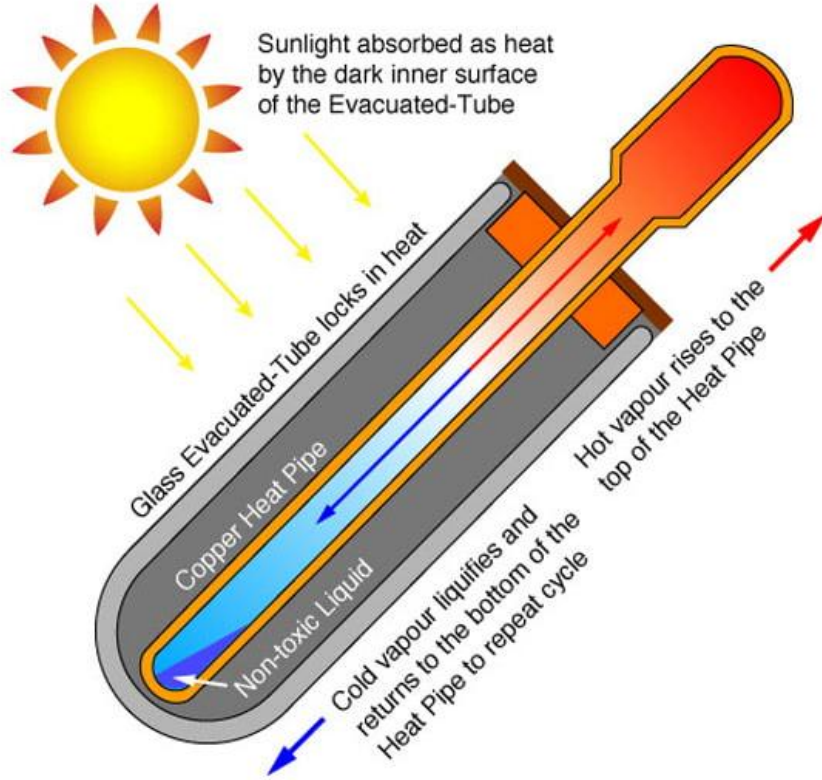


Figure 1.2: Solar Evacuated Tube Heater [15]

Applications of solar evacuated tube heating systems are diverse. They are widely used for domestic hot water supply, space heating, and industrial processes requiring low- to medium-grade heat [14]. In high-latitude regions, evacuated tube systems can be integrated with thermal energy storage tanks to store excess heat generated during sunny periods for later use, capitalizing on intermittent solar availability. Additionally, they are often paired with auxiliary heating systems such as boilers or heat pumps to ensure continuous operation during periods of low solar input [14], [12].

Despite their advantages, solar evacuated tube systems face challenges. The initial cost of installation is typically higher than that of flat-plate collectors, which can deter use in cost-sensitive markets. The performance of evacuated tube collectors can also be affected by factors such as improper installation, shading, and degradation of selective coatings over time. Ongoing research aims to address these limitations by improving the durability of materials and reducing manufacturing costs [14], [17].

As global interest in sustainable and renewable energy technologies grows, solar evacuated tube heating systems are increasingly recognized as a critical component of low-carbon energy strategies. Their high efficiency, adaptability to diverse climates, and potential for integration with other renewable systems position them as a promising solution for meeting heating demands while reducing greenhouse gas emissions. This thesis examines the role of solar evacuated tube systems in hybrid heating configurations to evaluate their potential for improving energy efficiency and reducing fossil fuel dependence, particularly in high-latitude communities.

### **1.2.3 Hybrid Source Heat Pumps**

Hybrid source heat pumps (HSHPs) combine air source and water source heat pump technologies to provide efficient and versatile heating and cooling solutions. By leveraging the complementary characteristics of air and water as heat exchange mediums, these systems optimize energy efficiency across a range of environmental conditions [18]. HSHPs are designed to operate in both heating and cooling modes, functioning as heat pumps or air conditioners depending on the thermal demands of the space.

In heating mode, hybrid source heat pumps extract thermal energy from the ambient air or a water source, such as a groundwater well, lake, or thermal storage system. This extracted heat is then amplified using a vapor-compression cycle and delivered to the indoor space. In cooling mode, the system reverses this process, removing heat from the indoor environment and rejecting it into the outdoor air or water source. The ability to alternate between these modes enables HSHPs to meet year-round thermal needs efficiently [18].

A distinguishing feature of HSHPs is their capacity for incremental power modulation. Hybrid source heat pumps employ advanced technologies such as variable-speed compressors and electronic expansion valves to modulate their output based on real-time thermal demand. This allows the system to adjust its capacity incrementally, operating at partial loads when full capacity is unnecessary. This feature not only enhances energy efficiency but also ensures a more stable and comfortable indoor environment [19].

Another key advantage of hybrid source systems is their flexibility in choosing the most efficient heat source. For instance, when ambient air temperatures are mild, the control system may prioritize the air source component to reduce reliance on water-based systems, minimizing energy and operational costs. Conversely, during extreme weather conditions, the water source component can provide a more stable and reliable thermal reservoir, enhancing the system's performance [19].

HSHPs are particularly well-suited for integration with other renewable energy technologies, such as solar thermal systems or radiative sky cooling panels. When paired with a thermal storage tank, these passive systems can store excess heat or cooling energy for later use, further improving energy efficiency and reducing operational costs [12], [18]. Additionally, hybrid source heat pumps systems are scalable and can be sized to meet a wide range of heating and cooling needs [19].

Despite their numerous advantages, hybrid source heat pumps face some challenges. The initial installation cost can be significantly higher than that of single-source heat pumps, and their performance depends on the proper design and integration of the air and water components. Additionally, maintaining the system's balance between air and water source operations requires advanced controls and careful calibration [18]. In addition to the required instrumentation and control systems, there is more infrastructure associated with HSHPs than with a single source heat pump. Because HSHP may gain from or reject heat to two or more different sources, the installations are always more complex than a single source heat pump. This infrastructure requirement increases significantly when HSHPs are integrated with passive heating and cooling systems, and even more so with thermal storage systems.

As global efforts to reduce carbon emissions and increase energy efficiency intensify, hybrid source heat pumps are emerging as a critical technology for sustainable heating and cooling. Their ability to operate flexibly, efficiently, and reliably across varying environmental conditions makes them an ideal solution for both residential and commercial applications. This thesis explores the potential of HSHPs in high-latitude climates, focusing on their integration

with thermal storage and passive heating and cooling systems to optimize year-round performance and energy efficiency.

### **1.3 Literature Review**

The integration of hybrid source heat pumps with solar heating, RSC, and thermal storage technologies has emerged as a promising approach for improving energy efficiency and reducing reliance on fossil fuels. High-latitude regions, characterized by harsh winters, extreme temperature fluctuations, and limited solar irradiance during winter months, present unique challenges for both heating and cooling systems. Although the results of combining these technologies in high latitude communities is not well explored, there are significant findings for different applications.

#### **1.3.1 Hybrid Heat Pumps and Solar Thermal Collectors for Heating**

Studies have demonstrated that coupling HSHPs with solar thermal collectors can significantly improve system efficiency, particularly during transitional seasons when solar availability aligns with moderate heating demands [12], [20]. In high-latitude regions, where direct solar gain is limited in winter, hybrid systems often utilize thermal storage tanks to capture and retain solar energy during peak availability. This stored energy can then be utilized to supplement heat pump performance during periods of low ambient temperatures.

Research from [19] analyzed hybrid solar-assisted heat pumps and highlighted significant energy savings when combined with optimized system switching algorithms tailored for extreme climates. Comparative tests from Jordan et al. [21] show that solar-heat pump hybrids can reduce energy consumption by up to 54.9% compared to electrical resistance heating. However, there exists an irradiation threshold above which direct use of solar heat is more advantageous than feeding it to the heat pump evaporator [22]. These hybrid heating systems demonstrate potential for reducing power consumption and emissions in building applications [23].

### **1.3.2 Thermal Energy Storage Integration**

Thermal energy storage (TES) systems are a critical component of hybrid source heat pump designs, particularly in high-latitude settings where temperature fluctuations can be extreme. Hybrid source heat pumps integrated with TES offer promising solutions for efficient heating and cooling. These systems can balance seasonal load variations and mitigate grid disturbances from renewable energy sources [24]. TES systems enable the storage of excess solar energy during peak daylight hours for later use during nighttime or periods of reduced solar availability [24]. Furthermore, TES systems can be used with radiative emitters to store cooling energy at night for use throughout the day, improving air conditioning performance [8]. Research by Cabeza et al. [25] shows that phase change materials are particularly effective in TES applications due to their high energy density and ability to stabilize temperature fluctuations. In hybrid systems, TES not only enhances energy efficiency but also contributes to grid stability by reducing peak electricity demand [25], [24]. However, limitations such as thermal losses over time and the high initial investment cost for TES systems remain significant barriers to widespread adoption. Overall, hybrid source heat pumps with TES show great potential for enhancing energy efficiency and flexibility in various applications.

### **1.3.3 Hybrid Systems for Cooling with Radiative Sky Cooling (RSC)**

While heating remains the dominant concern in high-latitude communities, cooling demands are also emerging, driven by climate change and the increasing adoption of energy-intensive indoor technologies. Radiative sky cooling (RSC) systems, which exploit the natural heat-sink characteristics of the night sky, have gained attention as a passive cooling strategy. Research by [9] demonstrates the potential for RSC to operate without energy input, leveraging radiative heat transfer to cool thermal fluids or building surfaces.

In hybrid heat pump systems, RSC can serve as a supplemental cooling source, reducing the load on active cooling systems during warmer months or unseasonably warm days. Studies by [26] suggest that combining RSC with air source heat pumps can lead to substantial energy savings, particularly when integrated with intelligent control systems that optimize switching between cooling sources based on ambient conditions. Furthermore, investigations by [12]

have shown that RSC systems integrated with TES and HSHP are able to reduce annual power consumption by 3 – 29% depending on the climate, compared to radiative assisted heat pumps. Research from Magrath [8] used an air conditioner with its condenser inside a TES system, which was cooled by a radiative emitter, and found an energy savings of 3.8% to 18.4% compared to a system without RSC [8].

#### **1.3.4 Intelligent Control and Optimization in Hybrid Systems**

Intelligent control systems for HVAC offer significant potential for energy savings and improved comfort in buildings. These systems utilize advanced technologies such as real-time data acquisition, machine learning algorithms, and predictive control to optimize HVAC operation [27]. The performance of hybrid heat pump systems heavily relies on advanced control algorithms that optimize switching between energy sources based on real-time environmental and operational data. Machine learning-based control systems have shown significant promise in improving energy efficiency and system reliability. Research by [18] demonstrates how predictive control strategies can account for weather forecasts, occupancy patterns, and real-time energy pricing to optimize hybrid system performance. Other studies have shown that integrating occupancy detection and weather condition evaluation with HVAC can lead to substantial energy savings, with one case demonstrating up to 64% reduction in HVAC energy consumption [28]. Intelligent HVAC systems adapt dynamically to user needs and building environments, unlike traditional fixed control methods [29]. Various prediction techniques are employed in these systems to forecast energy consumption and thermal comfort requirements, enabling proactive control strategies that minimize energy use while maintaining occupant comfort [30]. Overall, intelligent HVAC control systems are an integral part of HVAC energy savings, especially in complex systems which require optimized switching and operations.

#### **1.3.5 Research Gaps and Relevance to High-Latitude Communities**

Despite advancements in HSHP, RSC, TES, and solar thermal heating technology, research focusing specifically on their combined application in high-latitude climates remains limited. Key challenges include the variability of solar resources, extreme winter temperatures,

and high complexity of renewable systems. Additionally, many renewable energy systems have an extremely high capital cost, which increases with system complexity. Furthermore, many renewable systems including heat pumps struggle to operate efficiently in extreme temperatures, reducing cost effectiveness. Further studies are needed to explore optimal control strategies, long-term performance under extreme weather conditions, and cost-benefit analyses tailored to these unique environmental settings.

This thesis aims to address these gaps by simulating the performance of hybrid source heat pumps integrated with TES, solar thermal heating, and RSC systems in a high-latitude setting - specifically Fairbanks, Alaska. The findings are expected to contribute to the growing body of knowledge on sustainable and efficient heating and cooling solutions for extreme climates, with an emphasis on intelligent system control and thermal energy storage integration.

#### **1.4 Purpose**

The performance of HVAC systems is highly variable, depending greatly on many location-specific parameters. Some HVAC systems' performance depends primarily on the heating/cooling load characteristics, while other systems depend on other variables such as heat source/sink temperature, wind speed, and solar irradiance. Several HVAC systems are compared in this thesis, many of which are highly dependent on variable conditions which cannot be easily estimated or ignored. To address these variable conditions, a data-driven approach was proposed to simulate a typical year in Fairbanks, Alaska. This approach aimed to model meteorological conditions, building heat transfer characteristics, and HVAC system functionality using a year-long simulation in Python. This model drew from various data sets to accurately model these conditions and applied principles of heat transfer and thermodynamics to analyze the performance of various HVAC systems in Fairbanks. This approach allowed for a rigorous analysis of HVAC system performance, and a comparison of each system's applicability to a Fairbanks homeowner. This thesis shows the iterative development of the model, as well as the impact of the tested systems on HVAC cost and emissions reductions in Fairbanks. Furthermore, while the model was used to simulate Fairbanks' conditions, it was developed in

an adjustable manner which can be used to easily perform similar analyses in other locations which are not explored in this thesis.

An emphasis was placed on the performance evaluation of advanced HVAC technology including RSC, solar thermal heating, thermal storage systems, and hybrid source heat pumps. The HVAC system proposed in this thesis incorporates each of these components, as well as a backup boiler to meet the heating requirements at extreme winter temperatures. The proposed configuration as shown in Figure 1.3 consists of a hybrid source heat pump which can switch between an air source or water source as needed. The water source in this configuration is a thermal energy storage tank, which is configured to be passively cooled by an RSC panel in the summertime cooling season and heated by a solar evacuated tube heating array during the heating season.

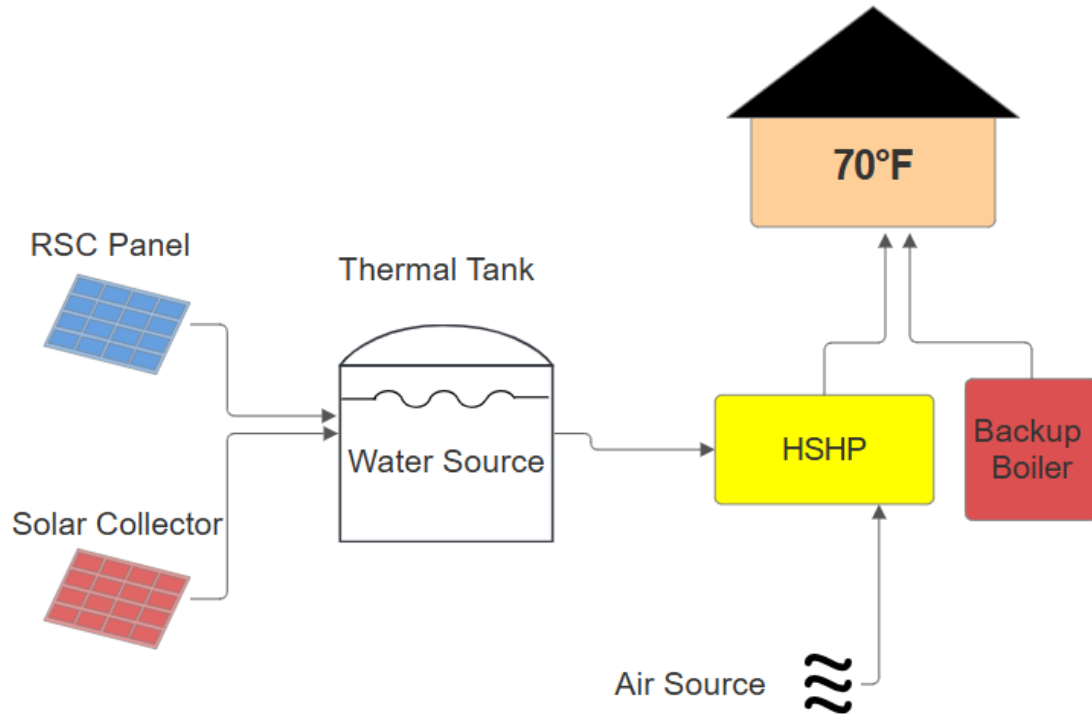


Figure 1.3: Proposed HSHP System

## Chapter 2: Steady State Analysis

### 2.1 Overview

In this model, several approaches were taken to perform a yearlong heating and cooling simulation, which are iteratively developed throughout this thesis. The model draws from various sets of data which must be well understood. TMY3, or Typical Meteorological Year version 3, is a dataset that provides hourly values of solar radiation and meteorological conditions for a one-year period, representing typical climatic conditions at specific locations based on historical data [31]. Modern day weather in Fairbanks follows a different pattern than it has in the past, with warmer winters than ever before [32]. However, the average temperature from the TMY3 data is very close to the modern-day average temperature in Fairbanks. Since TMY3 provides hourly weather data, the heating load was computed with an hourly resolution. This model also performed calculations which required spectral data. Since TMY3 only provides broadband irradiance data, SMARTS (Simple Model of the Atmospheric Radiative Transfer of Sunshine) was used iteratively to generate spectral irradiance data corresponding to the broadband TMY3 data [33]. This technique was required to accurately represent the RSC panel's heat dissipation at a given time from TMY3 data.

The first approach taken to calculate the heating and cooling load involved a steady state approximation. This method simulated the home at a constant setpoint temperature of 70°F and calculated the heat loss from the home to the environment. The HVAC system was assumed to be capable of providing or removing the exact amount of heat to maintain the home at the setpoint temperature and was set to be equal to the heat loss from the home each hour. This approach assumed that the heat loss from the home was perfectly replaced each hour by the HVAC system, and did not allow for thermal accumulation. A visual description of this energy balance is shown in Figure 2.1.

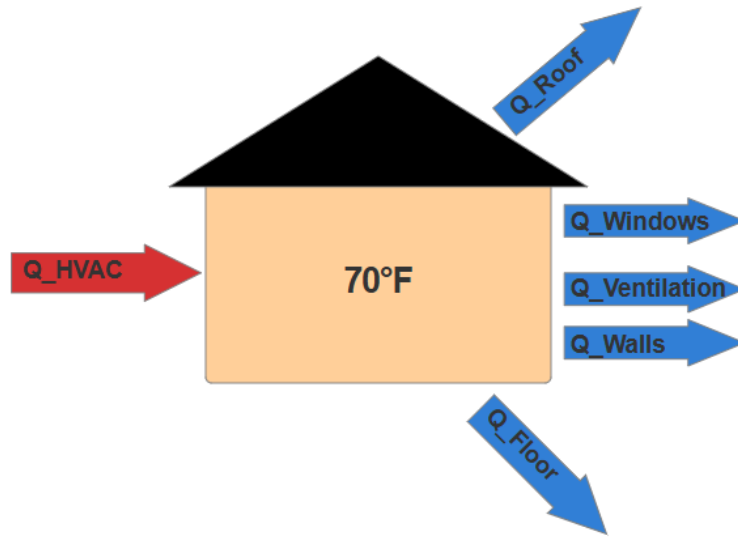


Figure 2.1: Steady State Energy Balance

The model home was based on a high-efficiency new construction home in the Fairbanks area. The material properties and geometry of the home are well known from the home's as-built drawings and specifications and were provided by the builder. To assess the validity and accuracy of the heating load calculation, a case study analysis was performed over the home and compared to other standard models. This study is detailed in the validation/verification section of this chapter. The following section shows the technical breakdown of the methodology used for the steady state analysis. The values, sources, and units for material properties and constants can be found in the nomenclature section of this thesis.

## 2.2 Methodology

### 2.2.1 Input Data

TMY3 data from NREL [31] provided ambient temperature, diffuse horizontal irradiance, direct normal irradiance, wind speed, air pressure, and relative humidity data. The cost of electricity was taken from GVEA [34] for 2023, and the cost of heating oil was taken from the State of Alaska Geoportal [35] for 2023. These data points were exported to excel, and linearly interpolated across to generate 8760 data points, allowing for an hourly resolution. This method accounted for changes in heating oil and electricity cost throughout a given year. The

heating oil cost, electricity cost, and weather data were easily stored as arrays using the NumPy [36] package in Python.

The term “spectral” simply refers to a data set which varies with wavelength, while “broadband” refers to irradiance across the entire spectrum or “band”. Spectral data must take a different structure in Python than broadband data since it is a function of wavelength, not time. The spectral data used in this model includes spectral atmospheric transmissivity and spectral RSC surface emissivity. The spectral atmospheric transmissivity data is taken from [8] while the RSC surface emissivity data was provided from [12]. All spectral data is taken over a wavelength ( $\lambda$ ) range of .3 micrometers to 15 micrometers with a resolution of .01 micrometers, yielding 1471 data points. Although spectral atmospheric transmissivity is provided, the governing heat transfer equations require the spectral atmospheric emissivity. However, the emissivity can be directly calculated from the transmissivity  $\tau_{atm}(\lambda)$ , which is shown in equation 2.1, taken from [8].

$$\varepsilon_{atm}(\lambda, \theta) = 1 - \tau_{atm}(\lambda)^{\frac{1}{\cos(\theta)}} \quad (2.1)$$

This calculated emissivity  $\varepsilon_{atm}(\lambda, \theta)$  is not only a function of the wavelength  $\lambda$ , but also of the polar angle  $\theta$ . Here,  $\theta$  ranges from 0 to  $\frac{\pi}{2}$  with a resolution of  $\frac{\pi}{32}$ . Thus, the spectral atmospheric emissivity must be stored in a matrix with rows corresponding to wavelength and columns corresponding to the polar angle.

The final input data used in this model was the spectral solar irradiance data (SSI) generated by SMARTS, which is expressed in terms of global horizontal irradiance (GHI). Here, a 3D matrix (365 x 24 x 1471) was dimensioned by the day of the year, hour of the day, and wavelength, respectively. The use of SMARTS in this study was a major improvement on past studies of high-latitude radiative sky cooling. The significance of this improvement is that the spectral distribution of solar irradiance across the electromagnetic spectrum can be calculated and accurately represented, according to input meteorological data from TMY3. This distribution is greatly affected by changes in location, time, and atmospheric/weather conditions, and must be calculated accordingly. In addition to location parameters such as

elevation, surface height, latitude, longitude, date, time, and climate classification, SMARTS also uses specific meteorological parameters from TMY3 which vary throughout the year. These input variables include site pressure, visibility, precipitable water, and albedo. Since these variables depend on time, the SSI data was computed at every time step throughout the model. To facilitate this, a process was implemented to run SMARTS iteratively for every time step, automatically using the TMY3 data corresponding to that time step. This process used a Python script which reads the TMY3 data file and generates a SMARTS input file using the TMY3 data for every time step. It is important to note that this spectral data is only needed for the RSC energy balance calculations, and it is therefore only necessary to have when the RSC panel is active. In this model, the RSC panel is active during the summer cooling season, from May 1<sup>st</sup> to August 31<sup>st</sup>. Once the Python script was used to generate the required SMARTS input files, a windows batch script was then used to automatically run SMARTS, iterating through each of the input files and generating the required SSI data as output. For each hour, an output file was generated with the SSI data in terms of spectral GHI displayed across the wavelength spectrum of .3 micrometers to 15 micrometers with a resolution of .01 micrometers, yielding 1471 data points. This is the third and final spectral data set that was used in this model. Note that all spectral data was defined over this same spectrum.

## 2.2.2 Ventilation

With the required input data stored in arrays, a few more values were calculated for use in the heating and cooling load computations. The Goff-Gratch equation was used to calculate the saturation pressure of water vapor as a function of ambient temperature as taken from [37], which was reformulated for ease of use in Python. The calculations are split up by terms for ease of display. Here,  $TB_{water}$  is the boiling point of water ( $K$ ),  $T_{amb}$  is the ambient temperature ( $K$ ), and  $P_{sat\ vapor}$  is the saturation vapor pressure of water ( $Pa$ ).

$$Term \#1 = -7.90298 \left( \frac{TB_{water}}{T_{amb}} - 1 \right) \quad (2.2)$$

$$Term \#2 = 5.02808 \left( \log_{10} \left( \frac{T_{amb}}{TB_{water}} \right) \right) \quad (2.3)$$

$$Term \#3 = -1.3816 \times 10^{-7} \left( 10^{11.344 \left( 1 - \frac{T_{amb}}{TB_{water}} \right)} - 1 \right) \quad (2.4)$$

$$Term \#4 = 8.1328 \times 10^{-3} \left( 10^{-3.49149 \left( 1 - \frac{T_{amb}}{TB_{water}} \right)} - 1 \right) \quad (2.5)$$

$$Term \#5 = Term \#1 + Term \#2 + Term \#3 + Term \#4 \quad (2.6)$$

$$P_{sat \text{ vapor}} = P_{atm} \cdot 10^{Term \#5} \quad (2.7)$$

With the water vapor saturation pressure known, the absolute humidity of the outside air was found. This analysis assumed a steady state mass balance over the home, where the mass entering was equal to the mass exiting. With the absolute air humidity known, the density of the moist air was calculated, following methodology from [38]. Here,  $P_{vapor}$  is the vapor pressure of water (Pa) as a function of  $T_{amb}$ ,  $RH$  is the relative humidity known from TMY3,  $\omega$  is the absolute humidity,  $P_{air}$  is the ambient air pressure (Pa) from TMY3,  $R_{vapor}$  is the gas constant for water vapor ( $\frac{J}{kg \cdot K}$ ),  $R_{air}$  is the gas constant for air ( $\frac{J}{kg \cdot K}$ ), and  $\rho_{air}$  is the density of the moist air ( $\frac{kg}{m^3}$ ).

$$P_{vapor} = P_{sat \text{ vapor}} \cdot RH \quad (2.8)$$

$$\omega = \frac{.622 P_{vapor}}{P_{air} - P_{vapor}} \quad (2.9)$$

$$\rho_{air} = \frac{\left( \frac{P_{air}}{R_{air} \cdot T_{amb}} (1 + \omega) \right)}{1 + \left( \frac{\omega \cdot R_{vapor}}{R_{air}} \right)} \quad (2.10)$$

With the air density and absolute humidity known, the specific enthalpy of the inside and outside air was calculated. These values were required to find the net heat loss from the home due to ventilation. Here,  $h_{dry}$  is the specific enthalpy of the dry air ( $\frac{J}{kg}$ ),  $cp_{air}$  is the specific heat capacity of the dry air ( $\frac{J}{kg \cdot K}$ ),  $q_{latent}^*$  is the latent heat of vaporization of water

$\left(\frac{J}{kg}\right)$ ,  $q_{sensible}^*$  is the sensible heat of the water vapor  $\left(\frac{J}{kg}\right)$ ,  $h_{vapor}$  is the specific enthalpy of the water vapor  $\left(\frac{J}{kg}\right)$ ,  $h_{out}$  is the specific enthalpy of the outside air  $\left(\frac{J}{kg}\right)$ ,  $h_{in}$  is the specific enthalpy of the inside air  $\left(\frac{J}{kg}\right)$ , and  $T_{set}$  is the setpoint temperature ( $K$ ). The notation  $T(^{\circ}C)$  indicates that the temperature value was converted to Celsius for calculations, while the  $q^*$  notation denotes that the heat value is in units of energy per mass. This methodology was borrowed from [39].

$$h_{dry} = cp_{air} \cdot T_{amb}(^{\circ}C) \quad (2.11)$$

$$q_{sensible}^* = cp_{vapor} \cdot T_{amb}(^{\circ}C) \quad (2.12)$$

$$h_{vapor} = q_{latent}^* + q_{sensible}^* \quad (2.13)$$

$$h_{out} = h_{dry} + (h_{vapor} \cdot \omega) \quad (2.14)$$

$$h_{in} = cp_{air} \cdot T_{set}(^{\circ}C) + q_{latent}^* + cp_{vapor} \cdot T_{set}(^{\circ}C) \quad (2.15)$$

Additionally, a few more ventilation parameters were required to find the heat loss from ventilation. The mass flow rate of air is calculated in equation 2.17, converting into the appropriate units. Here,  $ACH$  is the number of air changes per hour from [40],  $Vent\ Rate$  is the rate of ventilation  $\left(\frac{m^3}{h}\right)$ ,  $V_{house}$  is the heating volume of the home ( $m^3$ ), and  $\dot{m}_{air}$  is the mass flow rate of moist air  $\left(\frac{kg}{s}\right)$ .

$$Vent\ Rate = ACH \cdot V_{house} \quad (2.16)$$

$$\dot{m}_{air} = \frac{Vent\ Rate \cdot \rho_{air}}{\left(\frac{3600s}{1h}\right)} \quad (2.17)$$

Finally, the net rate of heat loss from the home due to ventilation was calculated. Here,  $q_{ventilation}$  is in units of Watts, which follows the typical notation in this thesis.

$$q_{ventilation} = \dot{m}_{air}(h_{inside\ air} - h_{outside\ air}) \quad (2.18)$$

### 2.2.3 Solar Irradiance

Another important series of calculations must be performed to find the view factor of the sun at any given time for a horizontal, vertical, and tilted surface. The view factors were required to calculate the incident radiation on each surface position from the TMY3 broadband irradiance data. Here, the tilt optimized tilt angle for solar absorption was taken to be the same as the latitude of Fairbanks. The calculation of the solar declination angle, zenith angle, and horizontal view factor were adopted from [8]. The tilted evacuated solar collector's cylindrical tube design allowed for steady solar absorption regardless of the azimuthal angle of the sun. This design eliminated the need for single axis tracking by allowing for a negligible effect from the lateral view factor of the sun. Here,  $\delta_{day}$  is the daily solar declination angle (*radians*),  $\delta_{hour}$  is the solar declination hour angle (*radians*), *day* is the day of the year,  $\varphi$  is the latitude of Fairbanks (*radians*),  $\beta$  is the tilt angle of the evacuated tube heater (*radians*),  $\theta_Z$  is the zenith angle (*radians*), and *TVF*, *HVF*, and *VVF* are the tilted, horizontal, and vertical surface view factors, respectively.

$$\delta_{day} = 23.45 \sin \left( \left( \frac{\pi}{180} \right) (360) \left( \frac{284 + day}{365} \right) \right) \frac{\pi}{180} \quad (2.19)$$

$$\delta_{hour} = \cos \left( 2\pi \left( \frac{hour + 1 + 11}{24} \right) \right) + \sin(\varphi) \sin(\delta_{day}) \quad (2.20)$$

$$\theta_Z = \cos^{-1}(\cos(\varphi) \cos(\delta_{hour})) \quad (2.21)$$

$$\beta = \theta_Z - \varphi \quad (2.22)$$

$$TVF = \cos(\beta) \quad (2.23)$$

$$HVF = \cos(\theta_Z) \quad (2.24)$$

$$VVF = \sin(\theta_Z) \quad (2.25)$$

With each of these view factors calculated, the effective irradiance on each surface was calculated according to the following equations. In each equation, the effective irradiance is some combination of the direct normal irradiance (*DNI*) and the diffuse horizontal irradiance (*DHI*), which were known from TMY3. The *DNI* is multiplied with the associated view factor according to the angle of incidence, while the *DHI* is assumed to be some fraction of the full amount depending on the position of the surface. For simplicity, a vertical surface was assumed to receive half the diffuse component, and a tilted surface is assumed to receive a scaled amount based on the tilt angle, as shown in 2.28. Here, *HI*, *VI*, and *TI* are the horizontal, vertical, and tilted irradiance  $\left(\frac{W}{m^2}\right)$ . *DNI* is the direct normal irradiance, and *DHI* is the diffuse horizontal irradiance, both in the same units  $\left(\frac{W}{m^2}\right)$  from TMY3 [31].

$$HI = DNI \cdot HVF + DHI \quad (2.26)$$

$$VI = DNI \cdot VVF + \frac{DHI}{2} \quad (2.27)$$

$$TI = DNI \cdot TVF + DHI \left( \frac{\pi - \varphi}{\pi} \right) \quad (2.28)$$

## 2.2.4 Simplified Conductive Heat Loss

In this simulation, the home experienced heat loss through every exterior surface. To simplify the calculation of this heat loss, the effects of solar irradiance and convection were simplified by using an effective temperature approximation of each outside surface. Here, it was assumed that the temperature of the outside surface of the home was close to the ambient temperature, and the radiation both from the home to the atmosphere and vice versa are neglected in calculations. The convection coefficient  $h \left(\frac{W}{m^2 \cdot K}\right)$  is calculated as an empirical function of windspeed as shown in equation 2.29, taken from [8]. Here, the roof is approximated as a horizontal surface for simplicity, and the effective roof temperature  $T_{sol-air\ roof} (K)$  is calculated separately from the effective wall temperature  $T_{sol-air\ walls} (K)$

to account for the different solar view factors, using a shading factor  $S$  to account for the natural shading of the home's exterior walls. Here,  $v_{wind}$  is the wind speed ( $\frac{m}{s}$ ) from TMY3 and  $\alpha_{house}$  is the absorptivity of the home.

$$h = 3.1 + (4.1 \cdot v_{wind}) \quad (2.29)$$

$$T_{sol-air\ walls} = T_{amb} + (\alpha_{house} \cdot S \cdot VI) / h \quad (2.30)$$

$$T_{sol-air\ roof} = T_{amb} + (\alpha_{house} \cdot HI) / h \quad (2.31)$$

The sol-air temperature approximation used to find the effective temperature of the outside surface of the house was taken from [12]. This approximation accounts for the convection and incident solar radiation at the home's exterior surface. It was also assumed that only  $\frac{1}{2}$  of the home's exterior walls are shaded to the sun at any given time. The temperature of the exterior surface of the bottom of the home was assumed to be equal to the ambient air temperature. With each mode of heat transfer accounted for, the effective rate of heat transfer was modeled as conduction through a plane wall. Here, the wall R values represent the total resistance to every mode of heat transfer. The plane wall simplification using the sol-air temperature is shown in Figure 2.2 for clarity.

## 2.2.5 Home Energy Balance

With these assumptions in place, the net rates of heat loss from each surface of the home were calculated. In equation 2.35 it was again assumed that  $\frac{1}{2}$  of the home's windows receive solar irradiance at any given time. Additionally, it was assumed that only 60% of the solar irradiance on the window is absorbed throughout the year, which accounted for variable window curtain shading denoted by  $WC$ . Here,  $q$  ( $W$ ) denotes the rate of heat loss from the facet of the home given by each respective subscript.  $U_{windows}$  ( $\frac{W}{m^2 \cdot K}$ ) gives the window's insulation efficiency, while  $\tau_{windows}$  is the transmittance rating of the windows. Additionally,  $A$  ( $m^2$ ) gives the area and  $R$  gives the thermal resistance of each surface ( $\frac{m^2 \cdot K}{W}$ ).

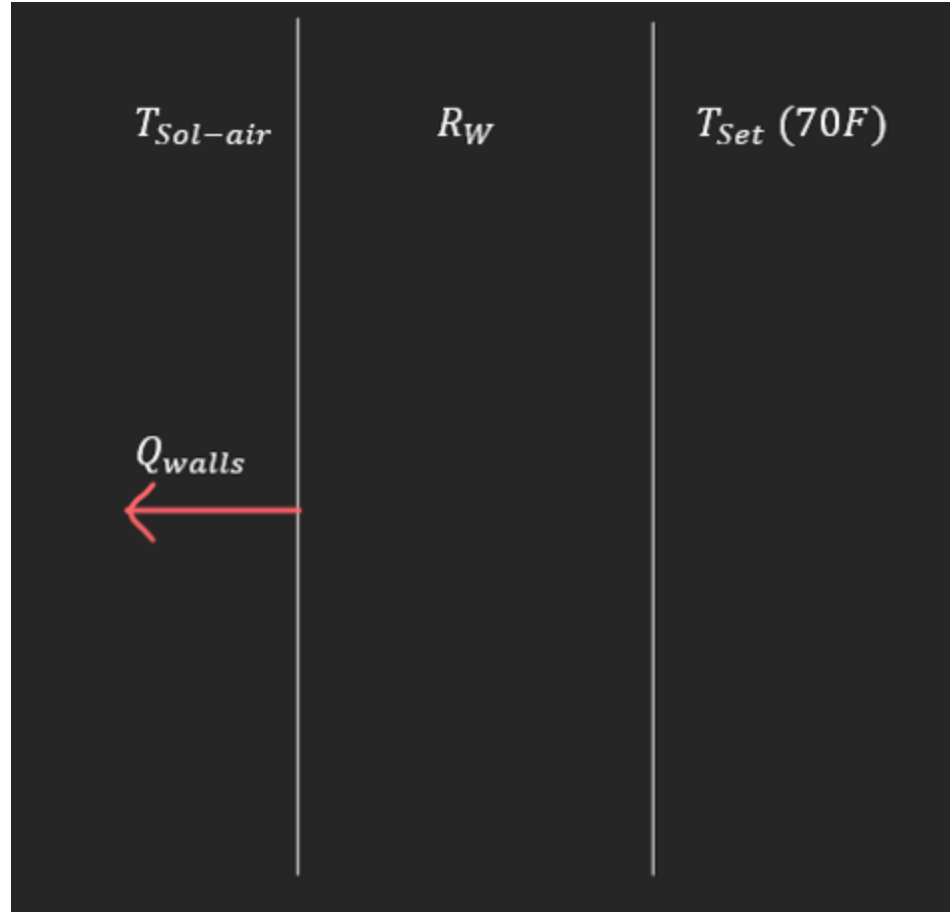


Figure 2.2: Plane Wall

$$q_{walls} = ((T_{set} - T_{sol-air\ walls}) A_{walls}) / R_{walls} \quad (2.32)$$

$$q_{roof} = ((T_{set} - T_{sol-air\ roof}) A_{roof}) / R_{roof} \quad (2.33)$$

$$q_{floor} = ((T_{set} - T_{amb}) A_{floor}) / R_{floor} \quad (2.34)$$

$$q_{windows} = (U_{windows} \cdot A_{windows}(T_{set} - T_{amb})) - (S \cdot VI \cdot A_{windows} \cdot \tau_{windows} \cdot WC) \quad (2.35)$$

The net heat loss from the home  $q_{Loss}$  ( $W$ ) was calculated as shown in equation 2.36. Here, the HVAC load  $q_{Load}$  ( $W$ ) was set equal to the hourly rate of heat loss from the home  $q_{Loss}$ . Looping through the year,  $q_{Load}$  was structured as an array which stored the corresponding heating/cooling load for the HVAC system each hour.

$$q_{Load} = q_{Loss} = q_{walls} + q_{roof} + q_{floor} + q_{windows} + q_{ventilation} \quad (2.36)$$

## 2.2.6 RSC Panel and Solar Evacuated Tube Collector Energy Balance

With the heating/cooling load calculated for the year, the energy balances for each component of the HVAC system were applied. The following section defines the rest of the energy balance functions, beginning with the RSC panel which was broken down into each mode of heat flux from the solar irradiance, convection, radiation to outer space, and atmospheric radiation.  $q''_{sun}$ ,  $q''_{conv}$ ,  $q''_{space}$ , and  $q''_{atm}$  are the respective rates of heat flux ( $\frac{W}{m^2}$ ) from each mode. The integrations were performed using the *SciPy* “*integrate.trapezoid*” function in Python [41] with a wavelength step size of  $.01\mu m$  denoted by  $d\lambda$ , and a polar angle step size of  $\frac{\pi}{32}$  denoted by  $d\theta$ . Note that these equations were adopted from [8] and [42].

Here,  $T_{tank}$  ( $K$ ) is the thermal tank temperature, which is assumed to be equal to the surface temperature of the RSC panel.  $C_1$  ( $3.74 \times 10^8 W \cdot m^2$ ) and  $C_2$  ( $1.44 \times 10^9 \mu m \cdot K$ ) are constants for Planck’s law, which calculates the spectral black body irradiance  $B(\lambda)$ . In equation 2.40, the previously used functional notation for  $B(\lambda)$ ,  $\varepsilon_{RSC}(\lambda)$ , and  $\varepsilon_{atm}(\lambda, \theta)$  has been dropped for clarity. It’s important to note that none of these values are constant, and all vary as they are integrated across their respective input variables in equation 2.40. Additionally,  $SSI(\lambda)$  denotes the spectral solar irradiance ( $\frac{W}{m^2 \cdot \mu m}$ ).

$$q''_{sun} = \int_{.3\mu m}^{15\mu m} \varepsilon_{RSC}(\lambda) \cdot SSI(\lambda) \cdot d\lambda \quad (2.37)$$

$$q''_{conv} = h(T_{amb} - T_{tank}) \quad (2.38)$$

$$B(\lambda) = \frac{C_1 \cdot \lambda^{-5}}{e^{\left(\frac{C_2}{\lambda \cdot T_{amb}}\right)} - 1} \quad (2.39)$$

$$q''_{atm} = \int_{.3\mu m}^{15\mu m} \int_0^{\frac{\pi}{2}} \varepsilon_{RSC} \cdot \varepsilon_{atm} \cdot B \cdot \sin(2\theta) \cdot d\theta d\lambda \quad (2.40)$$

$$q''_{space} = \int_{.3\mu m}^{15\mu m} B(\lambda) \cdot \varepsilon_{RSC}(\lambda) \cdot d\lambda \quad (2.41)$$

$$q_{RSC} = (q''_{sun} + q''_{conv} + q''_{atm} - q''_{space}) A_{RSC} \quad (2.42)$$

Finally, the net rate of heat gain ( $W$ ) from the RSC panel is shown in equation 2.42, denoted by  $q_{RSC}$ . The much simpler expression for the rate of heat transfer for the solar collector is given in equation 2.43 by  $q_{sc}$ . Here,  $FR$  is the heat removal factor, and all other constants are as previously discussed and shown in the nomenclature section. This methodology was followed from [12].

$$q_{sc} = A_{sc} (FR \cdot \tau_{sc} \cdot \alpha_{sc} \cdot TI - FR \cdot U_{sc}(T_{tank} - T_{amb})) \quad (2.43)$$

With these energy balance functions defined, the model implemented logic and controls and calculated performance metrics. The first control was implemented to keep the RSC and solar collector from wasting energy to the environment. This logic automatically turned off the solar collector heating loop for that hour if the solar collector was rejecting heat to the environment and turned off the RSC loop if the RSC panel was gaining energy from the environment.

While the boiler was assigned a fixed efficiency  $\eta_{boiler}$ , the coefficient of performance (COP) of the WSHP and ASHP were calculated to compare performance and select the optimal system. The empirical equations for ASHP COP for heating were gathered and provided by Samuel et al. [43]. The same COP calculation was also used for the WSHP in heating mode. However, these empirical relationships were only known over a temperature range of -35°C to 13°C. Beyond these limits, the COP was calculated at the respective limit rather than extrapolating. The COP calculations for heating mode are shown in equations 2.44 and 2.45.

$$COP_{ASHP} = .001745(T_{amb}(\text{°C}))^2 + .1508T_{amb}(\text{°C}) + 4.751 \quad (2.44)$$

$$COP_{WSHP} = .001745(T_{tank}(^{\circ}\text{C}))^2 + .1508T_{tank}(^{\circ}\text{C}) + 4.751 \quad (2.45)$$

In cooling mode, the COP calculation for each system was provided from Magrath [8] as shown in equations 2.46 and 2.47.

$$COP_{ASHP} = -.06627T_{amb} + 23.935 \quad (2.46)$$

$$COP_{WSHP} = -.06627T_{tank} + 23.935 \quad (2.47)$$

At this point, the Python script entered an optimization block. In this program the user chose to optimize the HVAC system based on either cost or  $CO_2$  emissions. To select the best system based on these parameters, the cost and  $CO_2$  emissions of each system were calculated and compared. Initializing the logic sequence, a minimum cost and minimum emission variable were defined and given an initial value. Note that a 200W pump from [44] was used to circulate fluid through the heating loop each of the WSHP, ASHP, and boiler, and is accounted for in hourly cost and emissions calculations, denoted by  $E_{pump}$  ( $kWh$ ). Here,  $\$_{WSHP}$ ,  $\$_{ASHP}$ ,  $\$_{boiler}$ ,  $CO2_{WSHP}$ ,  $CO2_{ASHP}$ , and  $CO2_{boiler}$  represent the respective hourly cost (\$) and emissions ( $kg$ ) of each operational system.  $Q_{Load}$  denotes the total energy ( $Wh$ ) entering the home from the HVAC system in one hour, which is numerically equal to  $q_{Load}$ . Additionally,  $\$_{electricity}$  gives the price of electricity ( $\frac{\$}{kWh}$ ) from [34] while  $\$_{oil}$  represents the price of heating oil ( $\frac{\$}{gal}$ ) from [35]. It's important to note that the price of heating oil and electricity vary throughout the year.  $CO2_{oil}$  gives the associated emissions from heating oil combustion ( $\frac{kg}{gal}$ ) taken from [45], while  $CO2_{electricity}$  gives the associated  $CO_2$  emissions of electricity consumption ( $\frac{kg}{Wh}$ ), from [46]. Here, the lower heating value and density of No. 2 heating oil are given respectively by  $LHV_{oil}$  ( $\frac{J}{kg}$ ), and  $\rho_{oil}$  ( $\frac{kg}{m^3}$ ). The appropriate unit conversions are shown for each calculation.

$$\$_{WSHP} = \left( \frac{|Q_{Load}|}{\left(\frac{1000W}{1kW}\right) COP_{WSHP}} + E_{pump} \right) \$_{electricity} \quad (2.48)$$

$$\$_{ASHP} = \left( \frac{|Q_{Load}|}{\left( \frac{1000W}{1kW} \right) COP_{ASHP}} + E_{pump} \right) \$_{electricity} \quad (2.49)$$

$$\$_{boiler} = \frac{\$_{oil} \left( \frac{1gal}{.003785m^3} \right) \left( \frac{1}{\rho_{oil}} \right) |Q_{Load}| \left( \frac{3600J}{1Wh} \right)}{LHV_{oil} \cdot \eta_{boiler}} + (E_{pump} \cdot \$_{electricity}) \quad (2.50)$$

$$CO2_{WSHP} = CO2_{electricity} \left( \frac{\$_{WSHP}}{\$_{electricity}} \right) \left( \frac{1kW}{1000W} \right) \quad (2.51)$$

$$CO2_{ASHP} = CO2_{electricity} \left( \frac{\$_{ASHP}}{\$_{electricity}} \right) \left( \frac{1kW}{1000W} \right) \quad (2.52)$$

$$CO2_{boiler} = CO2_{oil} \left( \frac{\$_{boiler} - (E_{pump} \cdot \$_{electricity})}{\$_{oil}} \right) + (E_{pump} \cdot CO2_{electricity}) \quad (2.53)$$

Once these costs and emissions were calculated for each system, the script entered one of two control blocks, preselected by the user. In each of these blocks, the program executed a series of logic and controls which allowed it to pick the most efficient system check that it met the operational criteria. Each block used the same logic and control. The only difference between the two blocks was that one chose the system with the minimum cost, while the other chose the system with the minimum  $CO_2$  emissions. This structure allowed for the user to easily toggle between cost or emissions optimization.

The HVAC control logic for each block was broken into 3 sections, one for each system, beginning with the WSHP. During the summer heating season, the WSHP was automatically switched on if it had the minimum cost or emissions. During the winter however, the WSHP could only run if  $T_{tank} > TF_{glycol}$ . This logic ensured that the WSHP was automatically turned off when it approached the freezing temperature of the tank's glycol solution. The WSHP's control logic is shown in Figure 2.3.

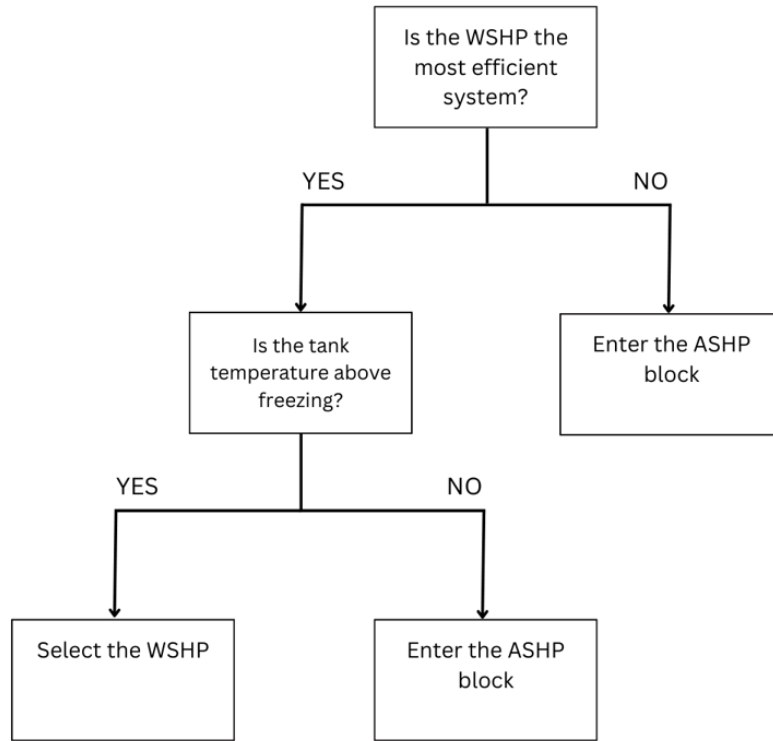


Figure 2.3: WSHP Control Logic

The ASHP had similar logic to the WSHP. It is commonly known that the heating capacity of an air source heat pump effectively drops to zero at a certain temperature [44], which was taken to be  $-35^{\circ}\text{C}$  in this simulation. Therefore, the ASHP was automatically turned off when  $T_{amb}(\text{ }^{\circ}\text{C}) < -35^{\circ}\text{C}$ . Otherwise, the ASHP was switched on when it had the minimum cost or emissions according to the user's preference. The ASHP's control logic is shown in Figure 2.4.

The boiler logic concluded the optimization block as the backup system for extremely cold temperatures. The boiler followed slightly different logic than the other systems. The boiler was turned on only when it had the lowest cost or emissions *and* there was a positive heating load. This logic ensured that the boiler did not incorrectly operate as an air conditioner. The control logic for the boiler is shown in Figure 2.5.

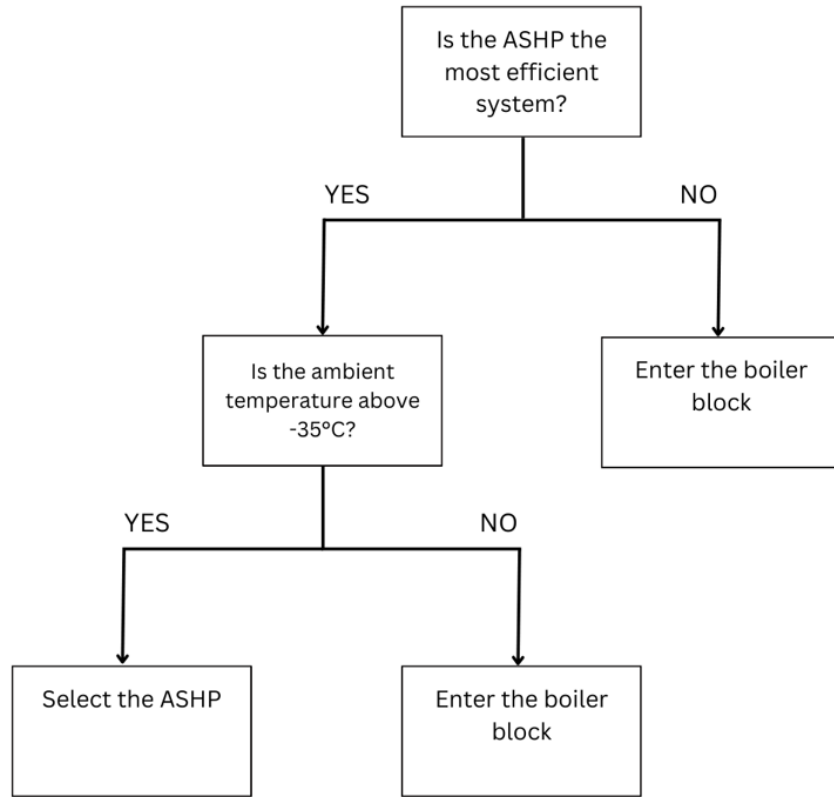


Figure 2.4: ASHP Control Logic

A final check determined if the WSHP or ASHP were active and turned the boiler on as a last resort if neither system was chosen. This default logic ensured that during extremely cold temperatures, the boiler kicks on when no other systems are viable, even if it isn't the most efficient system.

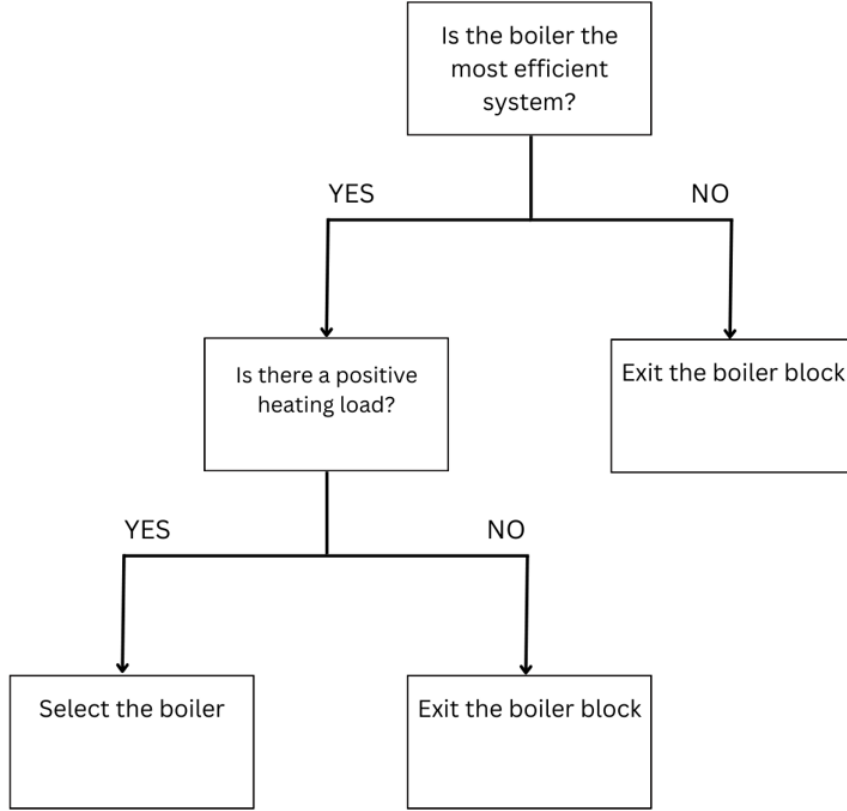


Figure 2.5: Boiler Control Logic

Following the optimization blocks, the final lines checked which system was active, calculated and recorded performance metrics, and balanced the tank temperature for the next iteration. Here,  $E_{WSHP}$ ,  $E_{ASHP}$ , and  $E_{boiler}$  are the electricity consumed by the respective systems during one hour of operation ( $Wh$ ),  $q_{WSHP\ Cond}$  is the rate of heat transfer into the WSHP's condenser ( $W$ ), and  $F_{boiler}$  is the heating oil consumed by the boiler ( $gal$ ). When the WSHP was selected as the active system, the following calculations were performed. Otherwise, the values in equations 2.54 and 2.55 were set to zero.

$$E_{WSHP} = \frac{\$_{WSHP}}{\$_{electricity}} \quad (2.54)$$

$$q_{WSHP\ Cond} = q_{Load} - \frac{q_{Load}}{COP_{WSHP}} \quad (2.55)$$

When the ASHP was the chosen system, the electricity consumption was calculated as shown in equation 2.56. Otherwise, it was set to zero.

$$E_{ASHP} = \frac{\$_{ASHP}}{\$_{electricity}} \quad (2.56)$$

When the boiler was selected as the operational system, the following calculations were performed. Otherwise, the values in equations 2.57 and 2.58 were set to zero.

$$F_{boiler} = \frac{\$_{boiler} - (E_{pump} \cdot \$_{electricity})}{\$_{oil}} \quad (2.57)$$

$$E_{boiler} = E_{pump} \cdot \$_{electricity} \quad (2.58)$$

Finally, the tank's energy balance was performed, and the new tank temperature was defined. Here, a few controls were implemented to ensure a physically representative system. Firstly, logic was put in place to cut off the RSC panel from the thermal tank when the tank temperature reached freezing. This way if the tank was too cold, the RSC panel could not continue to cool it. To avoid the RSC and SC panels counteracting each other, logic was placed which runs the RSC loop only during the summer cooling season and the SC loop during the winter heating season. During the summer cooling season, the net rate of heat transfer to the thermal tank is given in equation 2.59 by  $q_{net}$ .

$$q_{net} = q_{RSC} - q_{WSHP\ Cond} \quad (2.59)$$

During the winter heating season:

$$q_{net} = q_{SC} - q_{WSHP\ Cond} \quad (2.60)$$

The tank temperature was then balanced and updated. Here,  $m_{glycol}$  is the total mass of the glycol-water solution in the tank,  $cp_{glycol}$  is the specific heat capacity of the solution, and  $\rho_{glycol}$  is the density of the solution. Note here that while  $q_{net}$  was originally defined in units of power ( $W$ ), this value is numerically the same as the total heat transfer over one hour in Watt-hours. This equivalence was intended for ease of calculation and conversion between calculated heat transfer rates and net energy changes over an hour, which is the temporal resolution used in this model. Here,  $Q_{net}$  is in terms of energy ( $Wh$ ) and represents the net heat addition to the tank over one hour. This notation is typical in this thesis.

$$m_{glycol} = V_{tank} \cdot \rho_{glycol} \quad (2.61)$$

$$T_{tank} = \frac{Q_{net} \left( \frac{3600J}{1Wh} \right)}{m_{glycol} \cdot cp_{glycol}} + T_{tank} \quad (2.62)$$

Once the program completed the main loop's execution, it moved into post processing. During post processing, any significant data was converted into a Pandas data frame. An Excel sheet was then created, to which the data frames were exported accordingly. The program auto spaced columns, froze panes, added labels, and organized all data. Additionally, a graph was created on the final sheet of the workbook to show the system usage throughout the year.

### 2.3 Validation/Verification

Throughout the development of the model, each section was incrementally tested and validated. In addition to this incremental development, each critical set of generated data was tested and compared to other well-known data. This process included sampling small sections of the data and verifying that it matches the expected output, as well as verifying that the dataset followed expected overarching trends. The most critical values for validation in this model were those used the most directly in calculation, as well as those with the most complex methodology. These important values included  $q_{Load}$ ,  $q_{RSC}$ , SSI, VI, HI, and TI.

#### 2.3.1 Home Heat Loss Modeling

To validate the section of the model which computes  $q_{Load}$ , the heating and cooling loads of a recently built high energy efficiency home and the resulting yearly cost of space heating were computed. Comparing this data to a report from a professional energy assessor [47] it was determined that the model produced results very similar to industry standard methods. This validated the model's ability to accurately compute the space heating costs for a residential home, given information about the home's construction geometry and material properties. This is an impressive achievement considering that accurate energy assessments typically require a series of thorough home inspections and testing to determine the building's ability to retain heat.

For this analysis, a case study was performed over a high efficiency single family home built in Fairbanks in 2023. This 6-star energy rated home included high R-value walls and roof, high efficiency windows, well-sealed doors, and steam heating. The builder provided information from the home's construction including the insulation values, wall/window/door areas, heating volume, and external surface materials/colors. These constants are documented in the nomenclature section and were used to represent the model home for every analysis in this thesis, as provided from (C. Hnilicka, personal communication, September 17<sup>th</sup>, 2024). Using this information and assuming the ASHRAE standard minimum ACH of .35 from [40] the yearly space heating cost was found to be \$671. This estimation was roughly 9.9% lower than the energy assessor's estimation of \$745 [47]. From this analysis it was concluded that the model generated an accurate and comprehensive energy assessment over a given home.

### **2.3.2 Spectral Solar Irradiance Data Modeling**

Throughout this research, accurately representing the spectral solar irradiance absorbed by the RSC proved to be difficult. To truly understand how much heat would be absorbed by the panel through sunlight, the solar irradiance needed to be expressed in spectral terms. As explained in the previous methodology section, this SSI data was not available through TMY3. While converting broadband irradiance to spectral irradiance is a non-trivial task, it was imperative to the accuracy of the model to consistently use the TMY3 data for all weather inputs. For this reason, SMARTS was used to generate spectral solar irradiance data from broadband TMY3 data. Upon the completion of this complex task, it was important to observe the trends in the data to ensure that it was generated accurately. Here, it was demonstrated that the generated SSI data accurately reflected changes in the sunlight's power and distribution across the EM spectrum. This was a major improvement on previous studies which have assumed constant distribution for each hour of the day. A series of validation analyses were performed to verify the correctness of the generated data, beginning with the AM1.5 reference spectra as a control to compare the generated data to, shown in Figure 2.6 from [48].

The ASTM G173 – 03 Reference Spectra shown in Figure 2.6 give the spectral solar irradiance assuming typical atmospheric conditions, which are designed to be representative of

conditions in the contiguous US [48]. The red graph represents the direct and circumsolar irradiance, representing the total irradiance felt by a horizontal surface with a hemispherical view [48]. This most closely represents the measurable irradiance on the Earth's surface, and it includes direct sunlight as well as the scattered sunlight which appears as a ring around the sun. This data was chosen as a reference point for comparison. The generated spectral global horizontal irradiance data was then analyzed, beginning with the data generated for noon of summer solstice, shown in Figure 2.7. This is when the sunlight is the strongest throughout the year, most closely representing the AM1.5 reference spectra.

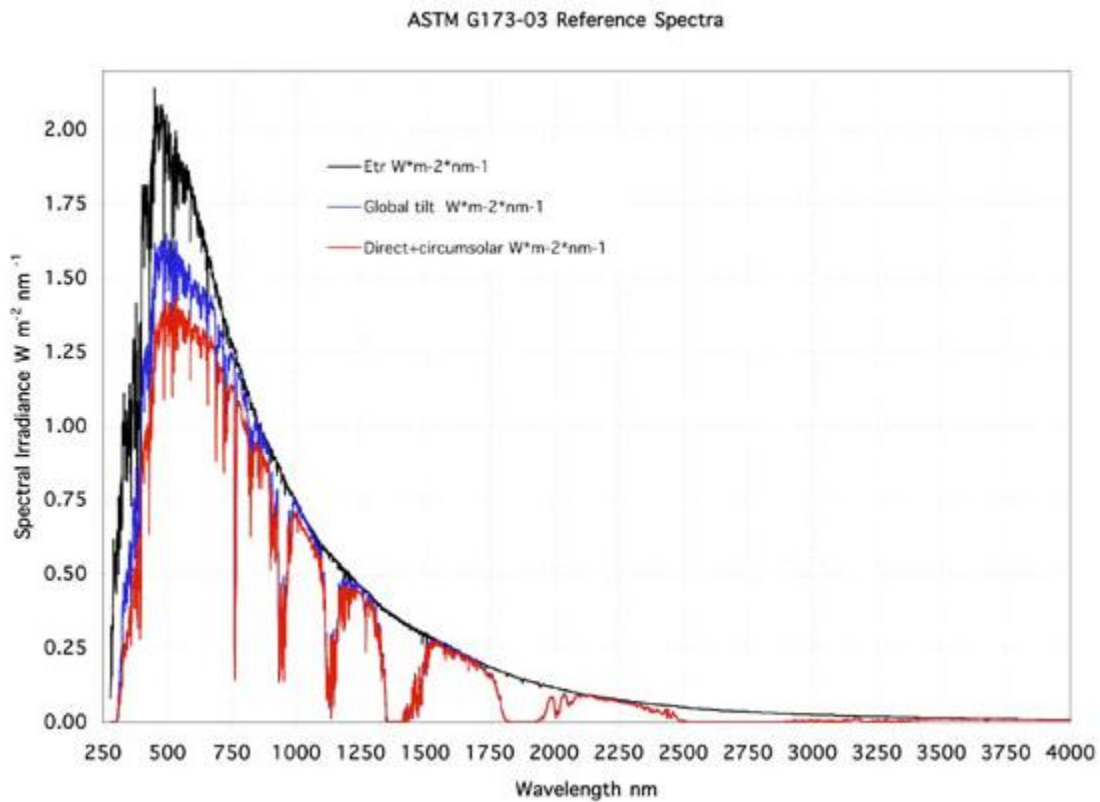


Figure 2.6: AM1.5 Reference Spectra from NREL [48]

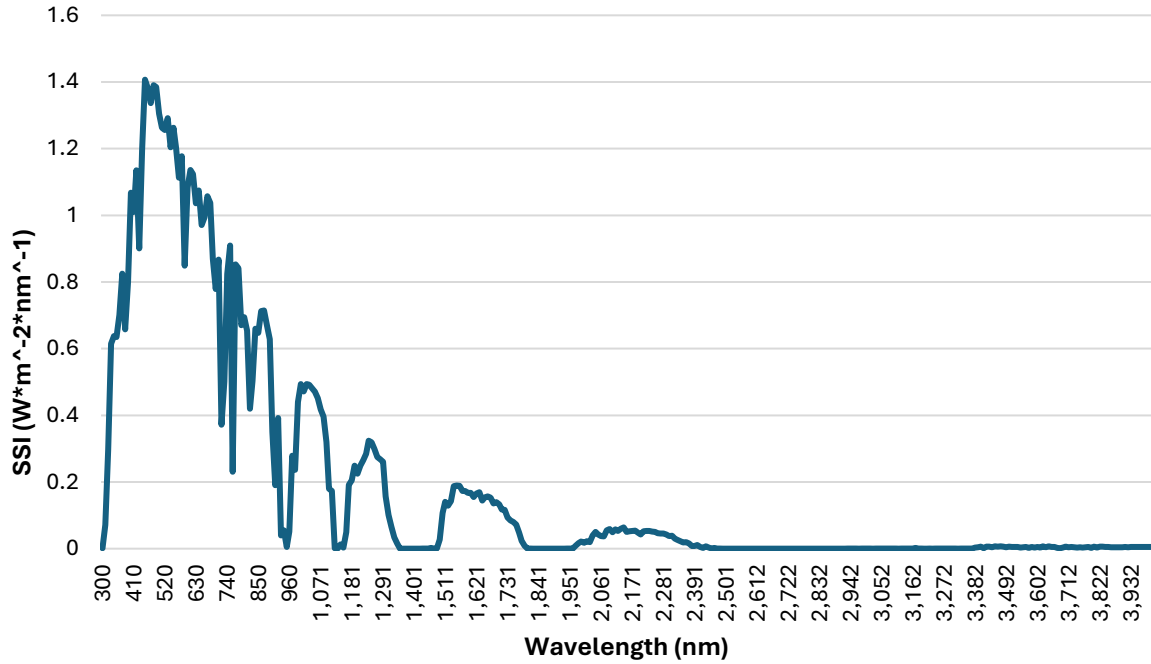


Figure 2.7: Spectral Solar Irradiance at Noon on Summer Solstice

Comparing Figure 2.6 and Figure 2.7, many similarities were observed. Both graphs peaked at the same value of  $1.4 \text{ } W \cdot m^{-2} \cdot nm^{-1}$ , and had a very similar distribution shape. These trends followed exactly what was expected at noon on the summer solstice in Fairbanks, Alaska. This analysis verified that the data generated closely matched the reference spectra as expected.

An analysis was also performed to observe the correlation between solar strength and spectral distribution with seasonal changes in the Earth's tilt. Here, the overall solar strength (the area under the curve) was expected to decrease when the Earth was tilted further away from the sun, given by seasonal changes. The spectral distribution at noon on May 1<sup>st</sup> is shown in Figure 2.8.

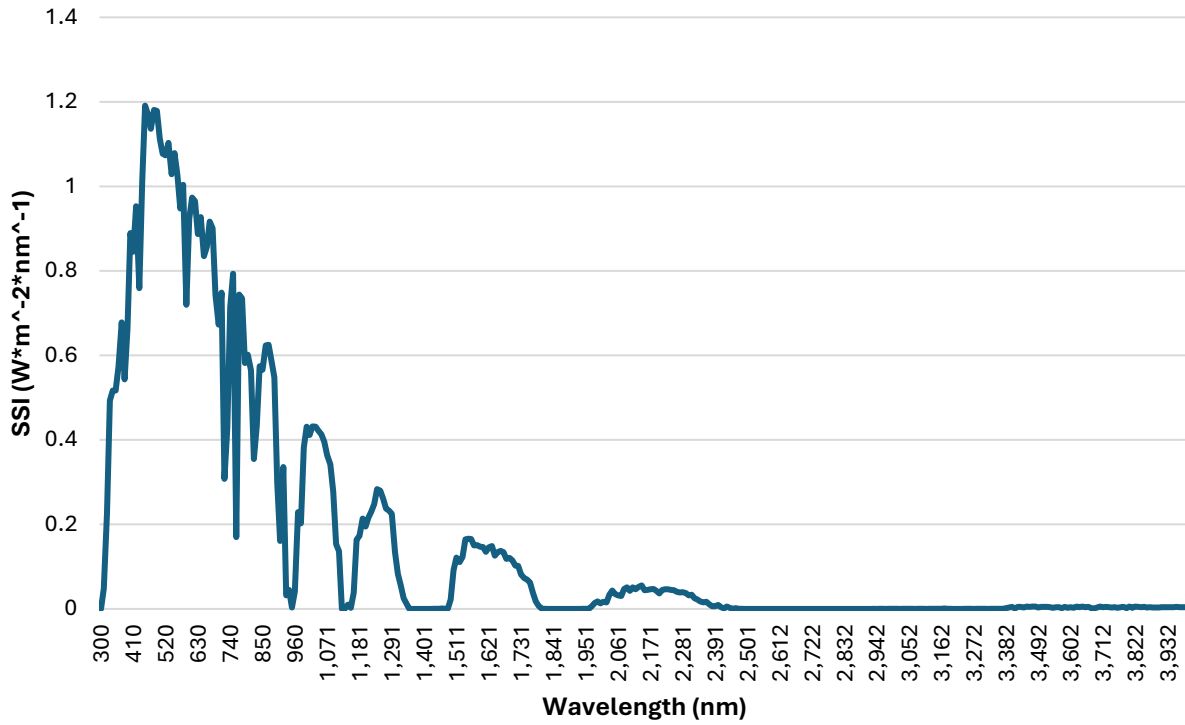


Figure 2.8: Spectral Solar Irradiance at Noon on May 1st

Given the time of day, strong sunlight was expected, however not as strong as the sun on the summer solstice due to the seasonally increased path length from the sun. As expected, the distribution took a very similar shape to the previous graph but peaked at a lower value of  $1.2 \text{ W} * \text{m}^{-2} * \text{nm}^{-1}$ . This lower peak indicated a decrease in overall solar strength, which followed the expected trend for seasonal changes and validated the correctness of the model.

An analysis was also performed to observe changes in solar strength and distribution throughout the day, given by changes in solar elevation. The spectral distribution at 8pm on the summer solstice is shown in Figure 2.9. As expected, the shape of the distribution changed significantly, and the highest peak decreased from 1.4 to just  $0.19 \text{ W} * \text{m}^{-2} * \text{nm}^{-1}$ . This showed that the data followed the expected trends and correctly varied with daily and seasonal changes.

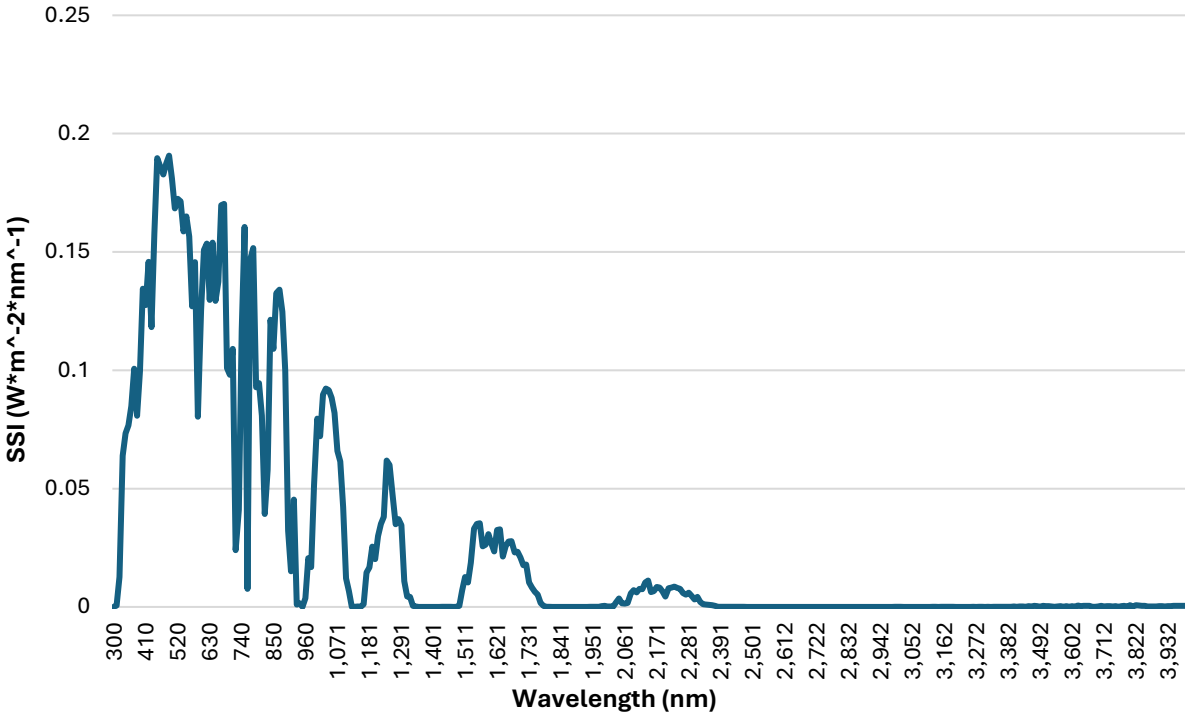


Figure 2.9: Spectral Solar Irradiance at 8pm on Summer Solstice

### 2.3.3 RSC Energy Balance

The RSC panel energy balance was easily the most complex calculation in the model due to the complex spectral integrations. The nature of these calculations required careful formulation and verification to ensure correctness. For this purpose, the RSC energy balance was thoroughly examined in development and post processing. The RSC panel was typically found to emit  $90 - 150 \frac{W}{m^2}$  passively to deep space and reached as high as  $200 \frac{W}{m^2}$  when surface temperatures exceeded 300K. This fell into the typical range for RSC cooling power densities from radiation to deep space (excluding other heat transfer modes). However, this system yielded a significantly larger net cooling power density than a typical RSC panel, which are known to net a cooling power density of around  $40 - 100 \frac{W}{m^2}$  [8] including all modes of heat transfer. When the RSC surface temperature exceeded 300K, the net cooling power density was found to be as large as  $1150 \frac{W}{m^2}$ . This cooling power density is very similar to findings from [11] which demonstrated  $1000 - 2000 \frac{W}{m^2}$  using advanced thermal management techniques. Power

density is not directly calculated in the model, but its value is given by  $\frac{Q}{A} \left( \frac{W}{m^2} \right)$ . This increase in power was resultant of the high surface temperature, allowing for  $950 \frac{W}{m^2}$  of convective heat dissipation along with  $200 \frac{W}{m^2}$  radiation to deep space. However, typical net cooling power density values were on the order of  $100 \frac{W}{m^2}$ , which agree well with typical findings [8].

#### 2.3.4 Solar Irradiance

Values of TI, VI, and HI were compared with one another as well as with values of DHI, DNI, and GHI from the TMY3 data. In Fairbanks at a latitude of  $64.8^\circ\text{N}$ , the sun appears low in the sky even during the summer. As the sun shines horizontally through the sky, it affects vertical surfaces but has the greatest view factor on surfaces tilted at an angle equal to the latitude. Since the sun is never directly overhead, the view factor on horizontal surfaces is always significantly lower than on tilted or vertical surfaces in Fairbanks even in the summer. From these known characteristics of the Fairbanks solar cycle, it was hypothesized that the VI and TI should be the highest, with the HI on the lower end. These values were found to meet expectations in relation to one another and were appropriately related to the TMY3 data. Additionally, these values varied as expected throughout the year and throughout the day. The mean irradiance values are shown in Figure 2.10, Figure 2.11, and Figure 2.12, demonstrating the adherence to daily and seasonal shifts in solar strength. During midwinter, the effects of the low solar altitude can be seen clearly as values of TI and HI dwindle down to zero.

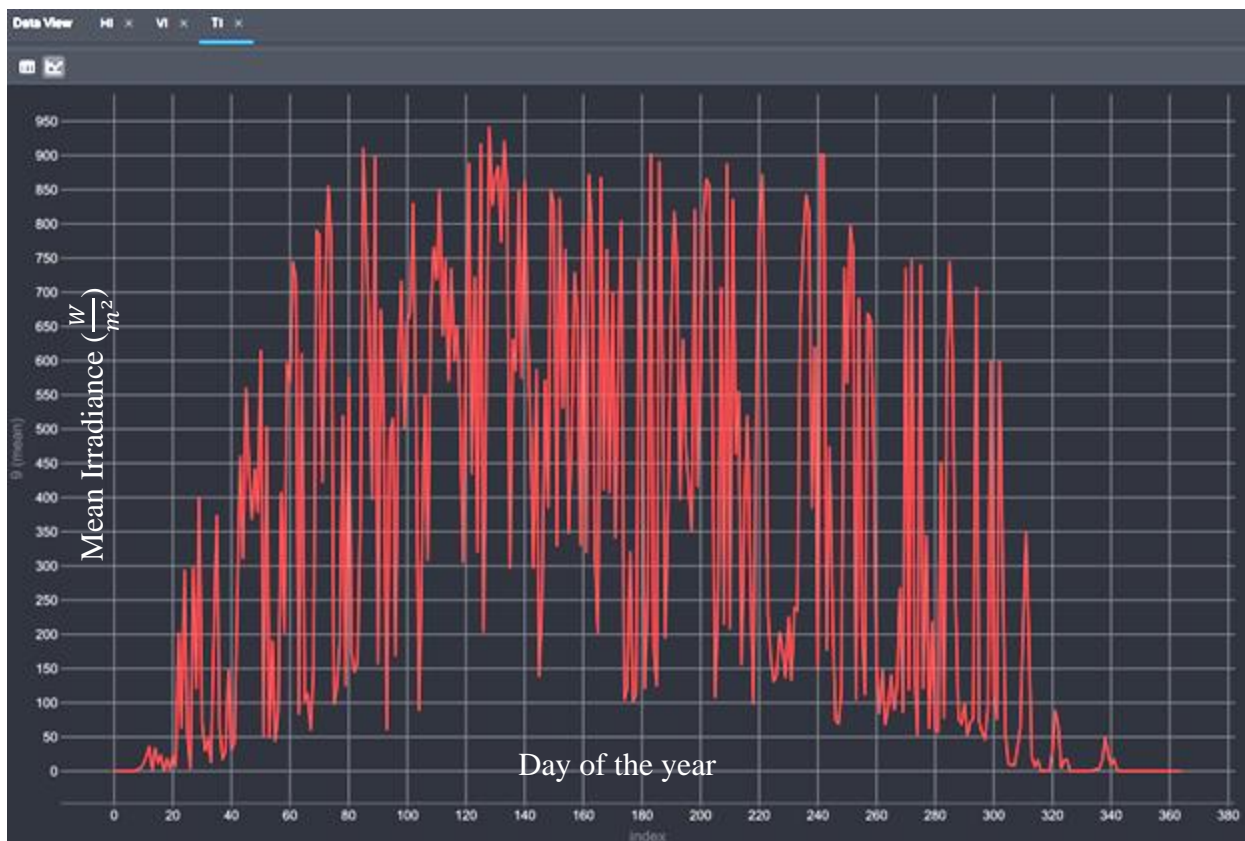


Figure 2.10: Tilted Surface Irradiance (TI)

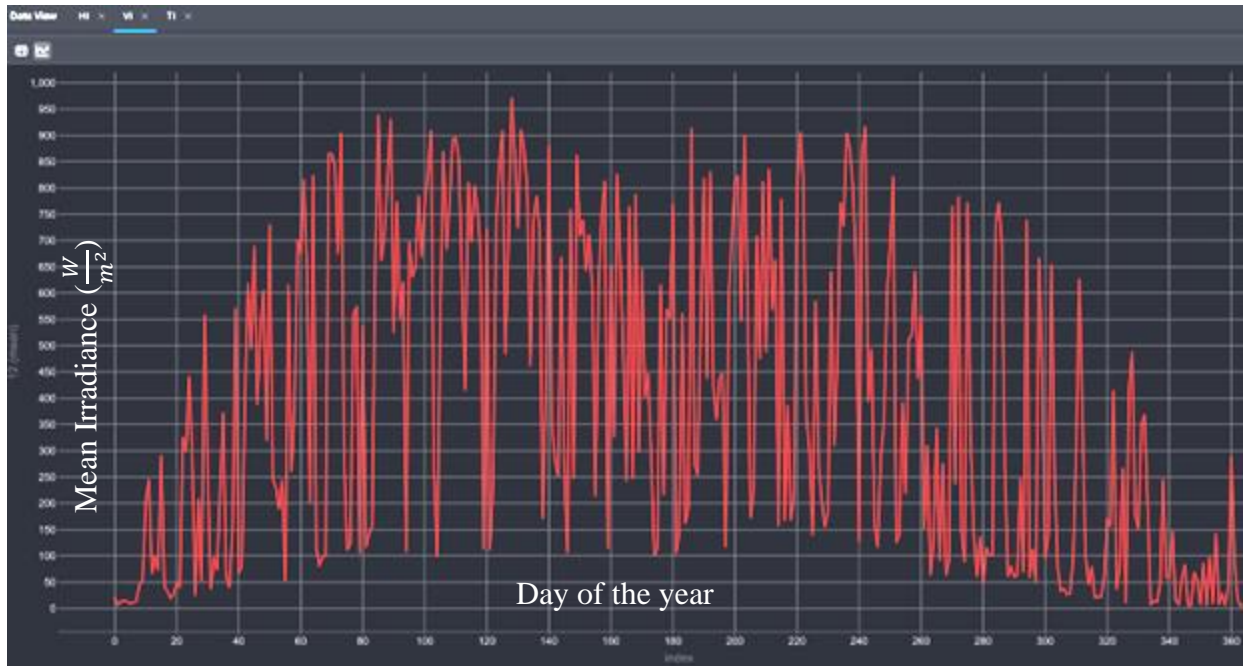


Figure 2.11: Vertical Surface Irradiance (VI)

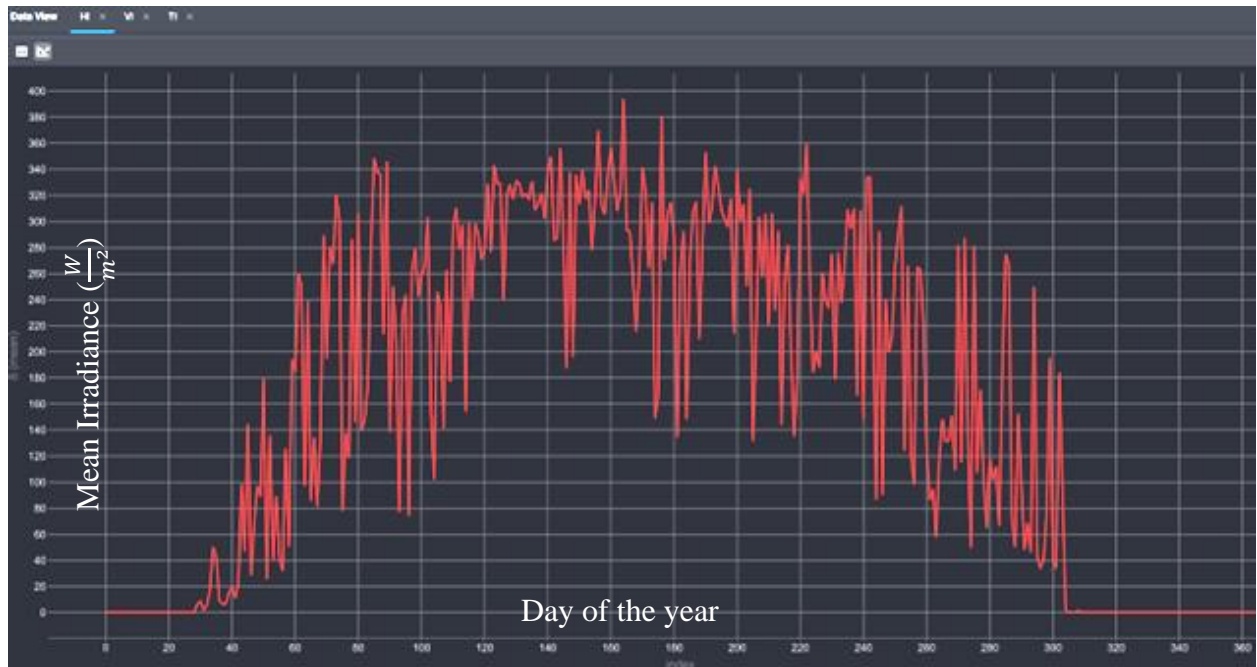


Figure 2.12: Horizontal Surface Irradiance (HI)

## 2.4 Results – Cost-Optimized Model

Using the specified input data and running the model using both cost and emissions optimization techniques, the simulation yielded promising results. Figure 2.13 shows the simulated system chosen for each hour throughout the year for both heating and cooling.

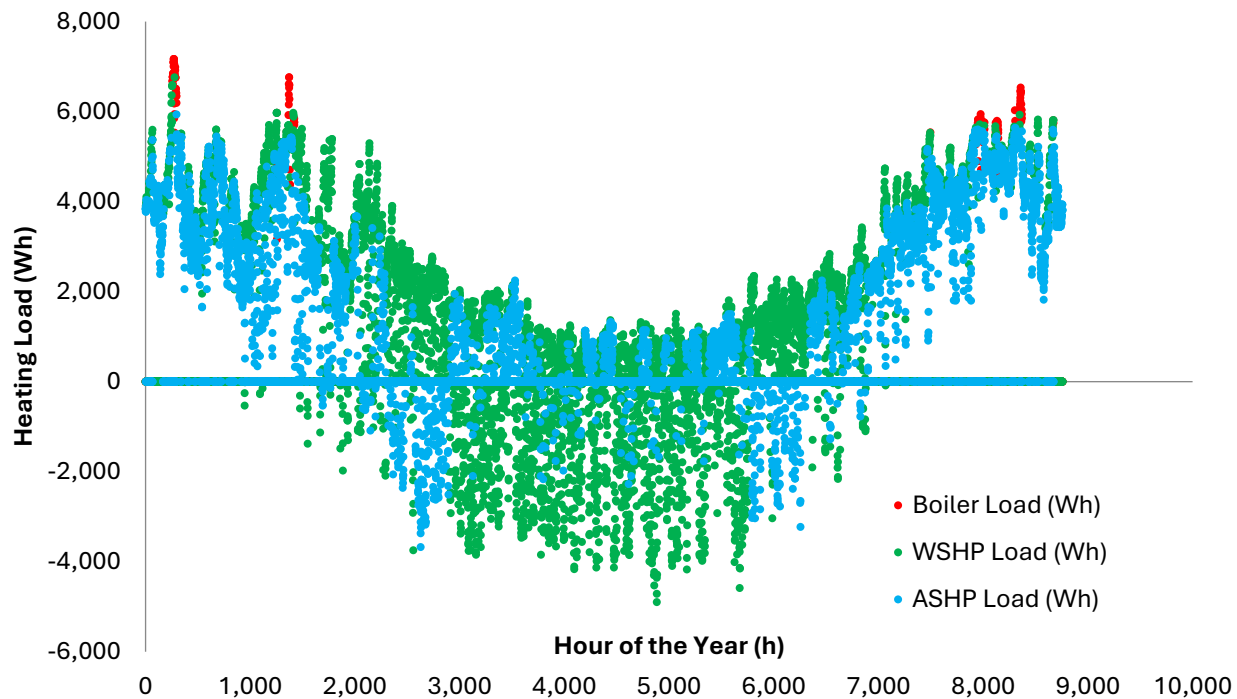


Figure 2.13: HVAC System Usage (Steady State, Cost-Optimized)

It is also important to observe the numerical results from the simulation to measure system performance. Here the total cost, operational  $CO_2$  emissions, energy consumption, average COP, and amount of space heating/AC provided for was documented for each system. This information helped to benchmark system performance, giving a baseline for comparison to future model iterations. The cost-optimized study results are shown in Table 2.1.

Table 2.1: HVAC System Performance (Steady State, Cost-Optimized)

	WSHP	ASHP	Boiler	Combined
<b>Yearly Cost (\$)</b>	903.95	1,113.34	124.90	2,142.19
<b>Yearly CO2 Output (Kg)</b>	1,410.65	1,769.68	279.21	3,459.54
<b>Average COP</b>	4.40	4.32	N/A	
<b>Energy Consumption</b>	3,617.04 (kWh)	4,537.63 (kWh)	26.19 (gal)	
<b>% Space Heating Provided</b>	39%	56%	5%	
<b>% Air Conditioning Provided</b>	82%	18%	0%	

## 2.5 Discussion – Cost-Optimized Model

The results gathered from this study clearly revealed that an 85% efficient heating oil boiler was rarely the economical choice for space heating, as shown by Figure 2.13. The boiler became economically viable only under extremely cold temperatures when the COP and heating capacity of the HSHP approached a minimum. However, Figure 2.13 also demonstrated that the implementation of a boiler is necessary for any given winter in Fairbanks. During extreme winter conditions, the heating capacity of a heat pump can fall to zero around -35°C [44]. Even before it reaches this extreme temperature, the heating capacity can drop so significantly that it may no longer supply the required heating load to maintain the home's setpoint temperature. For this reason, all heating systems in this thesis were modeled with a backup boiler to meet the heating load at the design temperature. Here, controls switch on the boiler and turn off the HSHP when the temperature is too extreme. Furthermore, additional controls could be implemented to allow the boiler to supplement the heating capacity of the HSHP so the heating load can be met. While not considered in this model iteration, variable heating capacity is discussed thoroughly in chapter 4. For simplicity, it was assumed in this model iteration that the HSHP can meet the required heating load, until -35°C where the heating capacity drops to zero.

In addition to the lack of boiler use throughout the year, a few interesting trends were observed between the ASHP and WSHP. As expected, the WSHP was the most efficient system for space heating during the shoulder seasons. This was a result of the increased solar resource as the days became longer and the path length of the solar irradiance decreased. With this increase, the solar collector provided a substantial amount of energy during the shoulder heating season, which allowed the WSHP to run at a high COP. On May 1<sup>st</sup> (hour 2920), the controller switched off the solar collector and turned on the RSC loop, effectively cooling the thermal tank in anticipation of the summer cooling season. From Figure 2.13, this is a clear turning point where the ASHP again dominated most of the heating for a while. After a prolonged period from May to June of ASHP heating, it was observed that the WSHP and ASHP began trading responsibility of heating and cooling back and forth. This oscillation was determined to stem directly from the temperature swings in the thermal tank. The WSHP claimed most of the air conditioning responsibility in the summertime as expected, but there were small spikes of ASHP cooling throughout. The oscillating cycle began as the RSC panel cooled down the thermal tank, chilling it to a cold temperature and giving the WSHP a high COP for air conditioning. Since the WSHP had a higher COP than the ASHP for AC at this point, the WSHP was the chosen system for AC. As it operated, heat was rejected from the home into the thermal tank. This heat rejection was often at a higher rate than the RSC panel could reject heat, which led to an accumulation of heat in the thermal tank and an increase in tank temperature. At a certain point, the thermal tank became warm enough that it was no longer efficient for AC. But, as the temperature continued to increase, it suddenly became the most efficient system for space heating. As it was chosen for space heating, heat was rejected from the tank into the WSHP's condenser, which led to a net tank cooling in addition to the RSC's cooling power. As the tank cooled off by heating the home, the tank temperature eventually plummeted back down. At this point, it became efficient for AC again, and the cycle repeated itself. This phenomenon resulted in oscillatory switching between AC and heating roles for the ASHP and WSHP during the summer and is shown in Figure 2.13.

In the shoulder seasons, the solar collector loop was active and heated the thermal tank, allowing the WSHP to be useful for space heating. As a result of this warm temperature,

the ASHP was the most efficient system for AC in the shoulder seasons. It is important to note that this was solely a function of the system's controls. If the logic were switched so that the RSC loop ran during this time instead of the solar collector, the roles would have switched and the WSHP would become efficient for AC, and the ASHP efficient for heating. On September 1<sup>st</sup> after the cooling season ends (hour 5840), Figure 2.13 showed another abrupt switch back to the WSHP for heating, and to the ASHP for cooling.

Observing each system individually rather than overlaying their plots, it is more clearly shown how these systems contributed to heating and cooling. The individual plots are shown in Figure 2.14, Figure 2.15, and Figure 2.16.

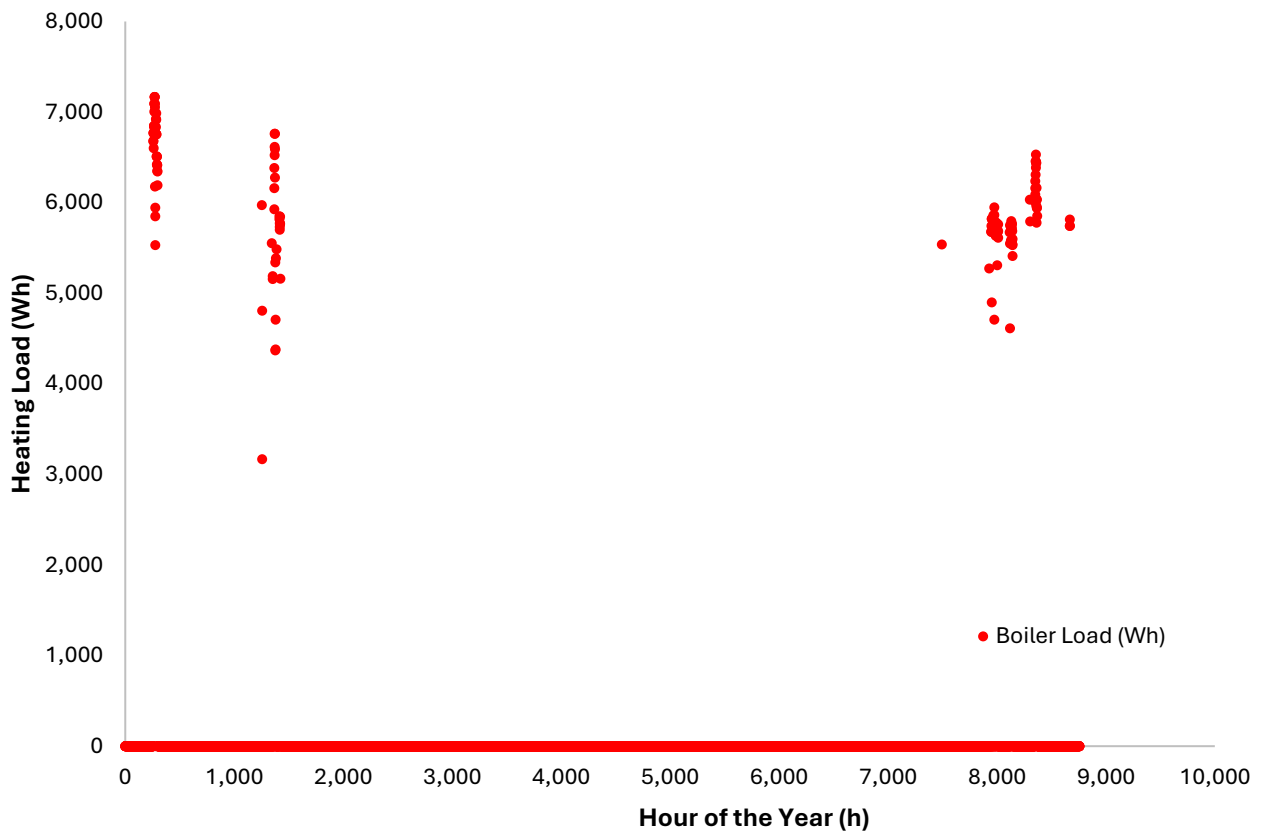


Figure 2.14: Boiler Usage (Steady State, Cost-Optimized)

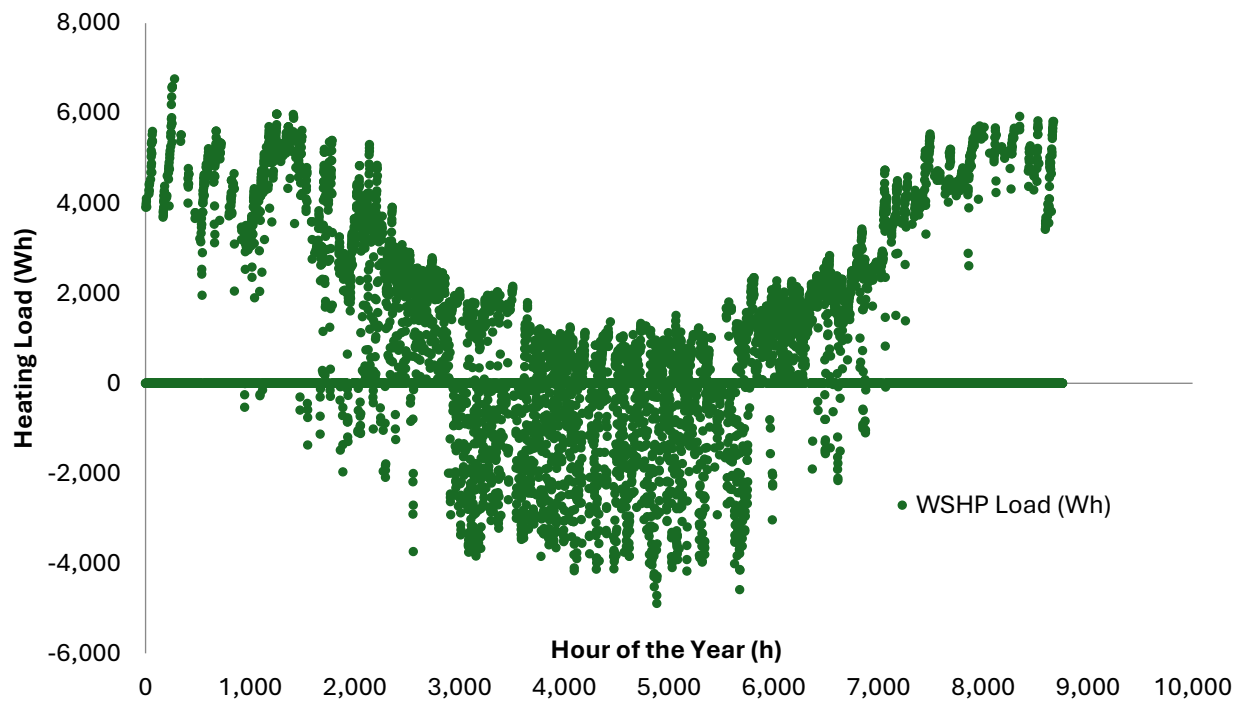


Figure 2.15: WSHP Usage (Steady State, Cost-Optimized)

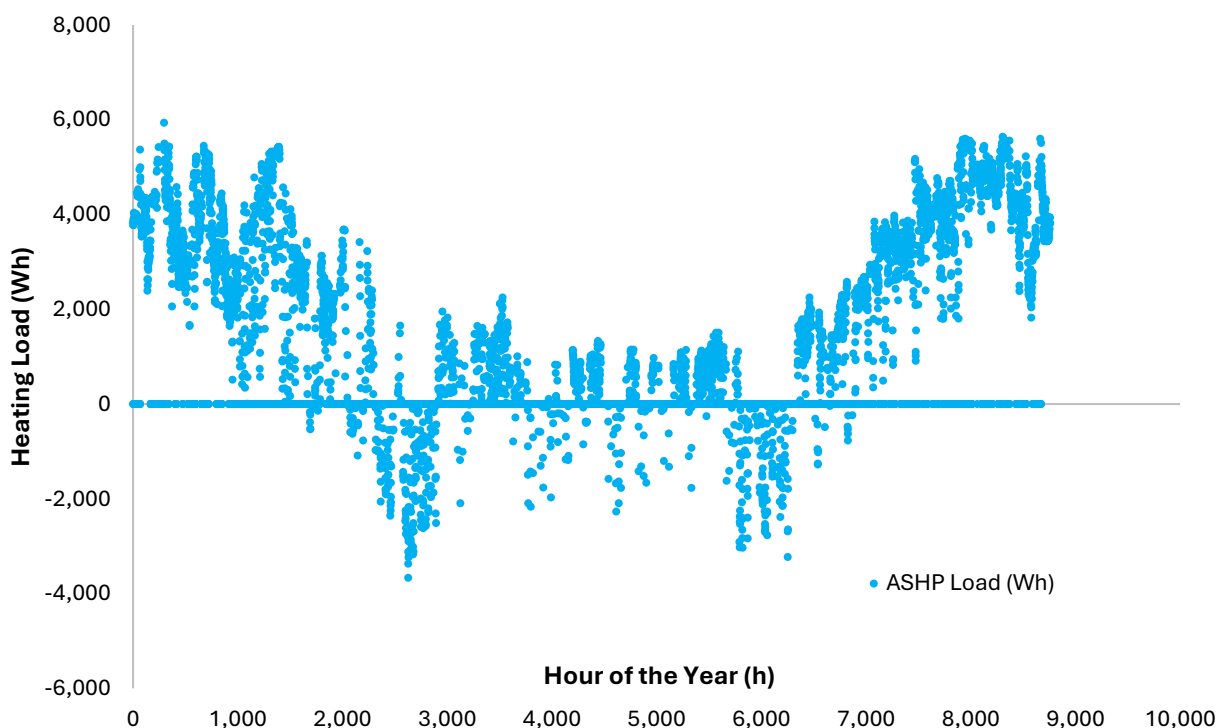


Figure 2.16: ASHP Usage (Steady State, Cost-Optimized)

The WSHP assumed most of the responsibility for heating and cooling in the summer months as shown by Figure 2.15. In the shoulder seasons, the WSHP mainly was responsible for heating while the ASHP took on the AC load. In the wintertime another interesting trend was observed. The ASHP was responsible for most of the heating load, especially when the heating load was between 0 and 4000W. This lower load represented times when the ambient temperature is cold, but not extreme. For heating loads around 4000W, the WSHP began to share some of the heating responsibility. This confirmed the expected result and showed that the WSHP was often more efficient during extreme ambient temperatures. As the heating load climbed to around 6000W, the boiler became the economical option. The trends observed in this section helped to improve future methodology. Chapters 3 and 4 in this thesis focus on changes in methodology and system configuration that improve real system performance.

Another interesting comparison was shown between thermal tank and ambient air temperature, shown in Figure 2.17. This comparison helped to shed light on why one type of heat pump might provide a higher COP than the other.

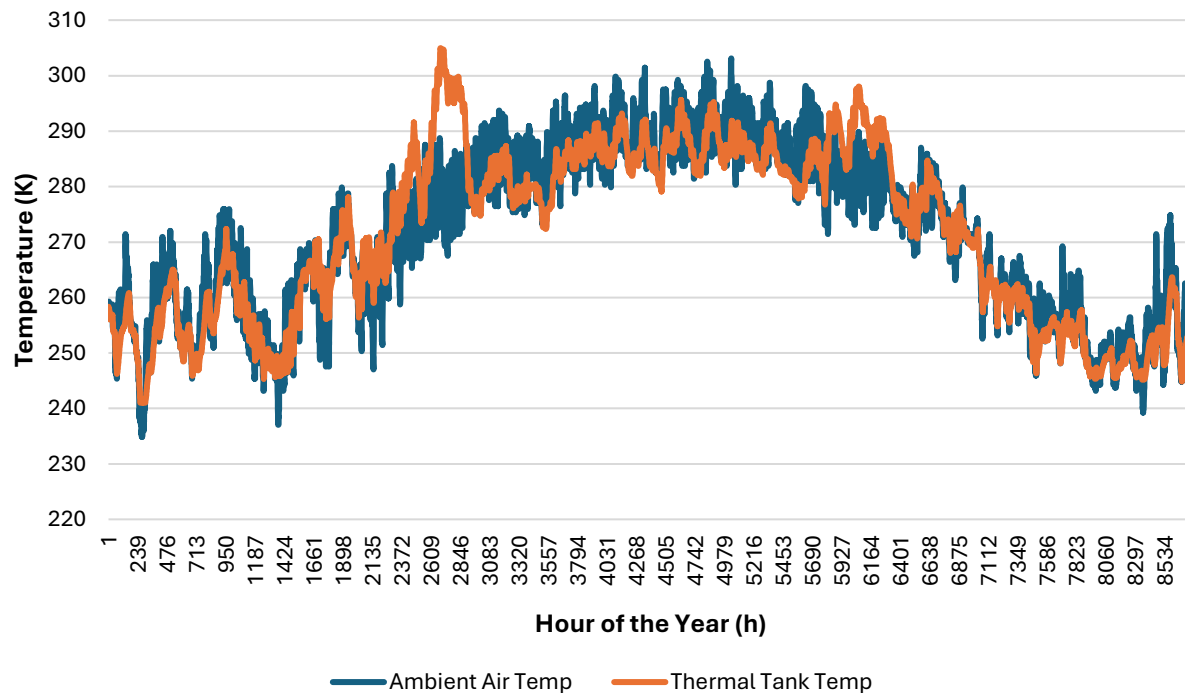


Figure 2.17: Thermal Tank Versus Ambient Temperature (Steady State, Cost-Optimized)

The thermal tank temperature followed a similar trend to the ambient air temperature for most of the year. However, there were spikes in the thermal tank during times of strong input from the solar collector or RSC panel. Additionally, the thermal tank lagged slightly behind the overall trend of the ambient air temperature and did not reach the same highs and lows. With the data analyzed well for the cost-optimized model, the results were analyzed for the emissions-optimized version for comparison.

## 2.6 Results – Emissions-Optimized Model

This section provides a comparison between the cost-optimized and emissions-optimized model results. The emissions-optimized model followed the same logic as the cost-optimized version detailed in the methodology section but selected the system with the lowest  $CO_2$  emissions rather than the lowest cost. The emissions-optimized system utilization is shown in Figure 2.18, and the numerical results are shown in Table 2.2.

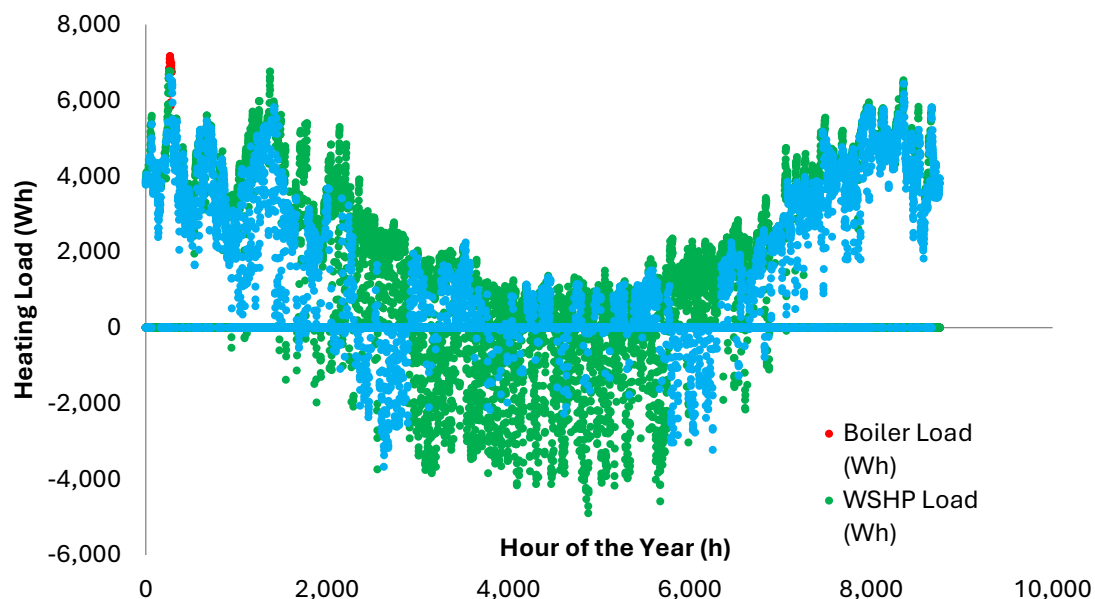


Figure 2.18: HVAC System Usage (V1 Emissions-Optimized)

Table 2.2: HVAC System Performance (Steady State, Emissions-Optimized)

	WSHP	ASHP	Boiler	Combined
<b>Yearly Cost (\$)</b>	934.72	1,190.17	22.59	2,174.48
<b>Yearly CO<sub>2</sub> Output (Kg)</b>	1,459.41	1,891.48	50.02	4,300.91
<b>Average COP</b>	4.40	4.32	N/A	
<b>Energy Consumption</b>	3,742.07 (kWh)	4,849.94 (kWh)	4.72 (gal)	
<b>% Space Heating provided</b>	40.5%	58.5%	1%	
<b>% Air Conditioning Provided</b>	82%	18%	0%	

A 4% decrease in boiler use was observed from prioritizing a low emissions system, of which 1.5% was taken by the WSHP and the remaining 2.5% was taken by the ASHP. As expected, there were no changes in the air conditioning system usage.

## 2.7 Discussion – Emissions-Optimized Model

Very little change was observed from switching the optimization technique. The main difference between optimizing emissions versus cost was that the emissions-optimized version used the boiler even less often than the cost-optimized version. Figure 2.13 and Figure 2.18 appear to be identical because of the lack of boiler use in both. The COP was found to be the determining factor in heat pump selection for both cost and emissions, so the two optimization techniques agreed for most of the year.

Due to the heating oil boiler's high  $CO_2$  output, the ambient air temperature had to be even more extreme for the boiler to be chosen in the emissions-optimized model, as shown by Figure 2.19. This resulted in less boiler use in the emissions-optimized version. Additionally, the tank and thermal temperature graph for this model version are shown by Figure 2.20 and were examined for differences from the cost-optimized version. As expected, both model versions had very similar thermal tank temperatures throughout the year.

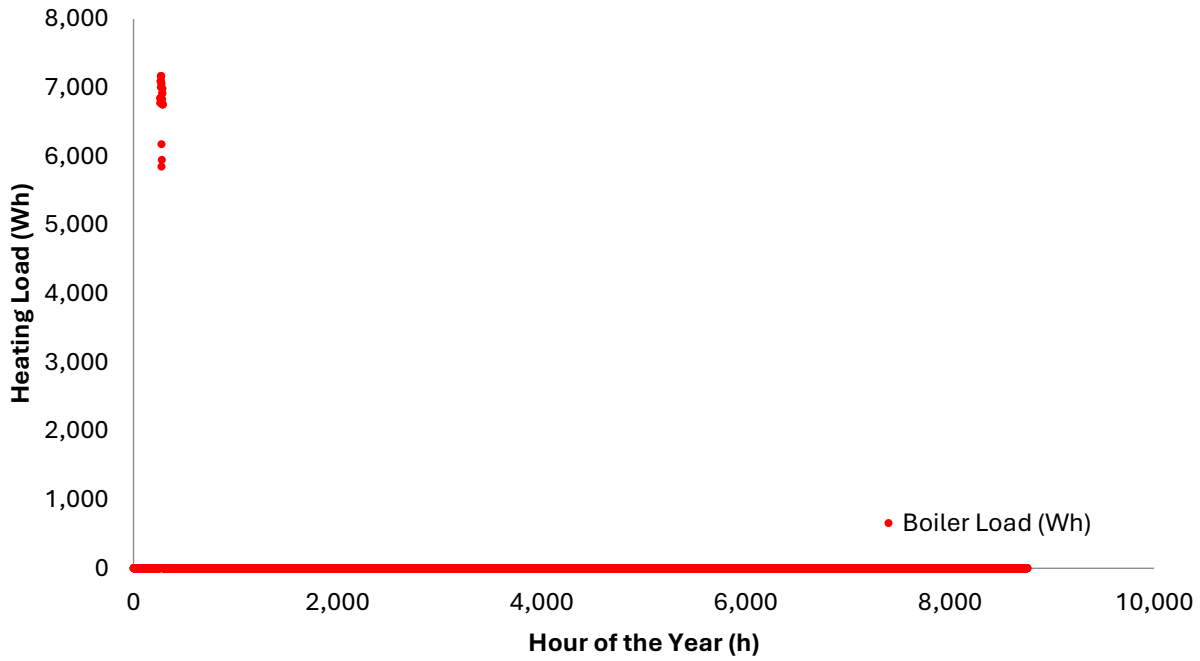


Figure 2.19: Boiler Usage (Steady State, Emissions-Optimized)

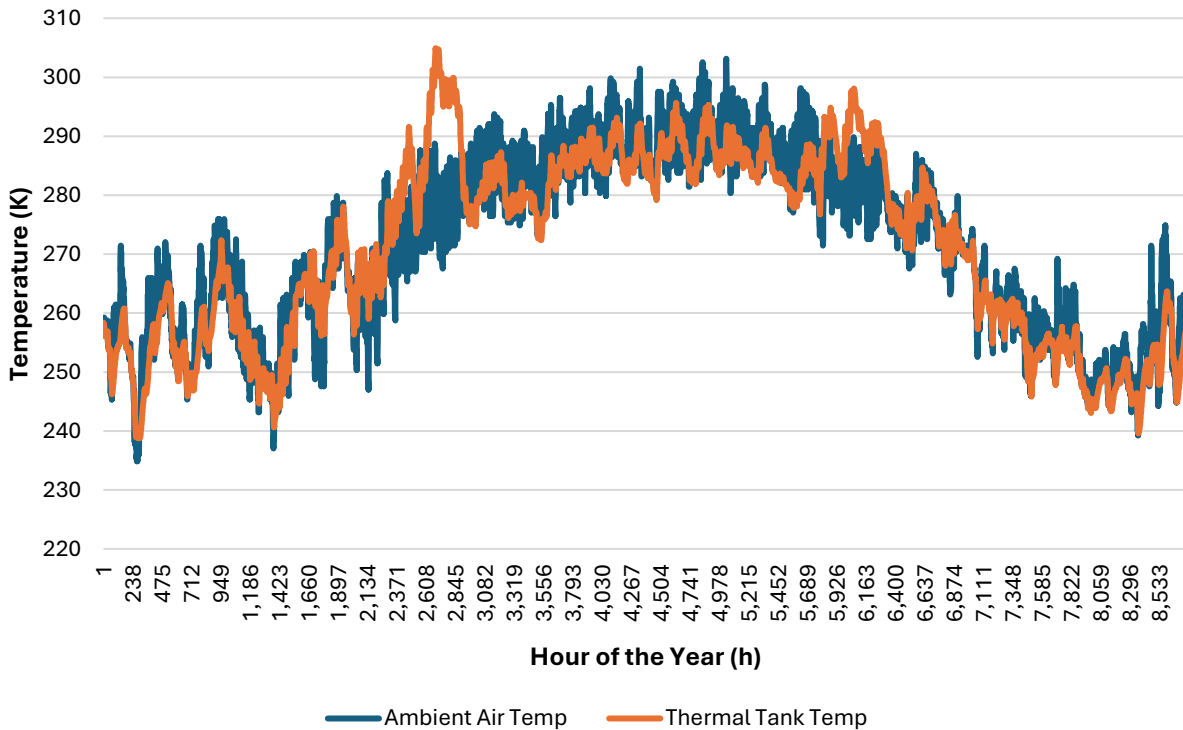


Figure 2.20: Thermal Tank Versus Ambient Temperature (Steady State, Emissions-Optimized)

The observations and comparisons made in this chapter highlighted the need for improved methodology. Inefficiencies in system switching were identified which prompted improvements in system controls and selection. Improvements to model logic and control are investigated in chapter 3. From the analysis in chapter 2, it was hypothesized that improvements to model controls and performance calculations would result in a more realistic representation of a physical HVAC system.

## Chapter 3: Controls Study

### 3.1 Overview

In this section, changes in the model logic and control were investigated to increase system performance and more accurately simulate the physical systems. The main purpose of this section is to improve upon the current methodology to implement the most efficient and realistic HVAC control system possible.

The first major control system change was the implementation of controls for a “deadband” temperature range. A deadband is a range of acceptable temperatures for which the HVAC system will remain inactive. The significance of this change was that the home’s energy balance was no longer performed using a steady state approximation. In chapter 2,  $q_{Load}$  was calculated by estimating the amount of energy input required to keep the building at a constant 70°F every hour. Because of this methodology, it was assumed that the home remained at a constant temperature or steady state, where the amount of energy entering the system was exactly equal to the amount of energy leaving the system. While this provided an accurate calculation of the home’s heat loss, there are significant inefficiencies associated with this type of HVAC control. This problem is accentuated in locations such as Fairbanks where temperature swings are extreme, and there are often heating *and* cooling loads throughout the day during the shoulder seasons. The use of a deadband temperature range allowed the home to oscillate around the setpoint temperature slightly before the HVAC system was activated. In this simulation, the temperature was allowed to swing from as low as 66°F to as high as 73°F without triggering the HVAC system. With this logic implemented, significant energy savings were observed throughout the year.

Once the deadband was implemented, a few other controls were implemented to achieve optimal system performance. One of the main goals of this study was to enable the model to accurately represent a physical system. This was a prerequisite for the system selection and optimization study of chapter 4, where specific models were chosen and simulated in the model. However, a few more changes were needed after the implementation of the deadband temperature to achieve these goals.

The next change that was implemented in this chapter was to spread out the required heating load over a few hours, rather than just one hour. HVAC systems are typically sized to meet the required heating load at extreme design temperatures. In Fairbanks, the winter design temperature is -40°F [40]. In this case, the HVAC system had to provide enough heat to counteract the rate of heat loss from the home at -40°F. In the previous model version, the heating load was set to be equal to the net rate of heat loss from the home. Once the deadband temperature controls were implemented, the HVAC system was expected to heat the home back up several degrees in addition to counteracting the active heat loss from the home, all in just one hour. In practice, it is not effective to design an HVAC system to provide this amount of heat in just one hour. A typical HVAC system may take a few hours to recover the home to its setpoint temperature under standard conditions. While it is important that an HVAC system can provide sufficient heat during extreme cold, it is equally important not to oversize the heating system. An oversized heating system can lead to inefficiencies and reduced lifespan. To prepare the model for sizing and selection of physical components, the controls were adjusted to allow for a lighter HVAC load over a longer period of time.

## **3.2 Deadband Controls**

### **3.2.1 Methodology**

While significant cost savings were expected from utilizing a deadband temperature zone, the implementation of this methodology was non-trivial and differs from the steady state analysis methodology of chapter 2. With the inside air temperature no longer constant but rather changing with time, a transient analysis was implemented over the previous steady state assumptions. A visual depiction of the home's transient energy balance is shown in Figure 3.1.

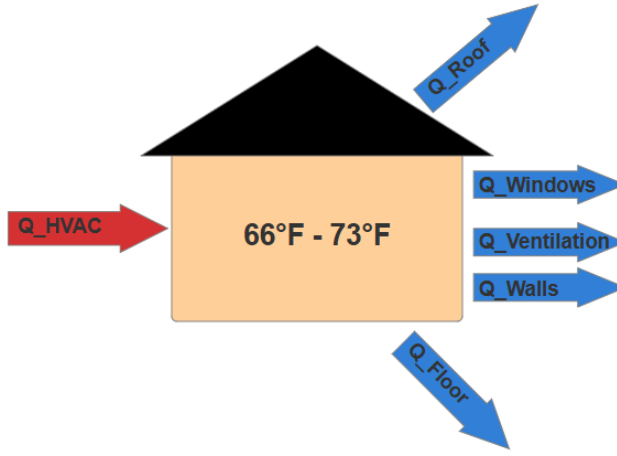


Figure 3.1: Transient Energy Balance

For this transient analysis, the change in inside air temperature was directly proportional to the difference in energy entering and leaving the system. Thus, the equation for the home's heating load was reformulated. Additionally, several new calculations were added to account for the thermal mass of the home and the variable enthalpy of the moist inside air.

$h_{set} \left( \frac{J}{kg} \right)$  represents the constant inside air enthalpy at the setpoint temperature, while  $h_{in} \left( \frac{J}{kg} \right)$  was redefined to represent the variable enthalpy of the inside air. An additional constant  $cp_{moist}$  was introduced as a combined specific heat capacity of the dry air and water vapor  $\left( \frac{J}{kg \cdot K} \right)$ .

$$h_{in} = cp_{air} \cdot T_{actual} ({}^{\circ}C) + \omega (q_{latent} + (cp_{watervapor} \cdot T_{actual} ({}^{\circ}C))) \quad (3.1)$$

$$h_{set} = cp_{air} \cdot T_{set} ({}^{\circ}C) + \omega (q_{latent} + (cp_{watervapor} \cdot T_{set} ({}^{\circ}C))) \quad (3.2)$$

$$m_{air} = \rho_{air} \cdot V_{house} \quad (3.3)$$

$$cp_{moist} = cp_{air} + \omega \cdot cp_{watervapor} \quad (3.4)$$

At this point, the energy balance function was called, calculating  $q_{Loss}$ . Following this call, the inside air temperature  $T_{actual}$  ( $K$ ) was checked. If it fell within the deadband range of 66°F to 73°F, then  $q_{Load}$  was automatically set to zero. If  $T_{actual}$  was outside of the deadband range, the model calculated the required energy input to bring the building back to 70°F, which was given by the total enthalpy change for an open system with a constant volume. The required enthalpy change of the system  $\Delta H_{sys}$  ( $Wh$ ) was broken down into separate

components for the building and the air inside, as shown in (67). Here,  $Q_{Loss}$  represents the total heat energy loss from the home ( $Wh$ ) over the one-hour heating/cooling cycle, which is numerically equal to  $q_{Load}$ .

$$\Delta H_{sys} = \Delta H_{building} + \Delta H_{air} + Q_{Loss} \quad (3.5)$$

Each component of the required air enthalpy change was broken down and equated to the previously calculated specific enthalpy values and converted to units of Watt-hours.

$$\Delta H_{air} = m_{air} \frac{(h_{set} - h_{in})}{\left(\frac{3600J}{1Wh}\right)} \quad (3.6)$$

The building's required enthalpy change was then calculated from (69), where  $C_B$  is the heat capacity of the building ( $\frac{Wh}{K}$ ).

$$\Delta H_{building} = C_B(T_{set} - T_{actual}) \quad (3.7)$$

From these equations, the total required enthalpy change to bring the system back to 70°F was calculated, thus giving the hourly heating/cooling load. The relationship between heating power and heat energy is shown in equation (3.9).

$$Q_{Load} = \Delta H_{sys} \quad (3.8)$$

$$q_{Load} = \frac{Q_{Load}}{1h} \quad (3.9)$$

A few more calculations were required to accurately simulate the building's transient energy balance. In chapter 2 a steady state energy balance was used, and thus the thermal mass of the system was negligible. In a transient analysis, the thermal mass of the system dictates how quickly a system will respond to energy input with changes in temperature. For this reason, the building's thermal mass  $C_B$  was calculated from the geometry and material properties specific to the home's construction. This adjustability allowed the model to be used for a variety of building applications, provided the input values were known or could be estimated. For the high efficiency home used in this model, the thermal mass was calculated ignoring the effects of internal furnishings or occupants.

$$C_B = C_{floor} + C_{framing} + C_{insulation} + C_{drywall} + C_{plywood} + C_{cladding} + C_{windows} \quad (3.10)$$

This thermal capacity included any construction materials with a significant thermal mass. These materials included the wall and roof framing, insulation, sheathing, siding, and drywall, as well as the windows and the concrete slab. The individual heat capacities for each component were calculated as shown in (3.11)(3.17, denoted by  $C \left( \frac{Wh}{K} \right)$ ). Note that in (74), a scaling factor  $ST$  was applied to account for 16" stud spacing of the 2" x 12" wood framing.

Here,  $c \left( \frac{kJ}{kg \cdot K} \right)$  denotes the specific heat capacity of the respective materials,  $\rho \left( \frac{kg}{m^3} \right)$  denotes the density,  $A (m^2)$  denotes the surface area, and  $t (m)$  denotes the thickness. The material properties used in these calculations are detailed in the nomenclature section of this thesis.

$$C_{floor} = \frac{t_{floor} \cdot \rho_{concrete} \cdot c_{concrete} \cdot A_{floor}}{\frac{3.6kJ}{Wh}} \quad (3.11)$$

$$C_{framing} = \frac{t_{wood} \cdot \rho_{wood} \cdot c_{wood} (A_{walls} + A_{roof}) ST}{\frac{3.6kJ}{Wh}} \quad (3.12)$$

$$C_{insulation} = \frac{t_{insulation} \cdot \rho_{insulation} \cdot c_{insulation} (A_{roof} + A_{walls})}{\frac{3.6kJ}{Wh}} \quad (3.13)$$

$$C_{drywall} = \frac{t_{gypsum} \cdot \rho_{gypsum} \cdot c_{gypsum} (A_{walls} + A_{floor})}{\frac{3.6kJ}{Wh}} \quad (3.14)$$

$$C_{plywood} = \frac{t_{plywood} \cdot \rho_{plywood} \cdot c_{plywood} (A_{walls} + A_{roof})}{\frac{3.6kJ}{Wh}} \quad (3.15)$$

$$C_{cladding} = \frac{t_{cladding} \cdot \rho_{cladding} \cdot c_{cladding} (A_{walls} + A_{roof})}{\frac{3.6kJ}{Wh}} \quad (3.16)$$

$$C_{windows} = \frac{t_{glass} \cdot \rho_{glass} \cdot c_{glass} \cdot A_{windows}}{\frac{3.6kJ}{Wh}} \quad (3.17)$$

As this construction is typical for residential homes, these calculations remain applicable for various homes. If the user varied the input for the roof, wall, floor, and window areas, the building's thermal mass was calculated accordingly in the model.

After the heating and cooling load was calculated from (71), the last step was to perform the home's energy balance and calculate the new resulting inside air temperature. Although this energy input was specifically calculated to bring the inside temperature back to exactly 70°F, the exact temperature was calculated every hour to avoid any error propagation. The new inside temperature was calculated at the end of the loop for use in calculation for the next hour as shown in equation (3.18).

$$T_{actual} = T_{actual} + \frac{Q_{Load} - Q_{Loss}}{\left( \frac{m_{air} \cdot cp_{moist}}{3600J} \right) + C_B} \quad (3.18)$$

### 3.2.2 Results

As expected, the implementation of a deadband temperature zone significantly improved the performance of the HVAC system over the year. Specifically, a large cost, energy consumption, and reduction of emissions was seen due to the natural heating and cooling of the home during the spring, summer, and fall. Only the cost-optimized model version results were considered here. After implementing the deadband temperature zone logic, the total cost of cooling and heating throughout the year was found to be \$1487.23, a 30.58% reduction from the previous cost of \$2142.19. The new  $CO_2$  emissions totaled to 2420kg, a 30.05% reduction from the previous 3459.53kg of emissions. The numerical results are shown in Table 3.1 while the system utilization throughout the year is shown in Figure 3.2.

Table 3.1: HVAC System Performance (Deadband Controls, Cost-Optimized)

	WSHP	ASHP	Boiler	Combined
<b>Yearly Cost (\$)</b>	619.08	782.23	85.92	1,487.23
<b>Yearly CO2 Output (Kg)</b>	975.88	1,249.15	194.99	2,420.02
<b>Average COP</b>	4.40	4.32	N/A	
<b>Energy Consumption</b>	2,502.25 (kWh)	3,202.94 (kWh)	19.01 (gal)	
<b>% Space Heating provided</b>	43%	53%	4%	
<b>% Air Conditioning Provided</b>	100%	0%	0%	

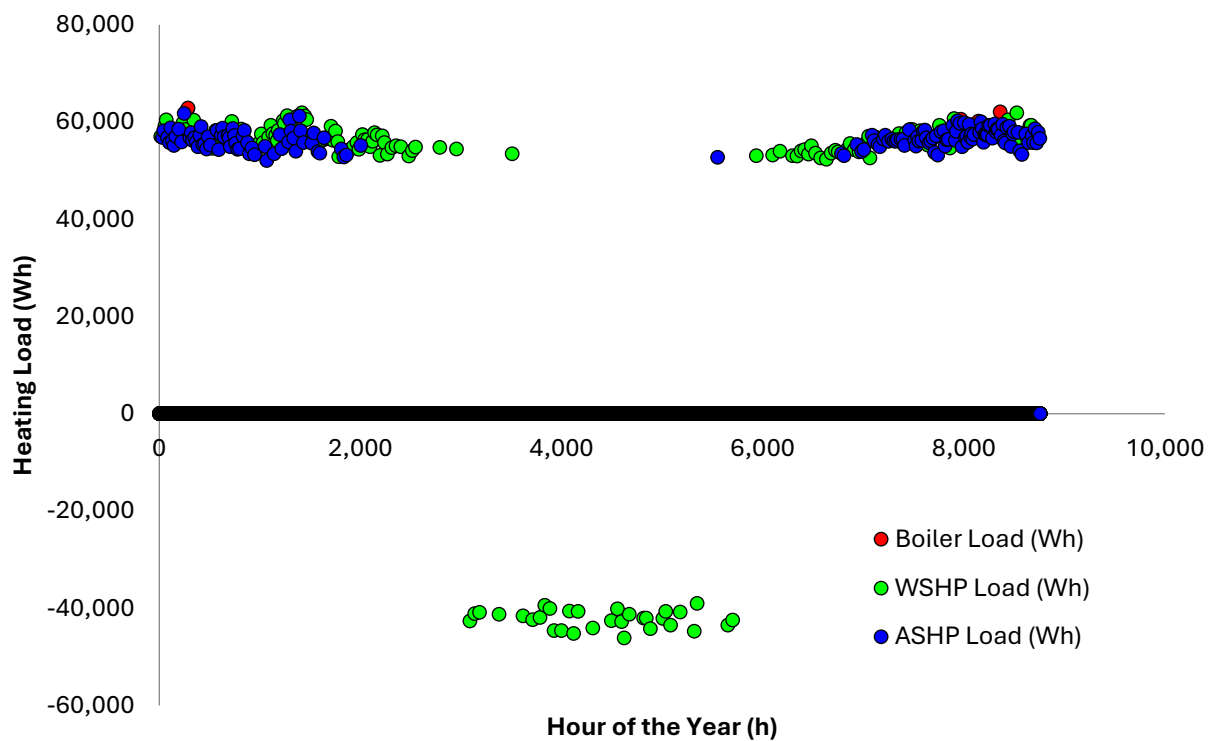


Figure 3.2: HVAC System Usage (Deadband Controls, Cost-Optimized)

### **3.2.3 Discussion**

Along with the decreases seen in cost, emissions, and energy consumption, there were some other notable resulting changes from the deadband implementation. The first observation noted here is a trade-off between HVAC operational frequency and load size. While the HVAC system activity frequency had decreased to just 10% of its former steady state activity, the system was also expected to make up all the heat loss during inactivity in the same period of one hour. This resulted in large heating loads which were problematic.

Air conditioning was taken 100% by the WSHP, eliminating the previous 18% that the ASHP provided in chapter 2. This was likely due to the infrequency at which air conditioning was needed during the cooling season. When a cooling load is assigned, another load doesn't appear for a while, giving the RSC panel time to cool down the tank temperature. This low tank temperature made the WSHP effective for providing the next cooling load.

A few critical changes from the steady state results can be seen from Figure 3.2. Since the HVAC system was only activated when the inside temperature leaves the deadband range, the required load to heat the building back up to the setpoint temperature was similar all year round. The total load varied slightly, depending on how far the inside air temperature dropped outside of the deadband, and how great the ambient heat loss/gain from the home was during the heating/cooling cycle. Since the HVAC system remained inactive inside of the deadband, the number of operational hours significantly decreased. Even in the heart of winter with ambient temperatures as cold as -36°F, the HVAC system remained inactive for a minimum of 8 hours at a time. This inactivity can be attributed to the home's excellent insulation rating and significant thermal mass. In the summertime, the HVAC system remained inactive for over a week at a time, depending on the extremity of ambient temperature swings. Isolating each component, a clearer representation of each system's contribution can be seen in Figure 3.3, Figure 3.4, and Figure 3.5.

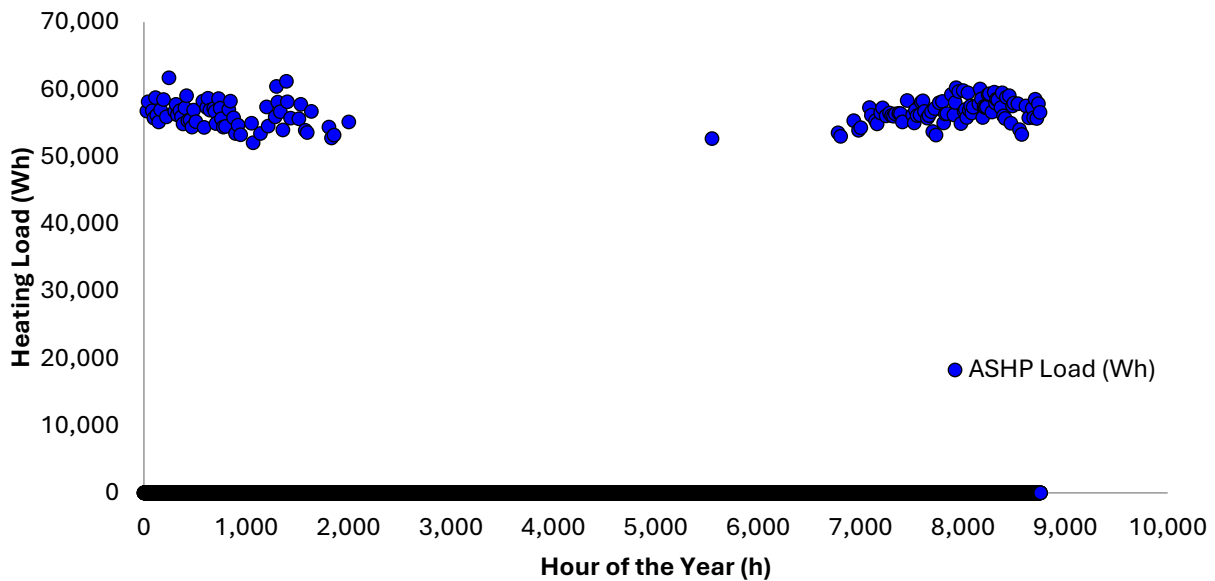


Figure 3.3: ASHP Usage (Deadband Controls, Cost-Optimized)

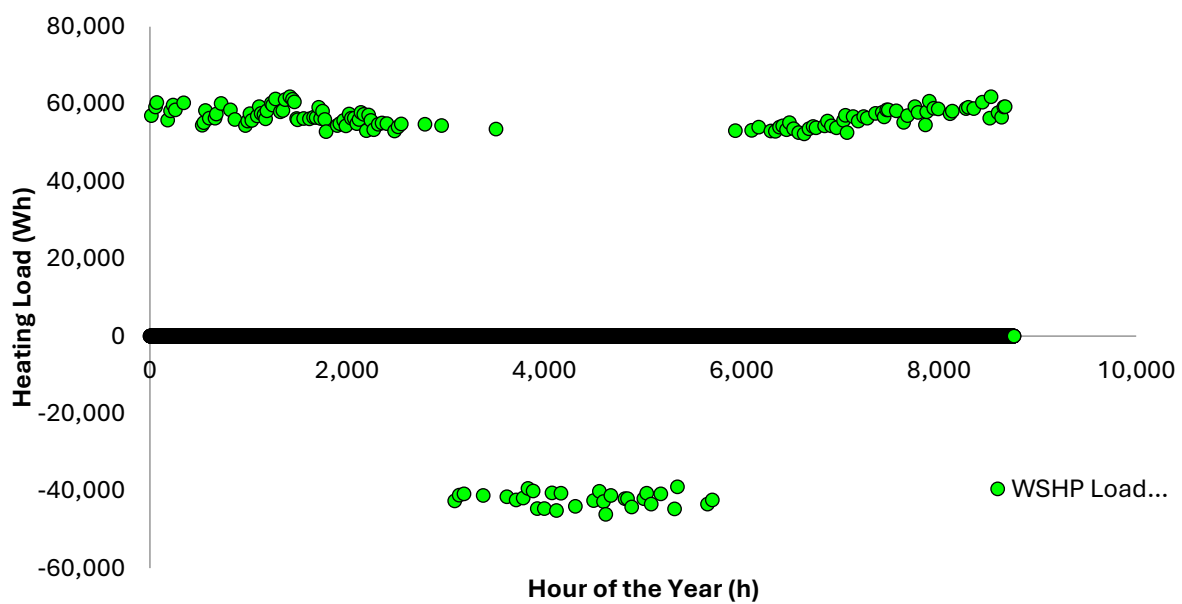


Figure 3.4: WSHP Usage (Deadband Controls, Cost-Optimized)

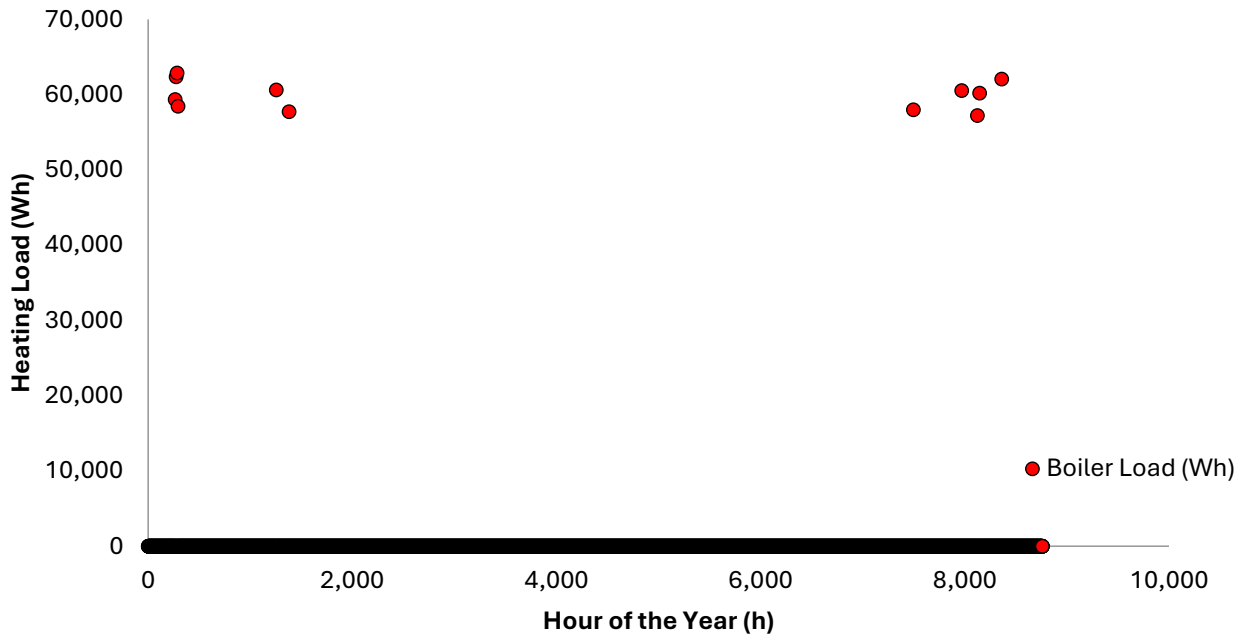


Figure 3.5: Boiler Usage (Deadband Controls, Cost-Optimized)

Although this control system allowed for less total energy usage and a lower cost for the user, it also necessitated a significantly more powerful HVAC system. The heating loads shown in Figure 3.2 are anywhere from 50-60kW, while the cooling loads are around 40kW. This is approximately a tenfold increase on the average HVAC loads from the previous steady state logic of chapter 2. There are multiple reasons for this substantial increase in heating load, both of which are addressed in this thesis. The deadband temperature control functioned as expected, allowing the HVAC system to remain inactive for extended periods of time. However, once the inside temperature fell outside of the deadband, the heating load required to heat the home back up to setpoint was massive. This massive load resulted from the cumulative loss or gain of heat during the hours of inactivity, eventually needing to be met all at once.

The other reason for this extremely large load is that the control system was designed to provide enough heat to return the home to 70°F in just one hour. After remaining inactive typically for around 10 hours in the winter, the HVAC system was expected to fully recover all the cumulatively lost heat in just one hour, thus the increase tenfold. In practice, sizing an

HVAC system to meet heating/cooling needs in one hour is unnecessary and will result in inefficiencies and additional system wear and tear. From this analysis, it was concluded that further controls were required to spread this large heating load out over a longer period.

The temperatures of the thermal tank and ambient air shown in Figure 3.6 were also compared to the steady state version.

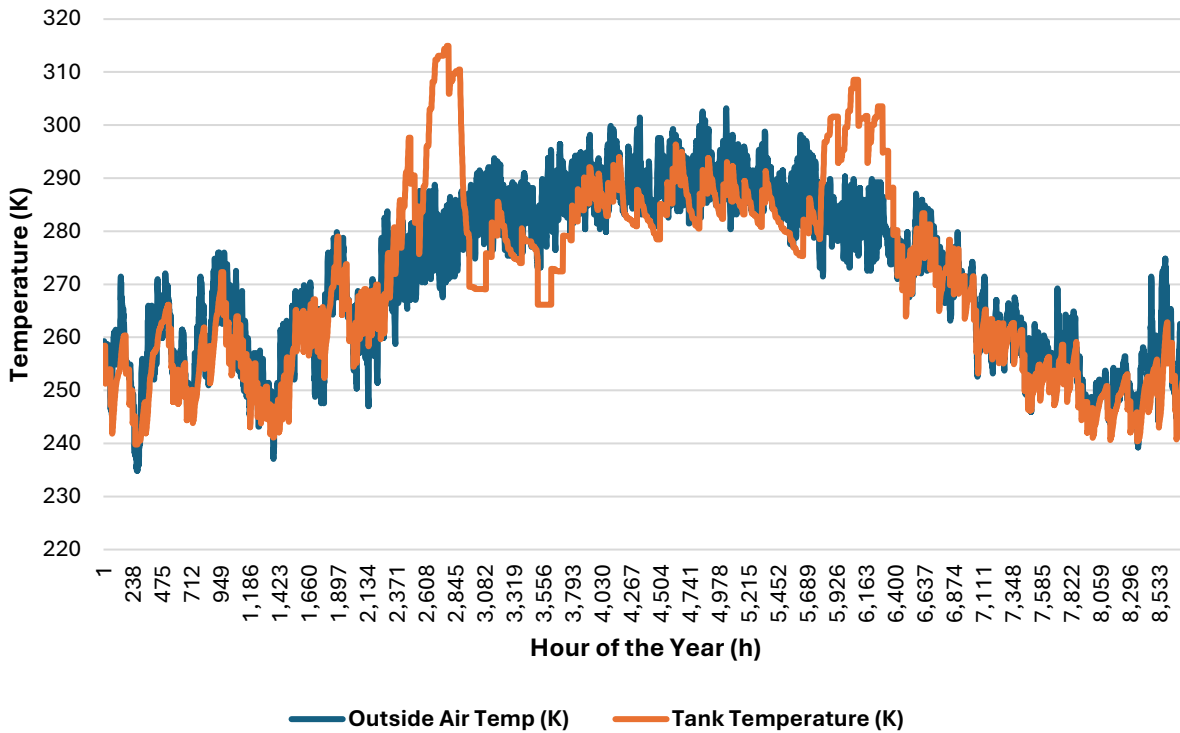
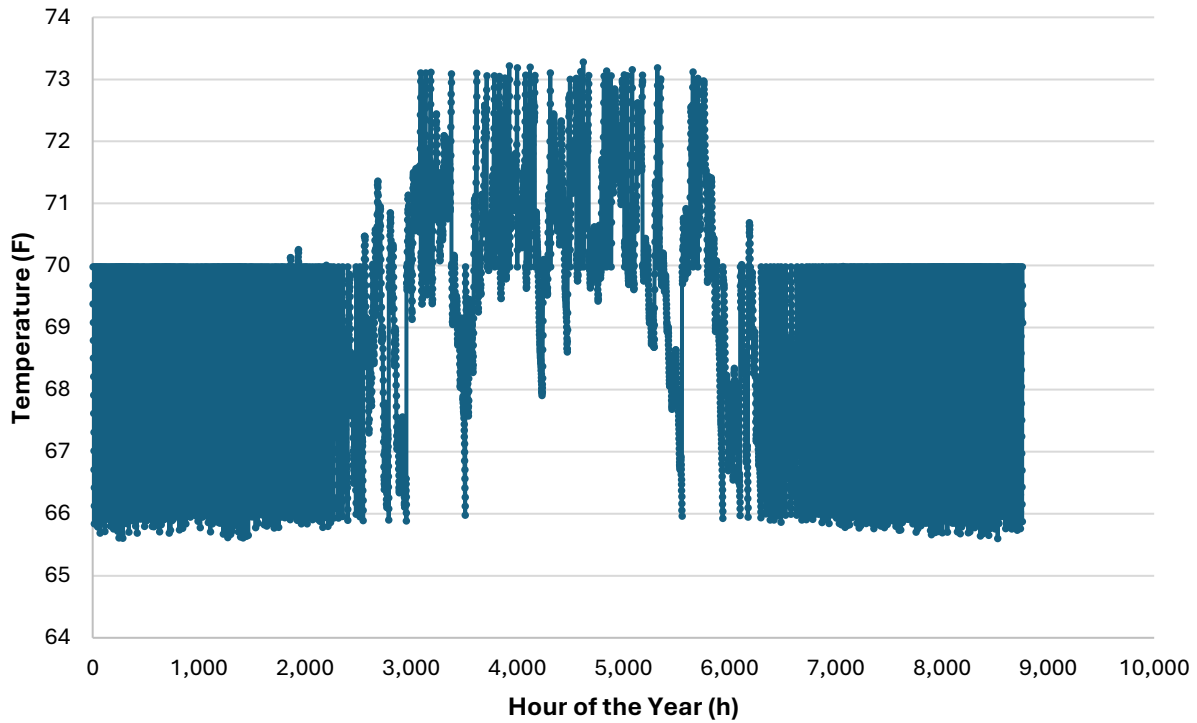


Figure 3.6: Thermal Tank Versus Ambient Temperature (Deadband Controls, Cost-Optimized)

Here, higher peaks in the thermal tank temperature were observed because of the deadband temperature controls. Reaching as high as 315K in the shoulder seasons, there was a 10K difference between the tank temperatures from the steady state model in Figure 2.17. Although the same trends were clearly identified, the deviation from the ambient air temperature was larger in the transient analysis. This greater deviation explains the WSHP's increased COP shown in Table 3.1.

Another interesting phenomenon can be seen by plotting the inside air temperature plotted against time, shown in Figure 3.7.



**Figure 3.7: Inside Air Temperature Versus Time (Deadband Controls, Cost-Optimized)**

From Figure 3.7, the inside temperature simply oscillated between 70°F and 66°F during the winter months. However, from March 12th (hour 1700) to October 20<sup>th</sup> (hour 6300) there was a clear oscillation between temperatures above and below the setpoint. This oscillation represents the times when the ambient cooling and heating throughout the day naturally regulates the temperature of the home, demonstrating the energy saving effect of the deadband temperature control implementation.

### **3.3 Variable Load Distribution Controls**

#### **3.3.1 Methodology**

As a result of implementing the deadband temperature zone, one significant issue arose in the model logic. Due to the infrequency of HVAC system activity the HVAC load became extremely large, reaching upwards of 60kW. This large HVAC load resulted from the system attempting to recover 8-10 hours' worth of heating or cooling in just one hour. Providing this amount of heating or cooling in just an hour is unrealistic and would require an oversized HVAC

system. A realistic solution to this problem is to break this load into manageable chunks, rather than handling it all at once. To achieve this, logic was added to convert operation at 60kW for one hour into 20kW for three hours, creating manageable heating and cooling loads.

In a realistic setting, it is appropriate for an HVAC system to heat a home by about one degree Fahrenheit per hour. Therefore, it would be appropriate for the HVAC system to take 3–4 hours to heat a home from 66°F back up to 70°F. In deadband control study, the highest HVAC loads experienced were just over 60kW. At this rate, an evenly distributed load of about 20kW would heat the home back up to setpoint in 3–4 hours. For this reason, 20kW was chosen to be the maximum allowable heating load for a single hour. Then, logic was implemented into the model distributing the calculated HVAC load over a few hours, up to 20kW per hour. When the HVAC load reached 20kW for a given hour, the script moved to the next hour and filled it with the remaining load, up to 20kW. This process continued until the heating load was distributed. This methodology allowed for variable load distribution, where small heating loads were provided in just an hour, and larger loads distributed over a longer period, up to 4 hours. It is important to note here that these numerical values were specific to the home used in this model. If a new home were used in the model, the maximum heating load would need to be calculated and distributed accordingly.

### **3.3.2 Results**

As a result of implementing variable load distribution in the model, a slight increase was found in the yearly cost, energy consumption, and  $CO_2$  emissions. The yearly cost increased 2.4% from the previous \$1487.23 to \$1523.59, and the yearly emissions increased from the previous 2420kg to 2500kg. Interestingly, the yearly heating load decreased from the previous 16.39MWh to 16.31MWh, and the cooling load decreased from 1.309MW to 1.307MW. While the total electricity usage from both heat pumps only increased by about 1kWh, the WSHP's consumption decreased significantly while the ASHP's consumption increased. Additionally, the boiler's fuel usage increased by about 7.5 gallons. The numerical results from implementing variable load distribution are shown in Table 3.2.

Table 3.2: HVAC System Performance (Variable Load Distribution Controls, Cost-Optimized)

	WSHP	ASHP	Boiler	Combined
<b>Yearly Cost (\$)</b>	556.05	845.99	121.56	1,523.59
<b>Yearly CO2 Output (Kg)</b>	875.92	1,349.50	274.58	2,500.00
<b>Average COP</b>	4.65	4.70	N/A	
<b>Energy Consumption</b>	2,245.95 (kWh)	3,460.25 (kWh)	26.46 (gal)	
<b>% Space Heating provided</b>	37%	58%	6%	
<b>% Air Conditioning Provided</b>	100%	0%	0%	

In Figure 3.8, the HVAC load reaches a limit of 20kW. Many loads are seen in between, representing both the smaller HVAC loads as well as the leftovers from the larger loads.

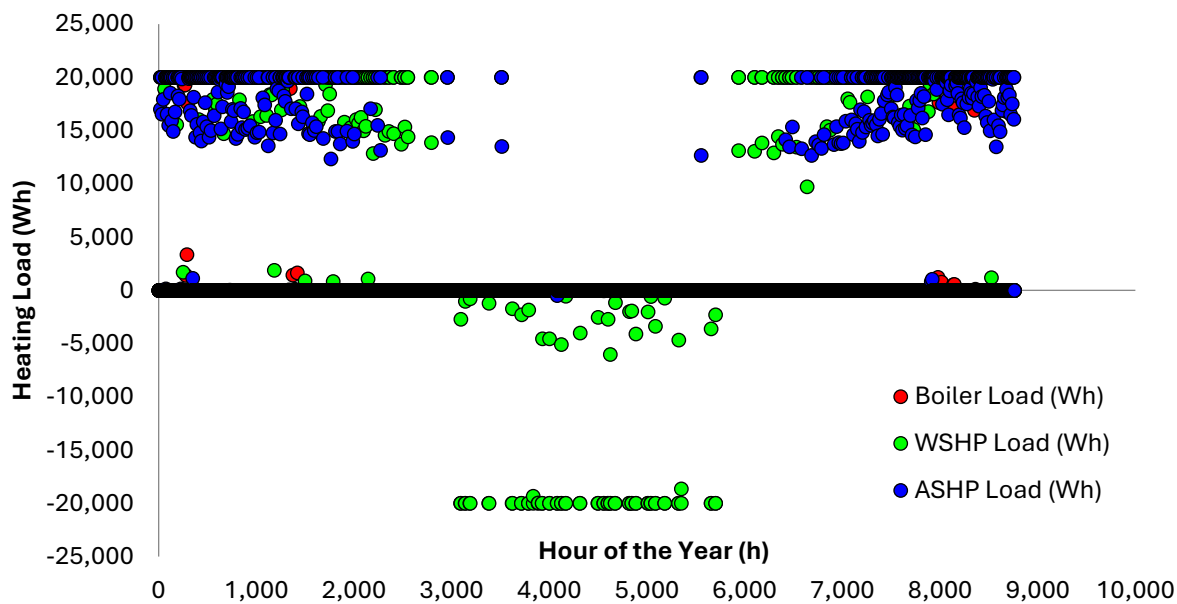


Figure 3.8: HVAC System Usage (Variable Load Distribution, Cost-Optimized)

### 3.3.3 Discussion

A few significant changes were noted with the implementation of the variable load distribution controls. Specifically, the yearly heating and cooling loads decreased, while the yearly cost, energy consumption, and  $CO_2$  emissions increased. These results required further investigation, as they appeared counterintuitive.

While there was not a major change in the yearly heating and cooling loads, there was a slight decrease in both that required an explanation. These values decreased despite using the same weather data due to the changes in the home's air temperature. With the HVAC load spread out over a few hours, it took longer for the inside air temperature to return to setpoint from HVAC activation. As a result, the home's air temperature was closer to the ambient temperature for longer periods of time than before. This phenomenon resulted in decreased heat loss from the home throughout the year, which in turn created less demand from the HVAC system. This effect can be seen in Figure 3.9.

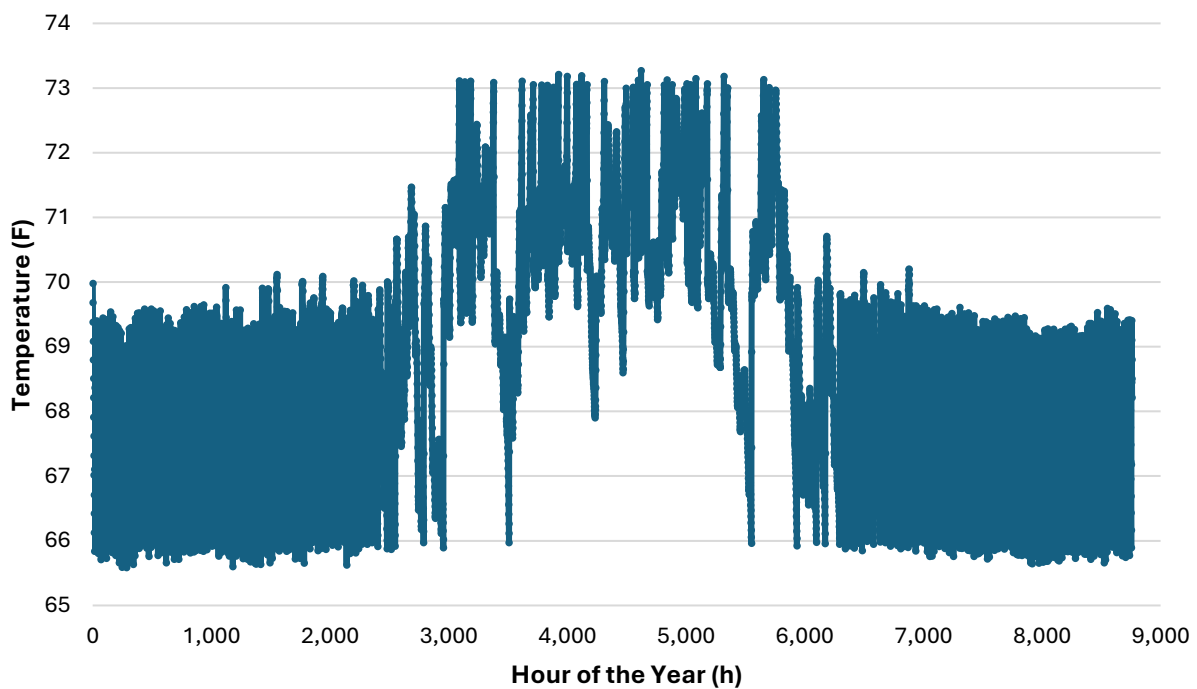


Figure 3.9: Inside Air Temperature Versus Time (Variable Load Distribution, Cost-Optimized)

While there were only a few small changes in the shape of Figure 3.9 compared to Figure 3.7, there was one significant observation worth noting. In Figure 3.7, there was a nearly solid line at 70°F, indicating that each time the HVAC system kicked on the inside temperature returned to exactly 70°F. With variable load distribution, the rate of heat being supplied by the HVAC system was smaller than before relative to the rate of heat loss from the home. Due to this opposition, the heat supplied often fell slightly short of returning the home to 70°F, often falling around 69.5F. This created natural energy savings while maintaining an ideal temperature for the home.

In the previous deadband controls section, the heating load was only distributed over one hour. As a result, the model logic only chose a system to provide that heating load once, since a system was chosen only once per hour. Due to the latency period from the deadband temperature implementation, there was often ample time for the thermal tank's temperature to balance before the next heating load was allocated. As a result of this, the calculated COP was often high for the WSHP after a period of inactivity. However, because the tank's temperature was not checked throughout the heating cycle, this calculated COP was not accurate throughout the heating cycle. In the new model version, the HVAC load was often distributed over 3-4 hours. As the thermal tank temperature and each system's COP were recalculated every hour, they were effectively recalculated and checked 3-4 times during each larger heating cycle. This change created a greater resolution in COP and tank temperature data relative to HVAC load data and greatly improved the accuracy of the tank's energy balance calculation. However, the WSHP's COP decreased throughout operation, which led to decreased WSHP utilization throughout the year. This decrease in COP also resulted in losses to overall system performance yielding higher cost, emissions, and energy consumption. While these consequences were not ideal, they were a telltale sign of model improvement. With these changes in place, the model was completely representative of a physical system to a high level of accuracy.

## **Chapter 4: System Selection and Optimization Study**

### **4.1 Overview**

In this section the operation of the proposed HSHP system was modeled with specified commercially available HVAC equipment. This study abandoned previously formulated COP calculations from Magrath [8] and from Samuel et al. [43], and implemented performance trends corresponding to commercially available heat pump and boiler systems. With these components modeled, an optimization technique was performed to select the most appropriate sizes for the RSC, solar collector, and thermal tank. In this technique, the size of one component was varied while the other component sizes were held constant. This optimization allowed the identification of optimal sizes for system performance. Following this component optimization, commercially available equipment was chosen according to the optimal sizes.

### **4.2 System Selection**

#### **4.2.1 Methodology**

The HVAC design process began by determining the minimum requirements of the system. According to the ASHRAE standards, Fairbanks has a cooling design temperature of 78°F and a heating design temperature of -40°F [49]. This means that to meet the ASHRAE design standard, a home's HVAC system must be able to fully meet the heating and cooling loads at these temperatures. In the model, the rate of heat loss of the home was found to be 7.06kW at -37°F. However, with the variable load distribution and deadband controls in place, a consistent load of 20kW was expected throughout the year, as shown in Figure 3.8. Since this 20kW load was much greater than the 7.06kW heat loss at the design temperature, 20kW was chosen as a minimum requirement for the HVAC system. This allowed for effective use of deadband controls to save energy throughout the year.

Since every configuration in this study was modeled with a backup boiler, the heat pumps were not sized to meet the required load at -40°F. However, to maximize savings, the heat pump units were sized to consistently provided most of the heat/AC throughout the year. Furthermore, the HVAC system logic was adjusted so that the boiler could supplement the heat

generated by the heat pump systems. The heat pumps were allowed to operate at full capacity even when they could not meet the heating load, and the boiler supplied the remaining required load. Thus, the boiler would be allowed to run simultaneously with a heat pump to provide the required heat. To achieve this, a section of code was implemented in the model which calculated the heating capacity of the heat pump units. With the heating capacity calculated, the most efficient system operated at full capacity, and any remaining heating load was delegated to the boiler. In addition to these changes in logic, product data for the specified equipment was implemented in the model to accurately calculate the COP for cooling and heating.

In Fairbanks, the ratio of heating requirements to cooling requirements is roughly 12 to 1 according to data generated by the model. The extreme winter temperatures can become dangerous when HVAC systems cannot provide enough heat. In the summertime however, the highest temperature experienced in the model is 85°F, and the AC design temperature is 78°F. However, Fairbanks homes typically rely solely on ventilation to regulate temperature in the summertime. The summertime high temperature is moderate in Fairbanks relative to other communities in the United States, and there is not a crucial need for air conditioning. For these reasons, all HVAC components were designed for heating provision. Thus, the cooling capacity of the HSHP system were not specifically designed to constantly provide 20kW. In the case where the cooling load exceeds the cooling capacity of the AC system, it was assumed that the AC system will continue operating slightly longer to meet the cooling needs, and the effects from this longer runtime will be negligible. In summary, it was assumed that the cooling capacity of the AC system was sufficient, and it was not considered in this analysis.

A commercially available boiler unit was selected which could provide a minimum 20kW of usable heat. The boiler in Figure 4.1 from Weil-McLain is a standard issue 75,000 BTU/hr (21.98kW) “high-efficiency cast iron boiler”, listed for sale from [50] for \$2432.07. The recommended burner for use with this boiler is the GO-2 Becket Oil Burner shown in Figure 4.1, which is also listed for sale from [51] for \$650.96. The system yields a combined efficiency of 86.7%, which was similar to that used in previous model calculations [52].



Figure 4.1: Weil-McLain Boiler and GO-2 Becket Oil Burner from Supply House [51], [50]

These units are affordable, available, and exceed the heating load requirement. This specific boiler model was chosen to represent the residential industry standard in Fairbanks, due to its low price and availability. This was the boiler model used in this study, and the boiler efficiency was implemented in all proceeding calculations.

For the ASHP, Arctic Heat Pump's model 050ZA/BE shown in Figure 4.3 was chosen due to its excellent heating performance at extreme temperatures. The performance data for this model shows that it can generate 22.068kW of heating power in ideal conditions [44]. According to Sam Thornton, PhD. with Arctic Heat Pumps, the chosen ASHP unit costs \$7,747, and one 80-gallon buffer tank costs \$2,578 (S. Thornton, personal communication, February 4<sup>th</sup>, 2025). Additionally, a circulating pump which costs \$595 was required for both the boiler ASHP,

and the ASHP required valves and fittings that total to \$400 (S. Thornton, personal communication, February 4<sup>th</sup>, 2025). The published performance data for 050ZA/BE has been plotted and fit with a trendline in Figure 4.2 assuming a water outlet temperature of 50°C (S. Thornton, personal communication, February 4<sup>th</sup>, 2025), [44].

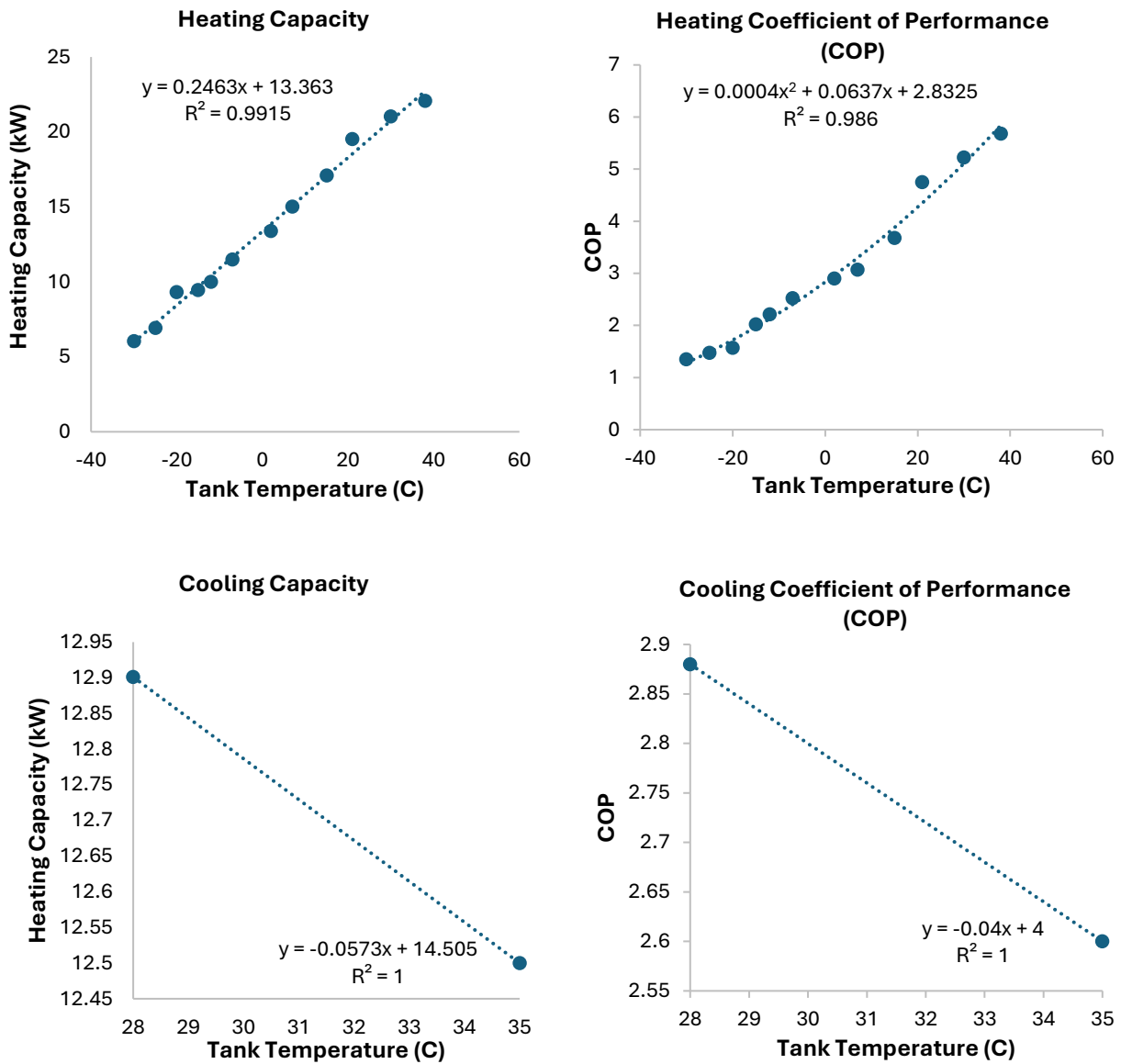


Figure 4.2: ASHP Model 050ZA/BE Performance Data

In the model, the ASHP's COP and heating capacity calculations were updated to follow the trends shown in Figure 4.2, excluding the cooling capacity. The 050ZA/BE ASHP and buffer tank from Arctic Heat Pumps are shown in Figure 4.3.



Figure 4.3: ASHP 050ZA/BE and Buffer Tank from Arctic Heat Pumps [44]

For the WSHP, the Bosch Model CE Residential Geothermal Heat Pump was selected as shown in Figure 4.4. The 5-ton unit (model CE061) can generate 29.94kW of heat at a thermal reservoir temperature of 80°F [53]. The product data for heating and cooling are plotted in Figure 4.5 for CE061 [53], using an inlet air temperature of 70°F for heating and 75°F for cooling. The Bosch WSHP model CE061 is shown in Figure 4.4.



Figure 4.4: Bosch WSHP Model CE061 [53]

The Bosch CE061 water to air heat pump is available through Ferguson, who offers it at a price of \$24,265. From the performance graphs for the ASHP and WSHP, the published data does not cover the full temperature range that is experienced in the model. For this reason, conditions were implemented which determined the values of COP and heating capacity outside of the known ranges. Here, a substantial improvement was made from the previous logic. In previous model versions, if the temperature exceeded the known range, the COP was calculated at the limit of the range. For example, if the ambient temperature was 27°C, then  $COP_{ASHP}$  was calculated at 13°C. However, this was not always a realistic assumption. For example, if  $COP_{ASHP}$  was taken at its lower limit of -35°C for heating when the actual temperature was -40°C, this assumed a value that is not realistic. Often the heat pump may not be operational outside of its temperature range, which is why extrapolation should be avoided.

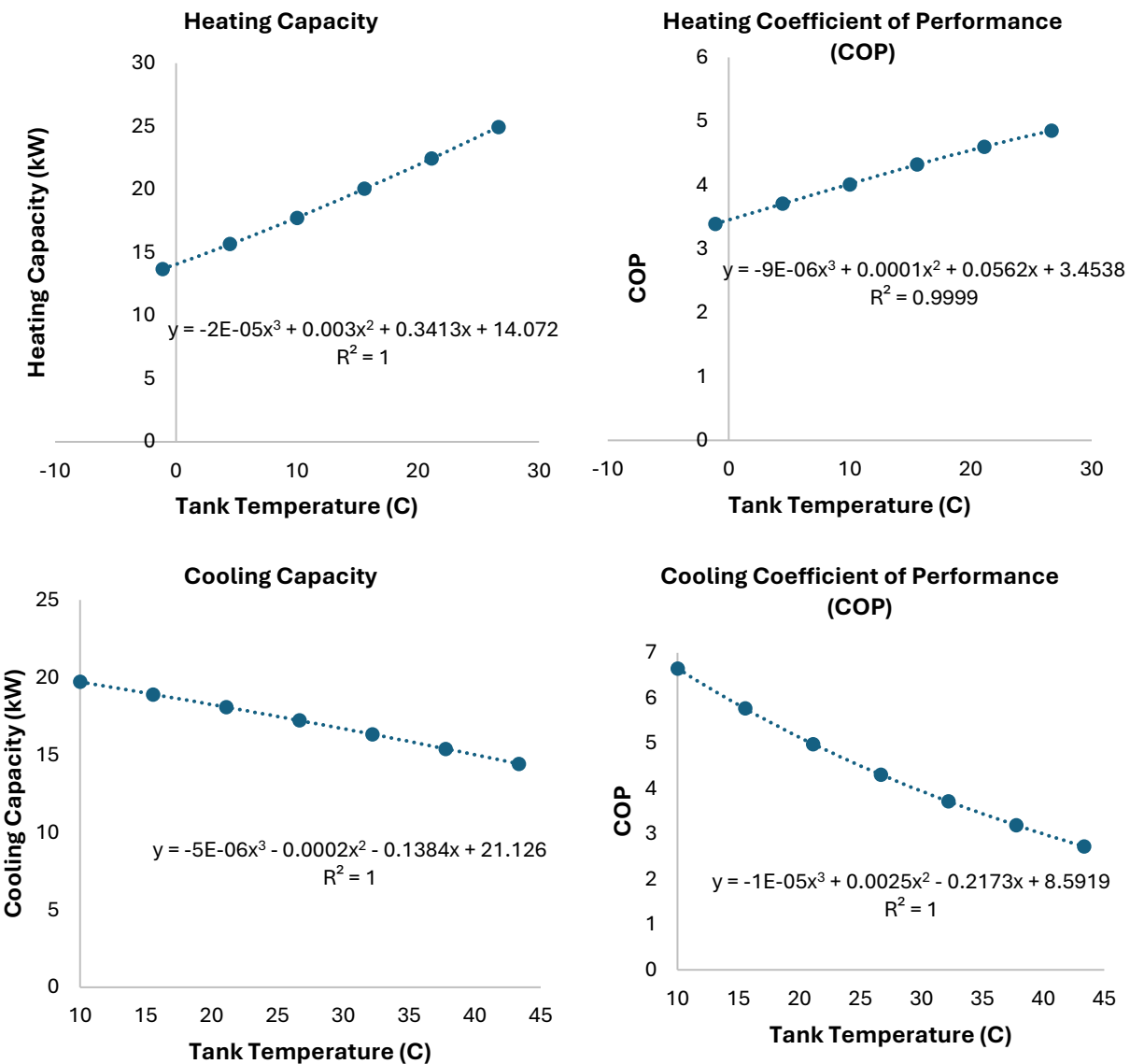


Figure 4.5: Bosch WSHP Model CE061 Performance Data

Aside from operational limit concerns, this method assumed a higher value than even extrapolation would suggest. Simply put, a more conservative estimation was needed at this level of detail. For these reasons, a new method of calculation beyond the known limits was taken. In the case that taking a value at its limit resulted in a bad assumption, that value was adjusted to be taken at its minimum. For heating, the COP was taken to be 1 and the heating capacity to be 0 when the temperature is below the known range. This method also reflected the “non-operational” default assumptions when a temperature dropped below the limit. Similarly for cooling, the COP was taken to be 1 when the temperature was above the allowable

range. These assumptions ensured that a conservative approach was taken to calculating system performance.

A condition was also implemented on the opposite boundary of the temperature range. This time, increased performance was expected when the temperature reaches outside of the boundary. However, since data was not available outside the boundary, it was more appropriate in this case to take the value at its limit rather than extrapolate. Here, COP and heating capacity were taken at the limit in heating mode when the temperature exceeded the upper boundary, and in cooling mode when the temperature dropped below the boundary (although cooling capacity was not considered in this analysis). This again ensured that a conservative approach was taken during performance calculations, improving on the previous methodology.

#### **4.2.2 Results – Cost-Optimized Model**

Several changes were made from the analyses in chapter 3 which have resulted in drastic differences in system performance. First, the heating capacity of the ASHP and WSHP is calculated and taken into consideration when distributing the heating load. Knowing that the heat pump systems are not designed to provide heat at the design temperatures, a backup boiler was selected and installed to run simultaneously with these systems and supplement their heating power. Additionally, product data for the selected and appropriately sized ASHP and WSHP was used to curve fit equations to calculate the heating and cooling COP, imitating the chosen equipment. Furthermore, a more conservative approach was taken for calculating performance metrics such as COP and heating capacity for temperatures outside the known limits. With these changes in place, the yearly cost of heating and cooling rose 29.14% from \$1523.59 to \$1967.57, while the total heating and cooling loads remained the same. The amount of space heating provided by the boiler rose from 6% to 66%, while the WSHP and ASHP dove from 37% to 16% and from 58% to 18%, respectively. The WSHP retained full provision of air conditioning. Notably the boiler fuel usage increased by 276.8 gallons, and the yearly  $CO_2$  output increased by a whopping 60% from 2500kg to 4067.19kg. The boiler itself produced 77.74% of the total  $CO_2$  emissions by mass. The results are shown in Table 4.1 for the

cost-optimized model version, while the typical performance plots are shown in Figure 4.6, Figure 4.7, and Figure 4.8.

Table 4.1: HVAC System Performance (System Selection, Cost-Optimized)

	WSHP	ASHP	Boiler	Combined
<b>Yearly Cost (\$)</b>	246.42	326.13	1,395.01	1,967.57
<b>Yearly CO2 Output (Kg)</b>	380.26	525.17	3,161.73	4,067.19
<b>Average COP</b>	2.79	2.82	N/A	
<b>Energy Consumption</b>	975.04 (kWh)	1,346.58 (kWh)	303.23 (gal)	
<b>% Space Heating provided</b>	16%	18%	66%	
<b>% Air Conditioning Provided</b>	100%	0%	0%	

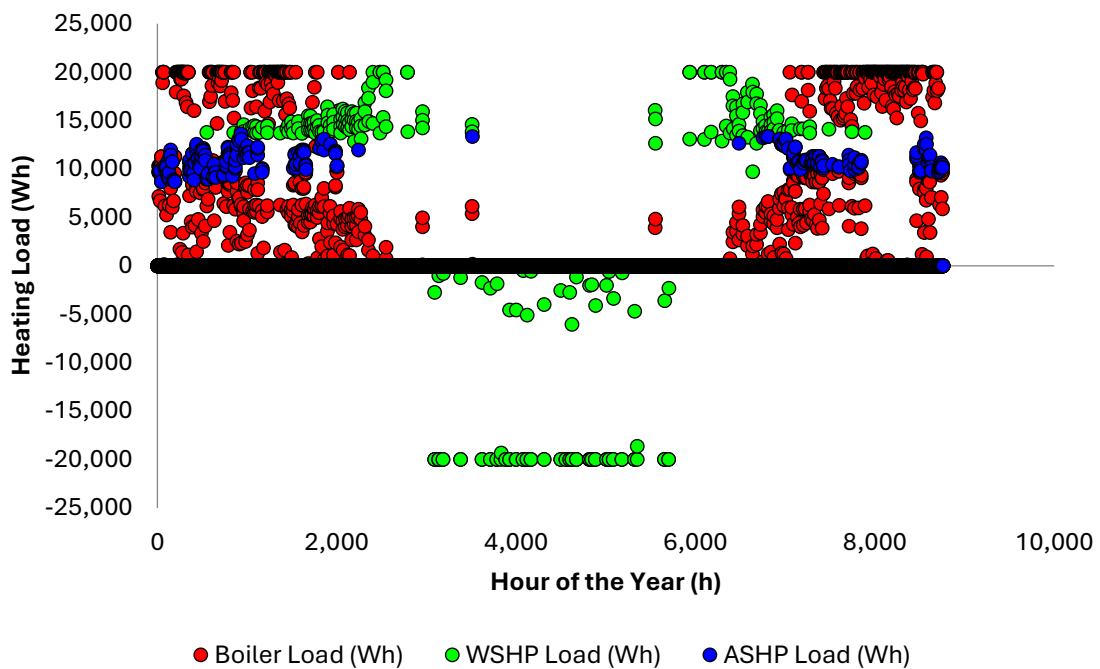


Figure 4.6: HVAC System Usage (System Selection, Cost-Optimized)

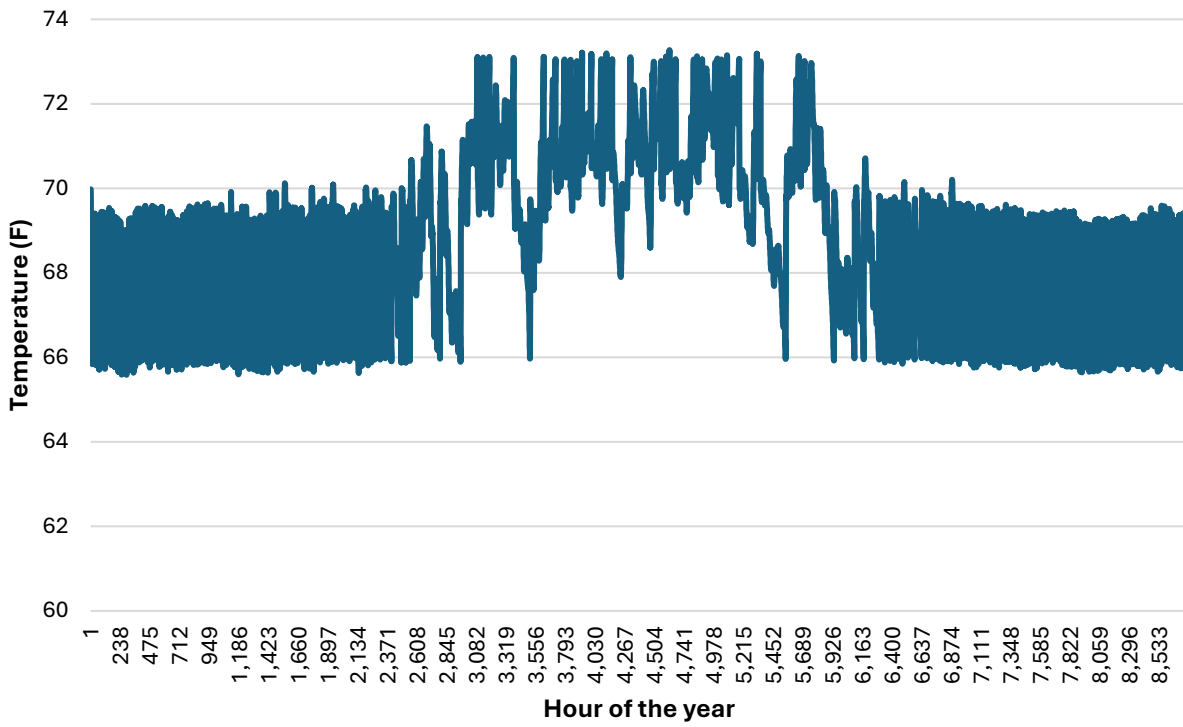


Figure 4.7: Inside Air Temperature (System Selection, Cost-Optimized)

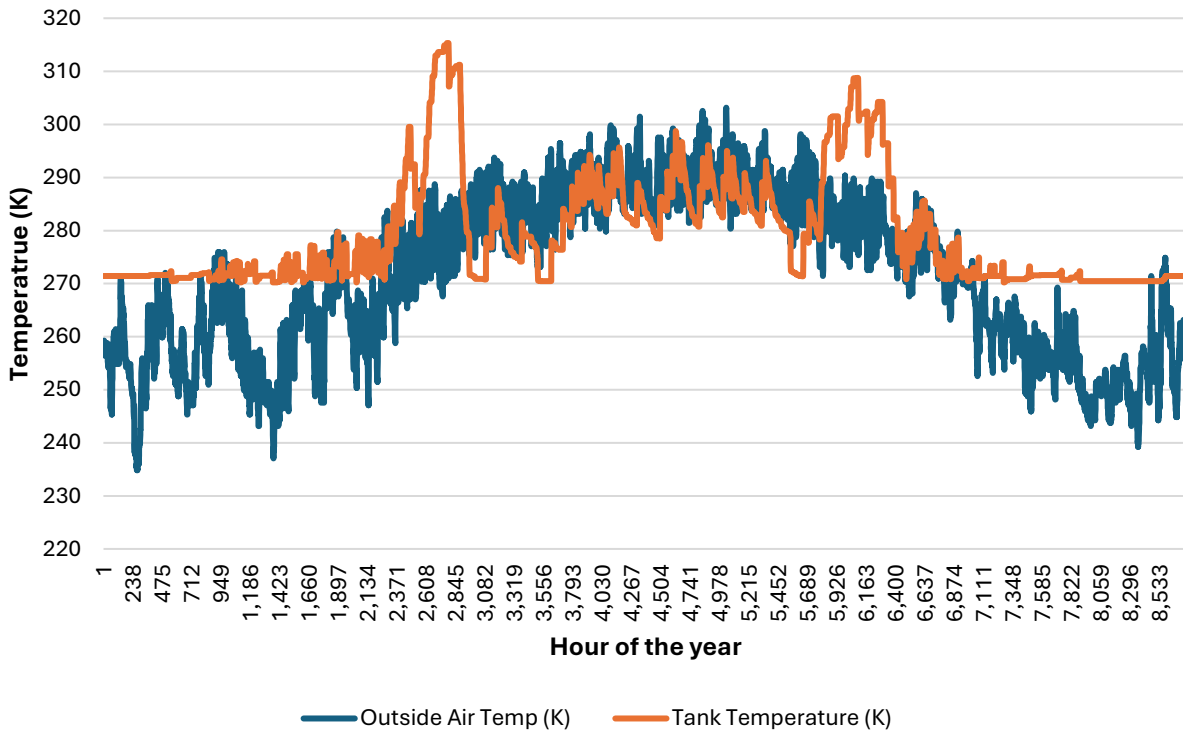


Figure 4.8: Thermal Tank Versus Ambient Temperature (System Selection, Cost-Optimized)

It's worth noting here that the initial tank temperature was set to match the converging tank temperature at the end of the year of 271.45K.

#### 4.2.3 Results – Emissions-Optimized Model

With the large increase in boiler utilization from the previous model version, it again becomes important to analyze separate results for optimization by cost versus by emissions. Even when the boiler is the most cost-efficient system, it will often give the highest emission of  $CO_2$  and will therefore be chosen less in the emissions-optimized version. For this reason, the emissions-optimized results must again be considered in analysis. The emissions-optimized results are shown in Table 4.2.

Table 4.2: HVAC System Performance (System Selection, Emissions-Optimized)

	WSHP	ASHP	Boiler	Combined
<b>Yearly Cost (\$)</b>	246.42	785.99	1021.19	2053.60
<b>Yearly CO2 Output</b>				
(Kg)	380.26	1255.03	2307.06	3942.38
<b>Average COP</b>	2.79	2.82	N/A	
<b>Energy Consumption</b>	975.04 (kWh)	3218.02 (kWh)	219.63 (gal)	
<b>% Space Heating</b>				
<b>provided</b>	16%	36%	48%	
<b>% Air Conditioning</b>				
<b>Provided</b>	100%	0%	0%	

Here, the emissions-optimized version results in Table 4.2 can be compared to the cost-optimized results shown in the last section. From switching the optimization criteria, the yearly cost increased 4.37% from \$1967.57 to \$2053.60. On the other hand, the yearly  $CO_2$  emissions decreased 3.07% from 4067.19 to 3942.38kg. The space heating provided by the boiler decreased from 66% to 48%, while the space heating provided by the ASHP increased from 18% to 36%. The total energy associated with heating and cooling remained unchanged, as well as

the heating and cooling provisions by the WSHP. Yearly electricity consumption increased 86.1% from 2321.62kWh to 4193.05kWh, while the yearly heating oil consumption decreased 27.57% from 303.23 gallons to 219.63 gallons. The average COP of the ASHP and WSHP remained unchanged. The system utilization plot is shown in Figure 4.9 for the emissions-optimized model. No significant changes in the thermal tank temperature and inside air temperature plots were noted from the cost-optimized results, thus those plots were omitted in this section.

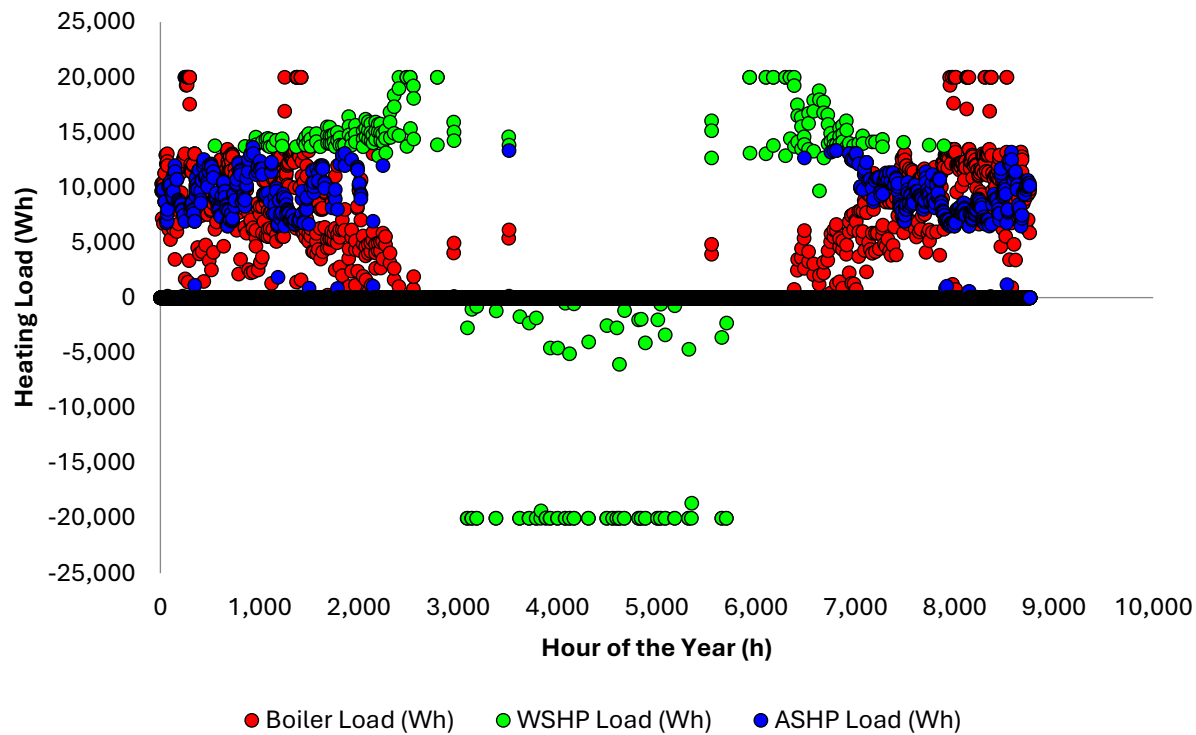


Figure 4.9: HVAC System Usage (System Selection, Emissions-Optimized)

#### 4.2.4 Discussion

By selecting real HVAC equipment, implementing conservative performance calculations, and allowing for supplemental boiler heating, some large-scale changes can be seen from the previous model version from the variable load distribution section. The most notable change is the increase in boiler utilization, from 6% to 66% in the cost-optimized version. This can be clearly seen in the utilization graphs, marked by a sea of red dots in the wintertime. This increased utilization is the result of a combination of changes in the model.

The main cause of increased boiler usage is the consideration of the heating capacity in ASHP and WSHP heating calculations. In the previous model, it was assumed that the heat pump systems were powerful enough to generate the required heating load and only considered the cost and emissions efficiencies of each system. Now taking the heating capacity into account, there is a massive drop in heat pump utilization in the wintertime due to the extreme temperatures. Although these heat pump systems were sized appropriately for the home, they clearly struggle to provide a significant heating capacity during the wintertime. This insufficiency results in, at best, the boiler supplementing the heat pumps to meet the load requirement. In addition to this supplementation, it is also clear from the cost-optimized utilization graph that the boiler is assigned the full heating load for a significant portion of the winter. To receive these assigned full heating loads of 20kW, the boiler must be chosen as the most cost-effective option. In past scenarios, the boiler was only chosen as the most efficient system during extreme winter temperatures close to -35°F. With the product data from the chosen equipment used to calculate COP, the average COP values have dropped significantly. As COP declines, the cost of operating the heat pumps increases, and the boiler becomes attractive. Furthermore, the more conservative approach taken to calculate COP and heating capacity beyond the known data contributes to the boiler's increased utilization. Now, the ASHP and WSHP are less tolerant of extreme temperatures, reaching an assumed COP of 1 and heating capacity of 0 when the temperature lands outside of the acceptable range. Since the range of allowable temperatures has changed, and the calculation of the performance metrics outside of the values has become more conservative, the boiler has become increasingly preferable to the heat pump systems.

While this increased utilization of the boiler leads to a higher yearly cost and  $CO_2$  output, it is also a telltale sign of a realistic scenario. This final model version most closely represents the physical components, modeling them accurately. While it is possible to increase the ASHP or WSHP utilization by using a larger unit, upsizing these units is costly and typically provides only a marginal benefit at colder temperatures. Rather than oversizing the heat pump unit, one method to increase utilization is to install an additional heat pump, effectively

producing twice the heating capacity. This method will be explored further in the system regime study.

There are also some noticeable changes between the cost-optimized and emissions-optimized results. Most notably, many of the larger heating loads that were given to the boiler in the cost-optimized version are now divided into smaller loads shared between the boiler and ASHP. This phenomenon occurred when was boiler is not the least emissive system. The ASHP was first chosen since it produced less  $CO_2$ , but in the winter months the ASHP's heating capacity was limited. So, the ASHP took on as much heating load as possible, and the boiler provided the rest. This difference between the ASHP and the boiler being chosen as the best system is exactly the tradeoff that is expected when optimizing for emissions versus cost. At extreme temperatures, the boiler may be the most cost-effective option, but it is almost never the least emissive option. While it is ideal to minimize both cost and emissions simultaneously, modern heat pump technology has its limits. In Fairbanks, poor air quality due to boiler emissions and high space heating costs are both problems, and so each of these criteria must be evaluated and compared. In this case, choosing low cost as the design criteria leads to a total cost of \$1967.57 and 4067.19kg of  $CO_2$  emissions. Selecting low emissions as the design criteria yields a total cost of \$2053.60 and 3942.38kg of  $CO_2$  emissions. This comparison highlights the trade-off between cost and  $CO_2$  emissions for competitive fossil fuel and renewable systems. However, an additional benefit is associated with the reduction of  $PM_{2.5}$  emissions in Fairbanks resulting from the reduction of heating oil consumption. Then, optimizing emissions has a potential benefit by greatly reducing heating oil combustion, and in turn reducing air pollution at a small additional cost to the user.

Although some major differences between the cost and emissions-optimized model versions were discussed, the inside air and tank temperatures are identical. The inside air temperature has not changed since the last model version, since the heating load distribution has not changed. While the ASHP and boiler trade some heating responsibility in the cost versus emissions-optimized versions, the WSHP's behavior remains the same, which explains the similarity in the tank temperature plots. However, the tank temperature has changed significantly since the last model version. While the tank reaches similar temperatures, it was

observed that it does not follow the outside air temperature trend nearly as close as in the last version. Especially in the wintertime, there was almost no correlation between the tank temperature and the outside air temperature. This is due to the reduction in WSHP utilization in the winter, from 37% to 16% as a result of the changes in this section. In the heart of the wintertime, the WSHP no longer plays a critical role in heating. Rather, the WSHP was heavily used during the shoulder seasons, and even into early and late winter. During this period of winter inactivity, the thermal gain from the solar collector was minimal. With little heat entering or leaving the tank, the temperature remained relatively constant throughout the wintertime.

### **4.3 System Optimization**

#### **4.3.1 Methodology**

With each of the heating/cooling components selected and sized appropriately for the home, a sizing technique was performed to determine the best sizes for the RSC, solar collector, and thermal tank. To size a component, the simulation was run several times while varying the size of that component and holding the other component sizes constant, using a single variable optimization technique to search for local minima. Since the component size which minimized the total yearly cost was expected to be very large, the minimization of cost was balanced with a reasonable component size. Large components are increasingly expensive to purchase and install, which was accounted for in this process. In this sizing process, a reasonable component size which achieved significant cost savings was chosen rather than selecting the component size at local minima. It's important to note here that up until this point, the areas of both the RSC and solar collector panels have each been  $10m^2$ , and the thermal tank size has been  $5m^3$ . In this study, two of the components were held constant at these respective sizes while one component size was varied. The optimization study began by varying  $A_{sc}$ , followed by  $A_{rsc}$ , and finally  $V_{tank}$ .

#### **4.3.2 Results and Discussion**

Assuming a solar collector size of  $10m^2$  and a thermal tank size of  $5m^3$ , the model was run iteratively for RSC panel sizes of 0, 2, 5, 7, 10, 15, 30, 50, 100, and  $150m^2$ . The optimal size

of the RSC panel,  $A_{rsc}$ , was chosen as  $5m^2$ . The resulting data and graphs are shown in Table 4.3 and Figure 4.10.

Table 4.3: RSC Panel Size Cost Optimization

Size ( $m^2$ )	Total Cost (\$)
0	2,020.95
2	1,977.83
5	1,970.14
7	1,968.86
10	1,967.57
15	1,966.83
30	1,966.00
50	1,965.97
100	1,965.88
150	1,965.98

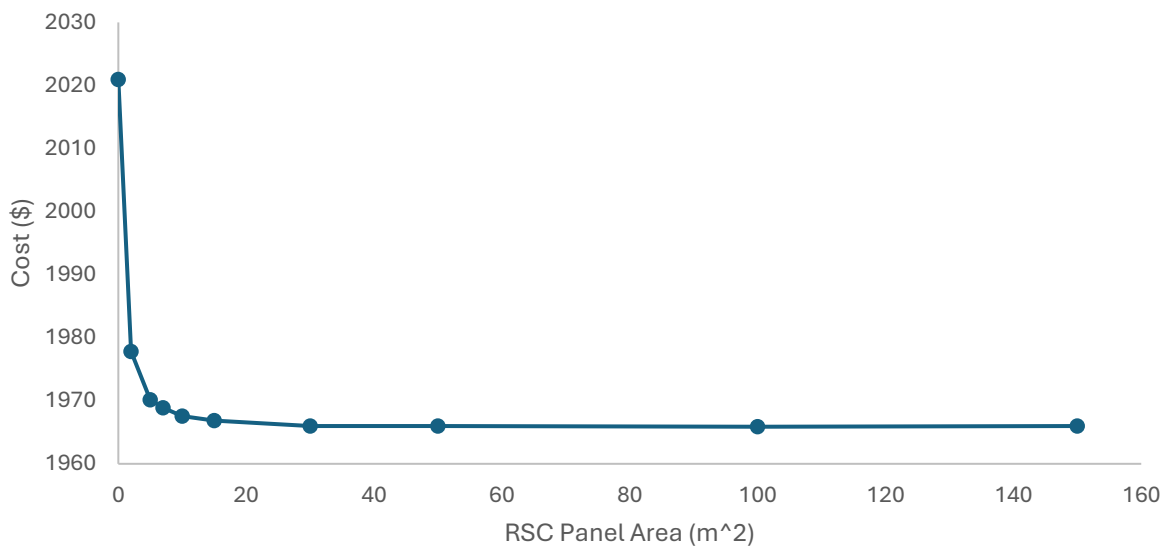


Figure 4.10: RSC Panel Size Cost Optimization

Here,  $5m^2$  was chosen as the optimal RSC panel size, balancing operational cost savings with upfront affordability. While pricing for commercially available RSC systems is not readily available, it is reasonable to assume that this younger technology might cost twice as much as solar evacuated tube collectors. Using this conservative estimate the total cost was assumed to be \$2000 for a  $5m^2$  panel.

Holding the thermal tank and RSC panel sizes constant, the model was then run iteratively for solar collector panel sizes of 0, 2, 5, 7, 10, 15, 30, 50, 100, and  $150m^2$ . The resulting table and graph is shown in Table 4.4 and Figure 4.11.

Table 4.4: Solar Collector Panel Size Optimization

Size ( $m^2$ )	Total Cost (\$)
0	2,067.53
2	2,042.32
5	2,009.81
7	1,992.38
10	1,967.57
15	1,936.96
30	1,875.05
50	1,827.65
100	1,767.74
150	1,739.80

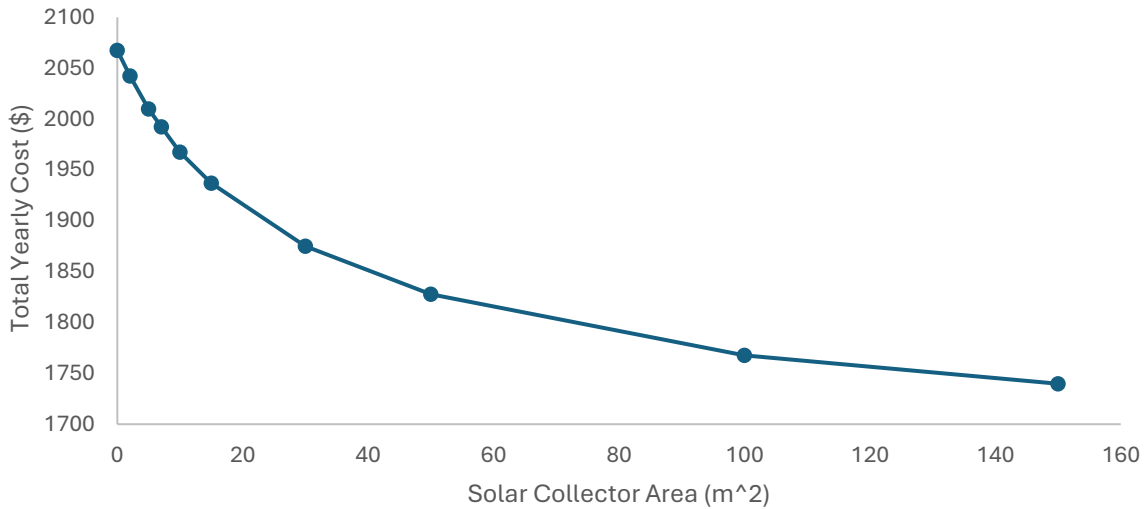


Figure 4.11: Solar Collector Size Optimization

The optimized panel size was chosen as  $50\text{m}^2$ , accounting for diminishing returns as size increased. To achieve this area, 10 collectors were selected from [54]. Each of the ThermoPower™ 30 Tube Evacuated Tube Solar Collectors from [54] are listed for \$2159.94, coming to a total of \$21,599.40 for the array.

Holding the RSC and solar collector sizes constant, the model was run iteratively for thermal tank sizes of 3.79, 5.68, 7.57, 9.46, and  $11.36\text{m}^3$ . These values represent typical commercially available tank sizes in the United States, taken from [8]. The resulting table and graph are shown Table 4.5 and Figure 4.12.

Table 4.5: Thermal Tank Size Optimization

Size (m <sup>3</sup> )	Total Cost (\$)
3.79	1,968.89
5.68	1,967.22
7.57	1,965.89
9.46	1,966.15
11.36	1,965.11

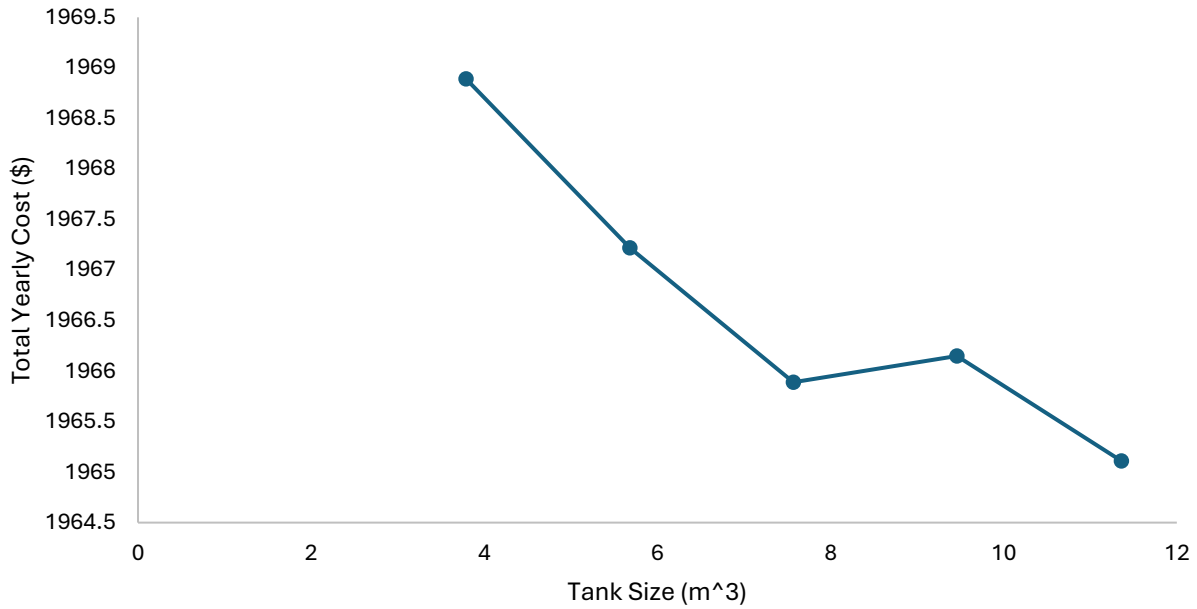


Figure 4.12: Thermal Tank Size Optimization

Here a clear local minimum was found at  $7.57m^3$  along with a diminishing return in total yearly cost savings as  $V_{tank}$  increased. For this reason, an optimized tank size of  $7.57m^3$  was chosen from this analysis. The chosen tank from this size is shown in Figure 4.13, made of HDPE material which is appropriate for storing water-glycol mixtures. This tank is available from [55] for \$1242.



Figure 4.13: Thermal Tank

Previously in this thesis, the differences in cost-optimized and emissions-optimized systems were compared. In this section along with chapter 5 and chapter 6, an economic approach is emphasized. For this reason, the cost-optimized model is used from this point on in this thesis. With these optimized sizes implemented in the model, the results from Table 4.6 were generated.

Table 4.6: HVAC System Performance (System Optimization, Cost-Optimized Model)

	WSHP	ASHP	Boiler	Combined
<b>Yearly Cost (\$)</b>	388.08	224.83	1,209.01	1,821.96
<b>Yearly CO<sub>2</sub> Output</b>				
(Kg)	602.32	366.46	2,734.24	3,703.10
<b>Average COP</b>	3.32	2.82	N/A	
<b>Energy Consumption</b>	1,544.42 (kWh)	939.65 (kWh)	262.20 (gal)	
<b>% Space Heating</b>				
<b>provided</b>	31%	12%	57%	
<b>% Air Conditioning</b>				
<b>Provided</b>	100%	0%	0%	

These results can be compared to the previous cost-optimized results from the system selection section earlier in chapter 3. From optimizing the sizes of these components, the yearly operational cost decreased 7.4% from \$1967.57 to \$1821.96. The yearly electricity consumption increased 7.00% from 2321.62kWh to 2484.07kWh, while the heating oil consumption decreased 13.53% from 303.23gal to 262.19gal. The yearly CO<sub>2</sub> emissions decreased 8.95% from 4067.19kg to 3703.10kg. While the ASHP average COP remained unchanged, the WSHP average COP increased 19.00% from 2.79 to 3.32. Along with this change in COP, the WSHP heating utilization increased from 16% to 31%, while the ASHP and boiler fell from 18% to 12% and from 66% to 57%, respectively. The system utilization, and thermal tank temperature plots are shown in Figure 4.14 and Figure 4.15.

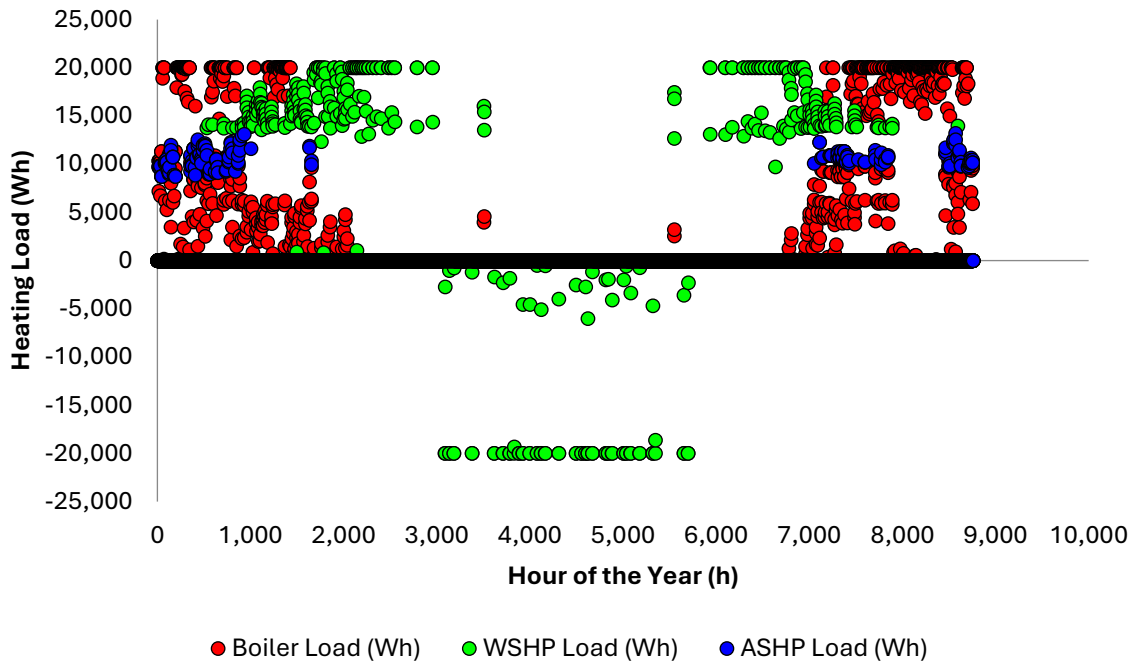


Figure 4.14: HVAC System Usage (System Optimization, Cost-Optimized Model)

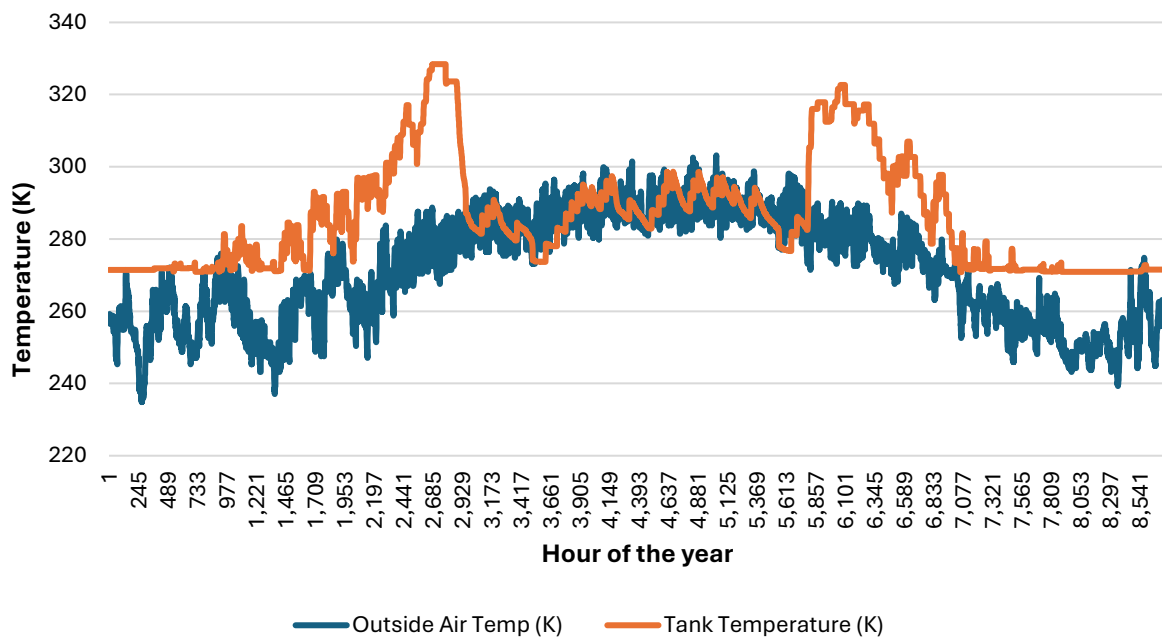


Figure 4.15: Thermal Tank Versus Ambient Temperature (System Optimization, Cost-Optimized Model)

In the system utilization graph, a heavier concentration of WSHP heating can be observed during the winter and the shoulder seasons. From the numerical data, it was observed that the WSHP is now more efficient than in the previous model version and therefore is chosen over the boiler and ASHP in a significant portion of the heating season. This improved COP of the WSHP is resultant of an increased thermal tank temperature throughout the year, as seen from the plot above. The increased size of the solar collector from the previous version has had a significant impact on the temperature of the thermal tank, which maximum temperatures reaching up to 330K. This is a great increase from the previous maximum tank temperatures of 317K. It can also be clearly seen from Figure 4.15 that at this point, there is a major temperature difference between the thermal tank and the ambient air during the shoulder seasons, leading to the WSHP's heating dominance.

## **Chapter 5: System Configuration Study**

### **5.1 Overview**

With commercially chosen HVAC equipment, optimized sizes for the RSC, solar collector, and thermal tank, and realistic controls implemented in the model, the operational performance of the proposed system can be properly analyzed. In this section a comparison will be made between the proposed hybrid source heat pump system and a series of other HVAC configurations. The cost of heating with the proposed system will be compared with the cost of heating with only a residential boiler, only an ASHP, and only a WSHP. The ASHP and WSHP will still be configured with a backup boiler to supplement heating since these systems are not designed to meet the heating load and design temperatures. Additionally, one more scenario will be added to show the results from adding a second ASHP, effectively doubling the heating capacity of the ASHP system. Analyzing the performance of these systems, the operational cost and emissions can be compared, and total energy savings, emissions savings, and cost savings can be determined for each system. The boiler-only configuration will serve as a baseline for comparison, since this is the typical heating system in Fairbanks homes. A separate analysis was also performed to analyze the cooling performance of the tested systems. This separation allowed for an emphasis on space heating, while still considering air conditioning in the analysis.

### **5.2 Methodology**

#### **5.2.1 Heating System Configuration**

In this analysis, the proposed HSHP system will be compared to various HVAC systems including a boiler, an ASHP, 2 ASHPs, and a WSHP. Each of the heat pump systems will be equipped with a backup boiler. In this study, the proposed system uses a hybrid source heat pump (HSHP) which can draw from or reject heat to a water source or an air source. The water source used in the proposed system is a thermal storage tank containing a glycol–water mixture. The thermal tank is passively cooled or heated by radiative sky cooling (RSC) and solar evacuated tube heating as appropriate. The proposed system combines the benefits of an ASHP and WSHP into one hybrid unit. When isolating the WSHP for its own analysis, it's important to

note that this configuration is also modeled with the thermal storage tank, RSC and solar collector as well, like the HSHP system. Since heating is the focus of this study, the cost and benefits of heating were recorded and compared separately from AC for each system.

Using the boiler-only system as a baseline, the performance of the other configurations were evaluated. To model these systems, the controls were adapted to isolate the system of interest. Starting with the boiler-only system, the controls were redefined in the model so that the ASHP and WSHP were turned off for the entire year. This resulted in the boiler as the only available system. Since the boiler is incapable of providing air conditioning, this analysis only considered the effects of heating as expected.

Following the isolation of the boiler, the ASHP was switched off in the model to isolate the WSHP and backup boiler. When the post processing of the resultant data was performed, only the heating loads that were greater than 0 were considered, ignoring AC loads. This method allowed comparison to the boiler-only baseline by isolating only the heating data for the year.

Similarly, the WSHP was then switched off to isolate the WSHP and backup boiler, again ignoring any AC utilization. These methods were used to generate data simulating the operation of the isolated components, allowing for comparison of heating data between each configuration. In each of these simulations, a yearly heating load of 16.3MWh and an AC load of 1.31MWh were found.

### **5.2.2 AC System Configuration**

While air conditioning is not the focus of this analysis, there is still a non-negligible cooling load during the summer cooling season in Fairbanks. This thesis aims to focus on heating system analysis, while providing a comparison for air conditioning as well. To compare the air conditioning performance of the different system configurations, some means of providing AC must be assumed in the boiler-only configuration. In Fairbanks, the most straightforward way to provide cooling power to a home configured with a boiler and baseboard heating system is to use a portable in-room AC unit. One affordable unit is the LG model LP0821GSSM, which is available from [56] for \$469. This unit performs at a listed

combined energy efficiency ratio (CEER) of 7.22, considering the energy used both when active and when in stand-by mode. During the summer in Fairbanks, this AC unit would have to run nearly constantly to provide the cooling load, since it is sized to provide cooling for only  $350\text{ft}^2$  [56]. Again, this type of unit is commonly used in Fairbanks to provide cooling to the bedroom of a residential home, which this unit is fully capable of doing. Since this unit would run often in the summertime, the CEER is a conservative estimate for the efficiency of the AC unit in this scenario. This LG unit was used to provide air conditioning in the boiler-only configuration, and the previously mentioned CEER  $\left(\frac{\text{BTU}}{\text{h}} \cdot \text{W}^{-1}\right)$  was used to calculate the cooling COP, associated cost and emissions of air conditioning. Here, the price of electricity  $\$/\text{electricity}$  was taken during the summertime high of \$.26/kWh. The electricity consumption  $E_{AC}$  ( $\text{kWh}$ ), associated cost (\$), and  $\text{CO}_2$  emissions ( $\text{kg}$ ) were calculated as shown in equations (5.1 and (5.4.

$$\text{COP} = \frac{\text{CEER}}{\left(\frac{3.412 \text{ BTU}}{1\text{h}} \cdot \text{W}^{-1}\right)} \quad (5.1)$$

$$E_{AC} = \frac{Q_{AC}}{\text{COP}} \quad (5.2)$$

$$\$/AC = E_{AC} \cdot \$\text{electricity} \quad (5.3)$$

$$\text{CO2}_{AC} = E_{AC} \cdot \text{CO2}_{\text{electricity}} \quad (5.4)$$

The chosen AC unit from [56] is shown in Figure 5.1.



Figure 5.1: Selected AC Unit (model LP0821GSSM) from LG [56]

With this AC system in place as a baseline, the performance of the HSHP, ASHP, 2 ASHPs, and WSHP systems were compared separately for air conditioning.

### 5.3 Results

#### 5.3.1 Boiler - Heating

With the boiler as the only operational system, the data from Table 5.1 was generated for space heating throughout the year.

Table 5.1: HVAC System Performance (Boiler Only)

Boiler	
<b>Yearly Heating Cost (\$)</b>	2,091.74
<b>Yearly CO<sub>2</sub> Output (Kg)</b>	4,775.52
<b>Average Heating COP</b>	N/A
<b>Boiler Fuel Consumption</b>	460.96 (gal)
<b>% Space Heating provided</b>	100%
<b>% Air Conditioning Provided</b>	100%

Using only the boiler, the yearly cost of space heating was \$2091.74 and the yearly  $CO_2$  emission from space heating were 4775.5Kg. These values are critical to the analysis in this section, since they will serve as a baseline for comparison to other system configurations. The system utilization and thermal tank temperature plots are shown by Figure 5.2 and Figure 5.3.

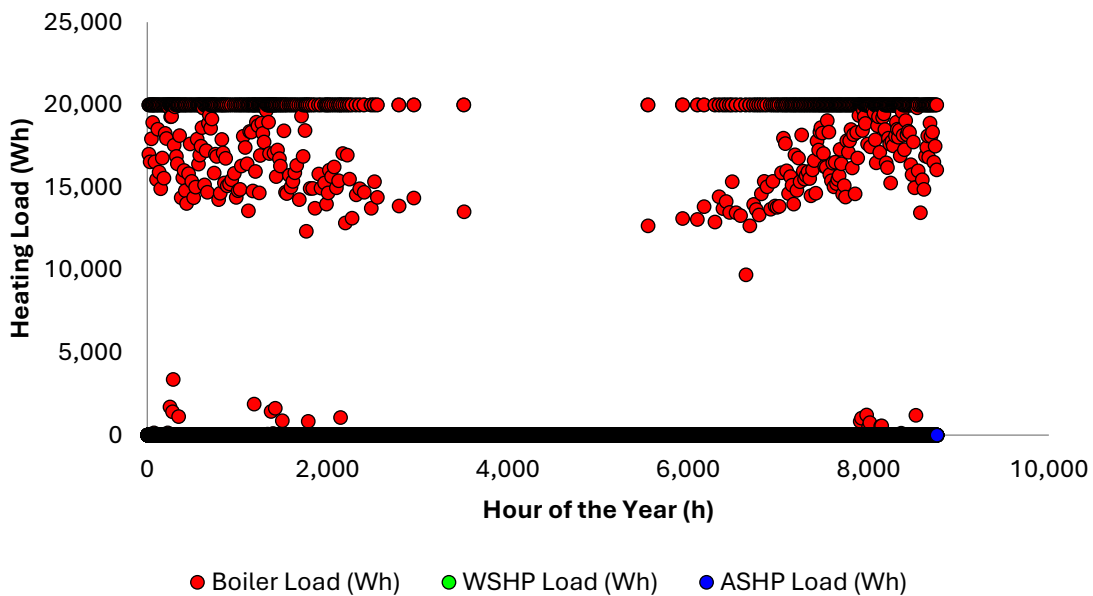


Figure 5.2: HVAC System Usage (Boiler Only)

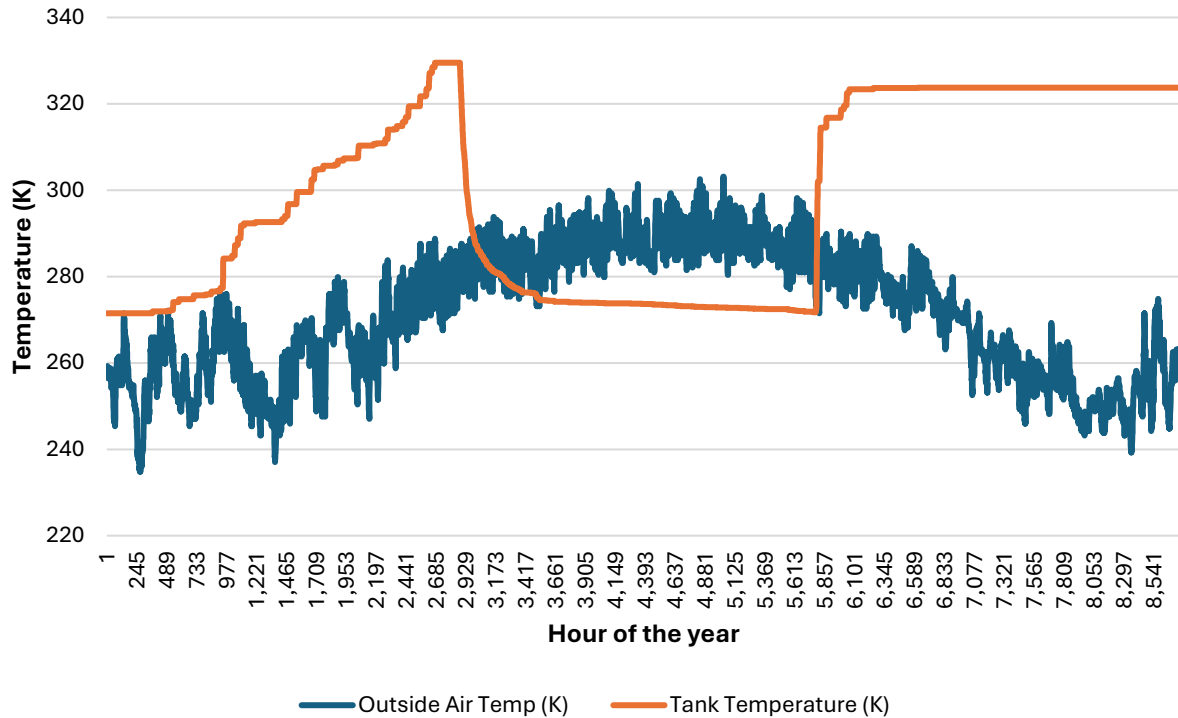


Figure 5.3: Thermal Tank Versus Ambient Temperature (Boiler Only)

### 5.3.2 LG Portable Unit - Air Conditioning

The LG model LP0821GSSM was used in this configuration to provide the required yearly AC load of 1.31MWh. The associated electricity usage of air conditioning using the LG unit was found to be 619.08kWh, and the cost of AC was found to be \$160.96. The emissions associated with electricity usage from this AC were found to be 242.12kg.

### 5.3.3 HSHP and Backup Boiler - Heating

With the HSHP and backup boiler as the active configuration, the data from Table 5.2 was generated for space heating throughout the year.

Table 5.2: HVAC System Performance (HSHP and Backup Boiler)

	WSHP	ASHP	Boiler	Combined
<b>Yearly Heating Cost (\$)</b>	326.20	224.83	1,209.01	1,760.04
<b>Yearly CO<sub>2</sub> Output</b>				
(Kg)	508.27	366.46	2,734.24	3,608.98
<b>Average Heating COP</b>	2.08	1.95	N/A	
<b>Energy Consumption</b>	1,303.27 (kWh)	939.65 (kWh)	262.19 (gal)	
<b>% Space Heating</b>				
<b>provided</b>	31%	12%	57%	

Using the boiler-only configuration as the baseline for comparison, the following changes were noted. The yearly cost of space heating declined 15.86% from \$2091.74 to \$1760.04. The yearly heating oil consumption decreased 43.1% from 460.96 gallons to 262.19 gallons, while the electricity usage from the heat pumps increased from 0 to 2242.91kWh. Additionally, the yearly  $CO_2$  emission decreased 24.43% from 4775.52kg to 3608.98kg. The system utilization and thermal tank temperature plots are shown in Figure 5.4 and Figure 5.5.

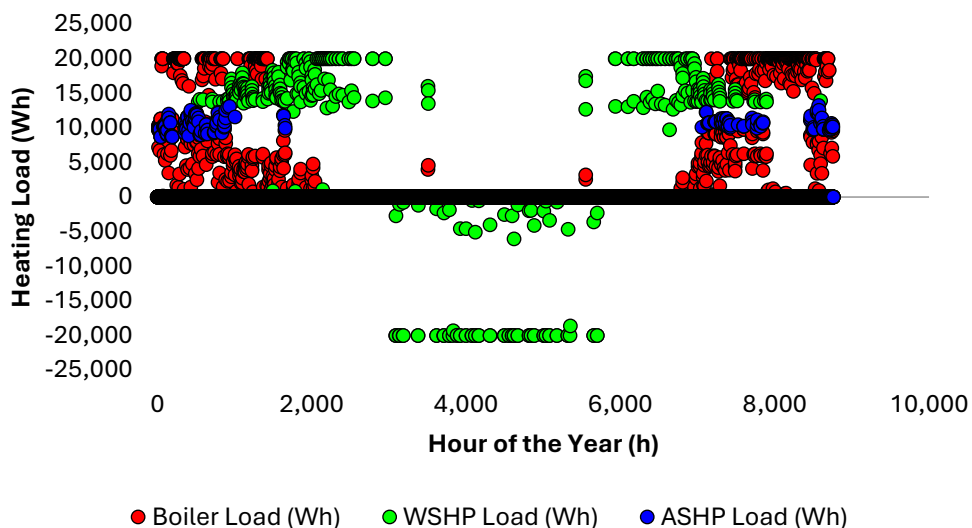


Figure 5.4: HVAC System Usage (HSHP and Backup Boiler)

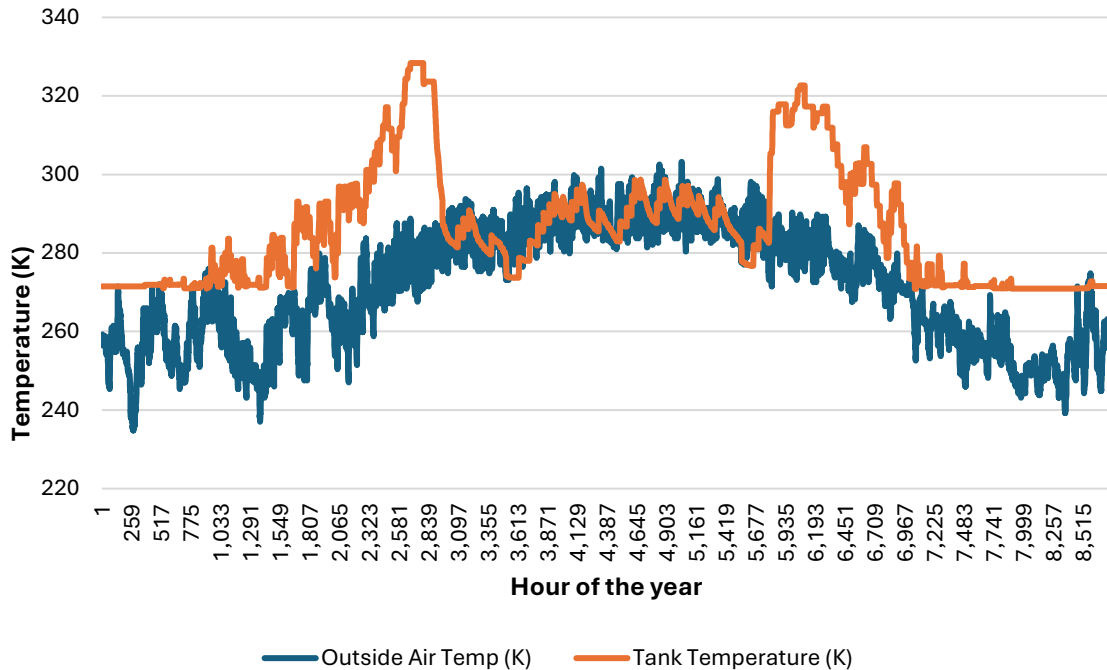


Figure 5.5: Thermal Tank Versus Ambient Temperature (HSHP and Backup Boiler)

### 5.3.4 HSHP - Air Conditioning

Using the proposed system, the WSHP was assigned 100% of the air conditioning load, achieving the cooling at an average COP of 5.82. The WSHP achieved the required cooling at a cost of \$61.88, which is 61.56% less expensive than the LG unit cost of \$160.96. The total electricity consumption decreased by 61.05% from 619.08kWh to 241.16kWh of electricity. The yearly emissions due to AC also decreased by 61.16% from 242.12kg to 94.05kg of  $CO_2$ .

### 5.3.5 ASHP and Backup Boiler - Heating

With the ASHP and backup boiler as the active configuration, the data in Table 5.3 was generated for space heating throughout the year.

Table 5.3: HVAC System Performance (ASHP and Backup Boiler)

	ASHP	Boiler	Combined
<b>Yearly Heating Cost (\$)</b>	489.02	1,521.41	2,010.43
<b>Yearly CO<sub>2</sub> Output (Kg)</b>	777.64	3,455.98	4,233.62
<b>Average Heating COP</b>	1.95	N/A	
<b>Energy Consumption</b>	1,993.95 (kWh)	331.81 (gal)	
<b>% Space Heating provided</b>	28%	72%	

From the boiler-only configuration, the following changes can be observed. The yearly heating costs decreased 3.89% from \$2091.74 to \$2010.44. The yearly heating oil consumption decreased 28.02% from 460.96 gallons to 331.81 gallons, while the electricity consumption by the ASHP rose from 0 to 1993.95kWh. The  $CO_2$  emissions associated with space heating fell 11.4% from 4775.52kg to 4233.62kg. The system utilization and thermal tank temperature plots are shown in

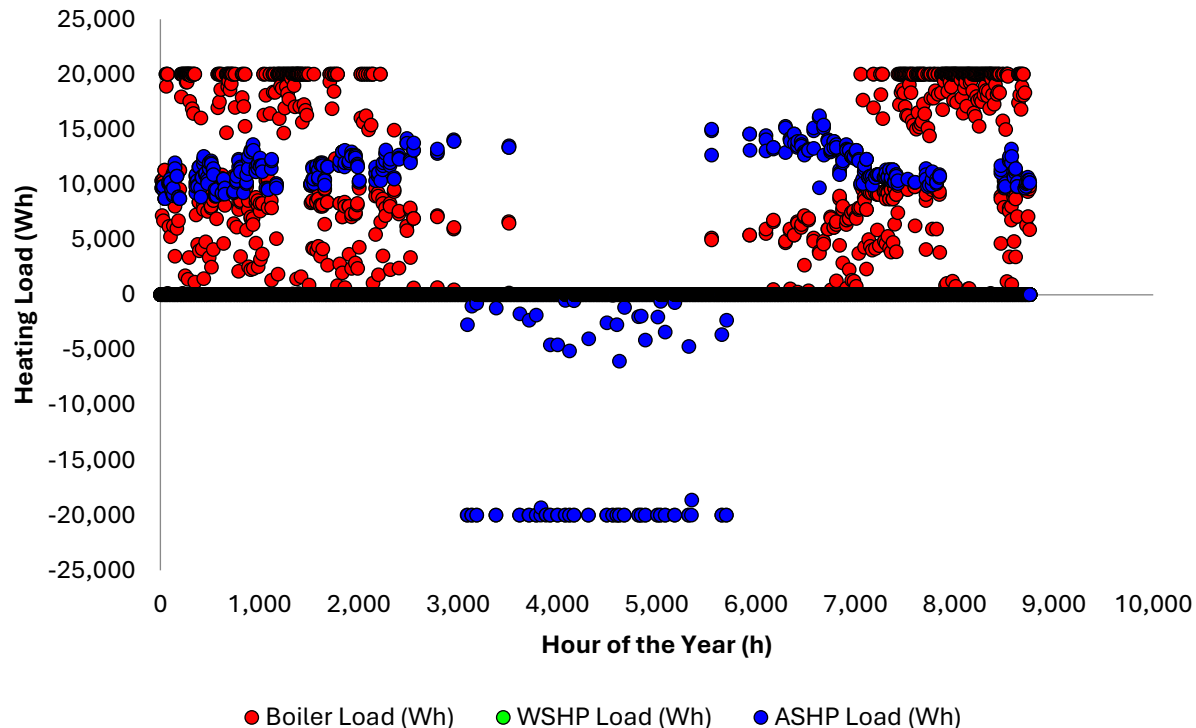


Figure 5.6 and Figure 5.7.

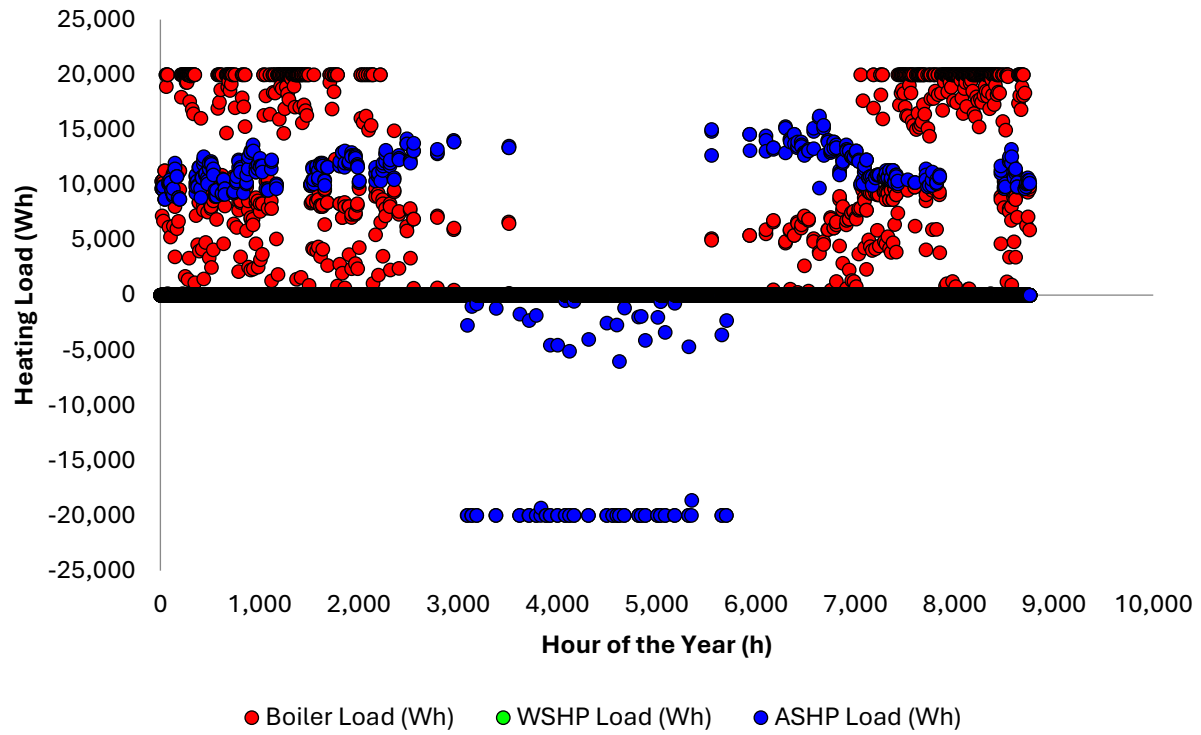


Figure 5.6: HVAC System Usage (ASHP and Backup Boiler)

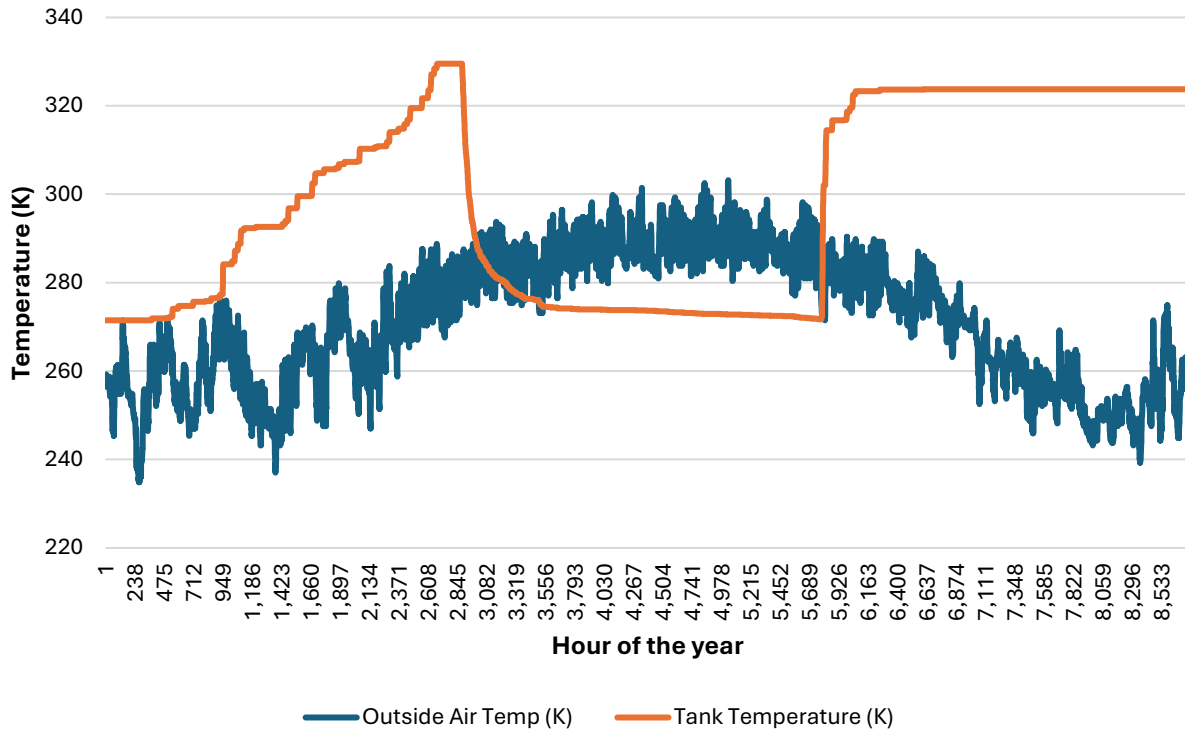


Figure 5.7: Thermal Tank Versus Ambient Temperature (ASHP and Backup Boiler)

### 5.3.6 ASHP - Air Conditioning

Using the ASHP and backup boiler only, the ASHP was assigned 100% of the air conditioning load, achieving the cooling at an average COP of 2.88. The ASHP achieved the required cooling at a cost of \$121.1, which is 24.76% cheaper than the LG unit cost of \$160.96. The total electricity consumption fell 23.81% from 619.08kWh to 471.71kWh of electricity. The yearly emissions due to AC also fell 24.02% from 242.12kg to 183.97kg of  $CO_2$ .

### 5.3.7 WSHP and Backup Boiler - Heating

With the WSHP and backup boiler as the active configuration, the data in Table 5.4 was generated for space heating throughout the year.

Table 5.4: HVAC System Performance (WSHP and Backup Boiler)

	WSHP	Boiler	Combined
<b>Yearly Heating Cost (\$)</b>	326.20	1,457.33	1,783.53
<b>Yearly CO<sub>2</sub> Output (Kg)</b>	508.27	3,298.71	3,806.98
<b>Average Heating COP</b>	2.08	N/A	
<b>Energy Consumption</b>	1,303.27 (kWh)	317.48 (gal)	
<b>% Space Heating provided</b>	31%	69%	

From the boiler – only configuration, the following changes can be observed. Heating with the WSHP and backup boiler resulted in a yearly cost decrease of 14.74% from \$2091.74 to \$1783.53. The heating oil consumption decreased 31.13% from 460.96 gallons to 317.48 gallons, while the electricity consumption by the heat pump rose from 0 to 1303.27kWh. The yearly  $CO_2$  emissions associated with heating decreased 20.28% from 4775.52kg to 3806.98kg. The HVAC system usage and thermal tank temperature plots are shown in Figure 5.8 and Figure 5.9.

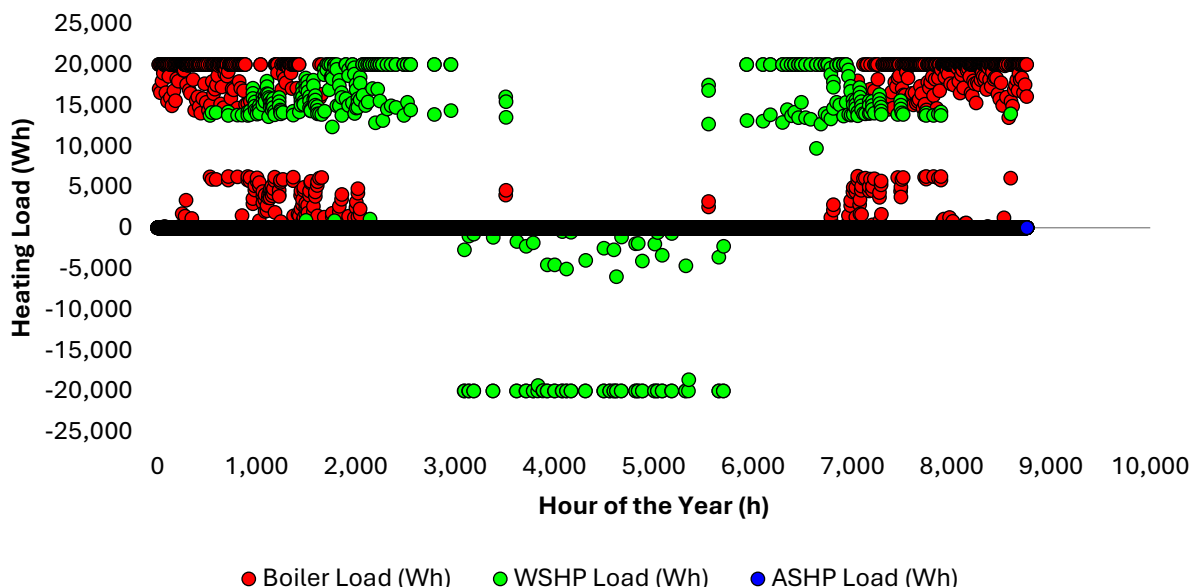


Figure 5.8: HVAC System Usage (WSHP and Backup Boiler)

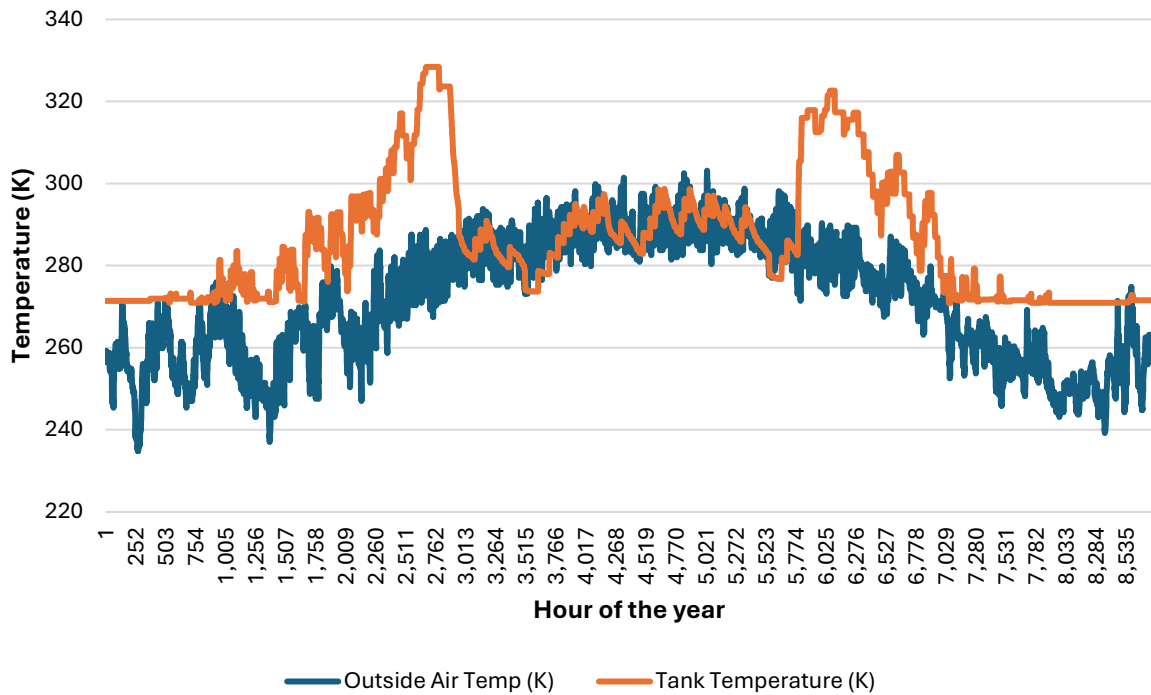


Figure 5.9: Thermal Tank Versus Ambient Temperature (WSHP and Backup Boiler)

### 5.3.8 WSHP - Air Conditioning

Using the WSHP and backup boiler only, the WSHP was assigned 100% of the air conditioning load, achieving the cooling at an average COP of 5.82. The WSHP achieved the required cooling at a cost of \$61.88, which is 61.56% less expensive than the LG unit cost of \$160.96. The total electricity consumption decreased by 61.05% from 619.08kWh to 241.16kWh of electricity. The yearly emissions due to AC also decreased by 61.16% from 242.12kg to 94.05kg of  $CO_2$ .

### 5.3.9 Dual ASHPs and Backup Boiler - Heating

With the 2 ASHPs and a backup boiler as the active configuration, the data in Table 5.5 was generated for space heating throughout the year.

Table 5.5: HVAC System Performance (2 ASHPs and Backup Boiler)

	2 ASHPs	Boiler	Combined
<b>Yearly Heating Cost (\$)</b>	782.69	1,163.04	1,945.73
<b>Yearly CO<sub>2</sub> Output (Kg)</b>	1,247.72	2,643.19	3,890.91
<b>Average Heating COP</b>	1.95	N/A	
<b>Energy Consumption</b>	3,199.28 (kWh)	254.80 (gal)	
<b>% Space Heating provided</b>	45%	55%	

From the boiler – only configuration, the following changes can be observed. Heating with the WSHP and backup boiler resulted in a yearly cost decrease of 6.98% from \$2091.74 to \$1945.72. The heating oil consumption decreased 44.72% from 460.96 gallons to 254.80 gallons, while the electricity consumption by the heat pumps rose from 0 to 3199.28kWh. The yearly  $CO_2$  emissions associated with heating decreased 18.52% from 4775.52kg to 3890.91kg. The HVAC system usage, inside air, and thermal tank temperature plots are shown in Figure 5.10 and Figure 5.11.

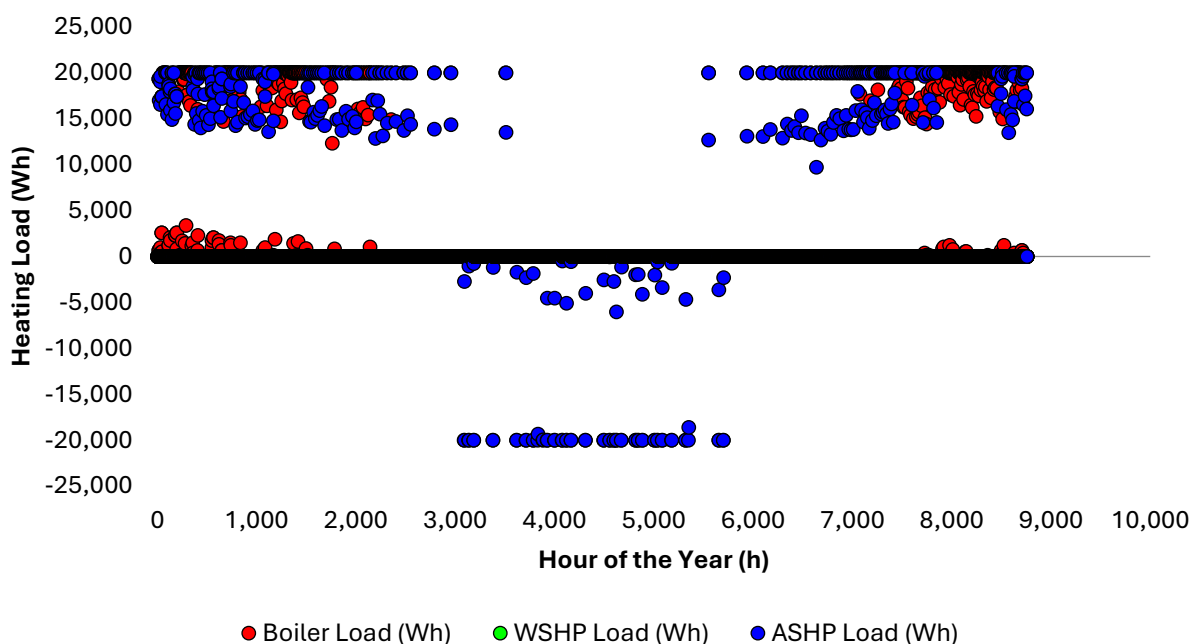


Figure 5.10: HVAC System Usage (2 ASHPs and Backup Boiler)

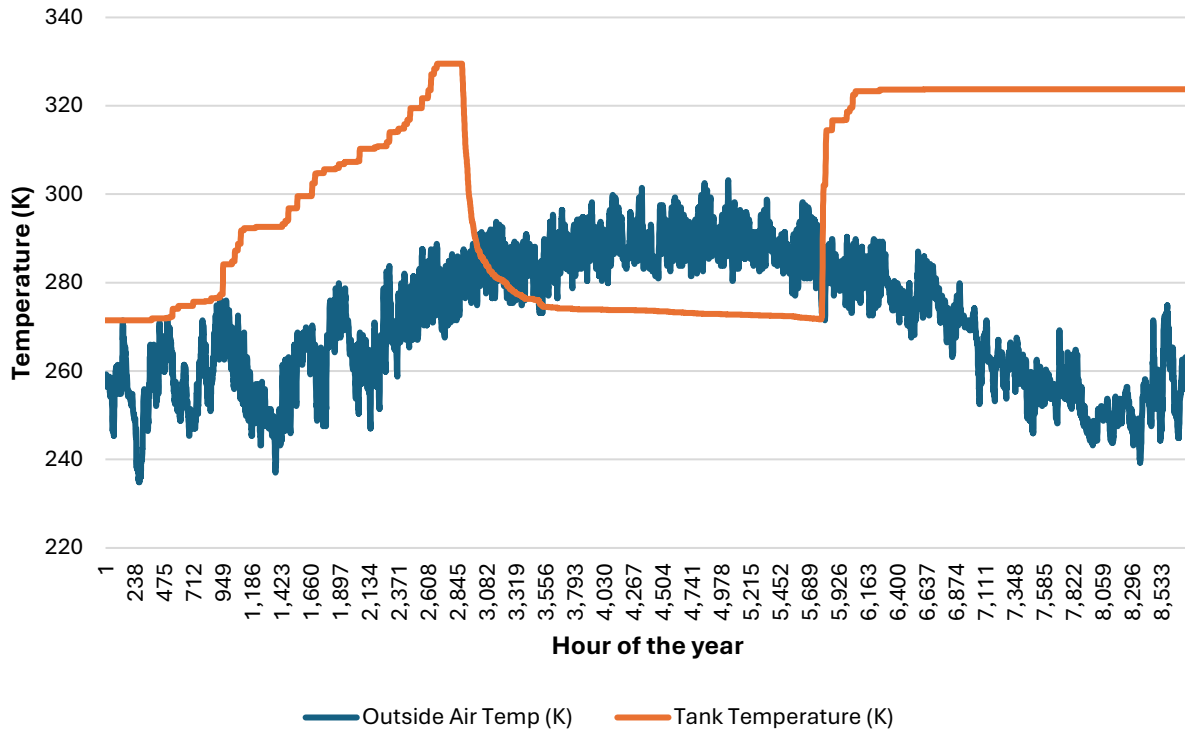


Figure 5.11: Thermal Tank Versus Ambient Temperature (2 ASHPs and Backup Boiler)

### 5.3.10 Dual ASHPs - Air Conditioning

Using the 2 ASHPs and backup boiler only, the ASHPs were assigned 100% of the air conditioning load, achieving the cooling at an average COP of 2.88. The ASHPs achieved the required cooling at a cost of \$121.1, which is 24.76% cheaper than the LG unit cost of \$160.96. The total electricity consumption fell 23.81% from 619.08kWh to 471.71kWh of electricity. The yearly emissions due to AC also fell 24.02% from 242.12kg to 183.97kg of  $CO_2$ .

### 5.3.11 Comparative Heating and Cooling

The summarized results can be tabulated and compared for a clear analysis. The summarized heating results for each system configuration are shown in Table 5.6 for comparison. Here, the COP for the HSHP is taken as the average values of the WSHP and ASHP's COP in the system. It should also be noted that while the boiler's electricity usage was considered when calculating cost and  $CO_2$  emissions, it was not recorded in the yearly electricity consumption.

Table 5.6: Summary of Results for Each Heating System Configuration

Heating Performance	WSHP and Boiler	ASHP and Boiler	HSHP and Boiler	2 ASHPs and Boiler	Boiler Only
<b>Yearly Heating Cost (\$)</b>	1,783.53	2,010.44	1,760.04	1,945.73	2,091.74
<b>Yearly CO2 Emissions (kg)</b>	3,808.89	4,233.62	3,608.98	3,890.91	4,775.52
<b>Yearly HP Electricity Consumption (kWh)</b>	1,303.27	1,993.95	2,242.91	3,199.28	N/A
<b>Yearly Heating Oil Consumption (gal)</b>	317.48	331.81	262.19	254.80	460.96
<b>% Cost Savings</b>	14.74	3.89	15.86	6.98	N/A
<b>% CO2 Emission Savings</b>	20.28	11.4	24.43	18.52	N/A
<b>% Heating Oil Consumption Savings</b>	31.13	28.02	43.1	44.72	N/A

The summarized cooling results for each system configuration are shown in Table 5.7 for comparison. Using the boiler-only system as a baseline, the savings for each system are tabulated as percent differences.

Table 5.7: Summary of Results for Each Cooling System Configuration

AC Performance	WSHP	ASHP	HSHP	2 ASHPS	LG Portable AC
<b>Yearly Cooling Cost (\$)</b>	61.88	121.07	61.88	121.07	160.96
<b>Yearly CO2 Emissions (kg)</b>	94.05	183.97	94.05	183.97	242.12
<b>Yearly HP Electricity Consumption (kWh)</b>	241.16	471.71	241.16	471.71	619.08
<b>% Cost Savings</b>	61.34	24.78	61.34	24.98	N/A
<b>% CO2 Emission Savings</b>	61.16	24.02	61.16	24.02	N/A
<b>% Electricity Savings</b>	61.05	23.81	61.05	23.81	N/A
<b>COP</b>	5.82	2.88	5.82	2.88	2.12

## 5.4 Discussion

In terms of heating cost, the proposed HSHP system was found to be the most efficient, with total cost savings of 15.86% from traditional boiler heating. Coming in close second, the WSHP yielded a 14.74% heating cost reduction from a traditional boiler. The ASHP system was far behind, yielding only 3.98% cost savings. Adding an additional ASHP achieved savings of 6.98%. Per year, the HSHP, WSHP, ASHP, and 2 ASHPs saved roughly \$331.75, \$308.32, \$81.37, and \$146.00 respectively.

It's also important to note the different energy consumption distributions for each system. Specifically, this thesis aims to explore cost savings as well as emissions reduction, particularly from the combustion of heating oil. While the ASHP performed rather poorly compared to the WSHP and HSHP systems for cost savings, it managed to reduce heating oil consumption by 28.02%, or 129.16 gallons per year. The ASHP also reduced the emission of  $CO_2$  by 11.4%, or 541.90kg per year. Improving on this performance, the WSHP reduced heating oil consumption by 143.48 gallons per year, or 31.13%. The WSHP also reduced the emission of  $CO_2$  by 20.28% or 966.63kg. The HSHP was the most effective in reducing  $CO_2$  emissions and the second most effective in reducing heating oil dependence, with a reduction in heating oil use of 43.1% or 198.77 gallons per year. The HSHP also reduced the emission of  $CO_2$  by 24.43%, or 1166.54kg. The most effective systems for heating oil consumption reduction and the second best for emissions reduction system were the 2 ASHPs, which reduced the heating oil consumption by 44.72% or 206.16 gallons, and reduced the emission of  $CO_2$  by 18.52% or 884.43kg.

In terms of cooling cost, the HSHP and WSHP yielded identical results. This is because the WSHP system was so efficient, yielding a cooling COP of 5.82, that it completely dominated air conditioning over the ASHP even in the HSHP system. Both the HSHP and WSHP systems saved 61.34% on air conditioning compared to the standard LG portable AC unit. The ASHP was a bit more efficient than the LG unit, yielding a COP of only 2.88 over the cooling season, earning a total 24.78% cost decrease from the LG system. In terms of cost, the HSHP and WSHP saved \$99.08 each year, while the ASHP saved \$39.89 per year as compared to the LG AC unit.

The dual ASHP system yielded identical results for cooling as the single ASHP, since the effects of cooling capacity were neglected in this analysis.

The WSHP and HSHP systems achieved significant cost and emissions savings for air conditioning as compared to the LG portable AC unit. The single and dual ASHP units also achieved significant cost and emissions reductions, although much less than the WSHP and HSHP systems. For heating however, The WSHP had a notable yearly improvement on all performance metrics, falling only shortly behind the HSHP system. The single and dual ASHP systems achieved menial cost savings but greatly reduced the consumption of heating oil.

## Chapter 6: Benefit-Cost Analysis

### 6.1 Overview

In the system configuration study, it was determined that the HSHP was the most effective system for combined heating and cooling when considering both operational cost and emissions. However, this analysis did not consider the cost effectiveness of the installation of each system. While the HSHP was the top performing system, it was very closely followed by the WSHP system in all performance metrics. Additionally, while the single and dual ASHP systems were far less economic than the HSHP or WSHP systems, they achieved competing reductions in  $CO_2$  emissions and heating oil consumption. To determine the relative cost effectiveness of these systems for a Fairbanks resident, the costs of each system must be weighed with the benefits provided from implementation. In this benefit-cost analysis, three categories were considered. The capital costs of each system were calculated to include equipment and installation costs. Operations and maintenance (O&M) costs were calculated yearly, accounting for variable system performance and maintenance needs. Finally, the social benefit of  $CO_2$  and  $PM_{2.5}$  emissions reductions was calculated. This calculation provided a means of monetarily quantifying the use of electric systems in place of fossil fuel, allowing for an “apples to apples” comparison of the tested systems.

Generally, a few relationships were noted between cost and benefit for the tested systems. While the boiler-only system was highly emissive, costly, and contributed significantly to air quality issues in the FNSB, it has an extremely low up front cost. This heating system provides the lowest barrier to entry for reliable heating for Fairbanks residents of all the tested systems. While the single and dual ASHP systems did not achieve significant cost savings, they provided a major environmental benefit by greatly reducing emissions from heating oil combustion. These units are far more expensive than a traditional boiler, yet far less expensive than complex WSHP or HSHP systems equipped with passively cooled and heated thermal storage systems. The proposed HSHP showed the highest overall performance of any system but was expected to have an astronomical upfront cost compared to the yearly cost savings. The WSHP achieved similar heating performance to the HSHP and identical AC performance,

falling just behind the HSHP in overall effectiveness. However, there is no ASHP component necessary in the WSHP system, resulting in a significantly lower upfront cost as compared to the HSHP. Although there are not readily available commercial HSHP systems, the cost difference between a HSHP and WSHP was expected to completely negate the marginal performance advantage seen by the HSHP. Relative to the boiler or ASHP systems, even the WSHP system is extremely cost prohibitive for Fairbanks residents.

## **6.2 Methodology**

To estimate the capital costs of each system, the equipment and installation costs must be fully determined for each system. According to [57], the average cost to install a thermal collector in Fairbanks is between \$1600 - \$2600. This analysis assumed the median value of \$2100 as the cost to install one of the chosen collectors. Since the cost of an RSC panel is not readily available, a few assumptions were made about equipment and installation costs. As previously described in the system selection section, an assumed equipment cost of \$2000 was taken for one  $5m^2$  RSC panel. Like solar evacuated tube collectors, RSC panels are installed onto the roof of a building and plumbed into an active cooling loop connected to a pump. Because of the similarity of installation, it is reasonable to assume that the cost to install an RSC system is the same as the cost to install a solar evacuated tube heating system. Additionally, a thermal storage tank installation in Fairbanks costs between \$1000 - \$2800, and parts (including the pump) to connect the solar collector to the thermal tank cost between \$800 - \$2800 [57]. Due to the large size of the chosen tank and the fact that it would need to be buried, insulated, and connected to both the RSC and solar collector plumbing loops, the costs of the tank installation and the required parts were each taken at the highest value of \$2800.

According to [58], the cost to retrofit a 5-ton heat pump unit is between \$7600 - \$10,300, and this price can decrease between \$400 - \$1000 if an existing heat pump does not need to be removed. For the chosen ASHP and WSHP, the cost of installation was taken at the median value of these ranges, for a total of \$8250 each. Furthermore, a buffer tank is required with the ASHP system, for which an installation cost of \$2800 was assumed, like that of the thermal tank.

Additionally, a HSHP has a very similar function and installation to an ASHP or WSHP. The main difference is that the HSHP will have two condensers, one in an air medium and one in a water medium. Therefore, two heating loops are necessary, requiring twice the number of fittings and twice the labor to install. From this, the installation cost of a HSHP was conservatively assumed to be twice the cost of a typical installation, for a total of \$16,500. Since the cost of a HSHP unit was not readily available, some assumptions were made based on the known cost of its components. Since a HSHP performs the duties of both an ASHP and a WSHP using multiple heating/cooling loops, it was assumed that the cost of a HSHP unit is equal to the sum of the costs of an ASHP, a WSHP, and the required buffer tank for the ASHP. This estimated cost comes to a total of \$34,590 for the HSHP unit alone.

According to [59], boiler installation labor and fitting in Fairbanks costs between \$1200 - \$3200. Due to the standard model of the selected equipment, the median value of \$2200 was assumed for this analysis.

With these installation costs known, the total cost of each system was calculated including the equipment costs from the system selection section. The costs for both parts and labor for the selected equipment as introduced in the system selection section of chapter 4 is shown in Table 6.1.

Table 6.1: Equipment and Installation Costs

Equipment	Cost (\$)
Boiler	2,432
Burner	651
ASHP	7,747
80-gallon buffer tank	2,578
Pump	595
HP Valves/Fittings	400
WSHP	24,265
Thermal Tank	1,242
Solar Collector Array	21,599
RSC panel	2,000
Tank to RSC parts	2,800
Tank to Solar Array Parts	2,800
LG AC Unit	469
Installation	Cost (\$)
Boiler	2,200
ASHP	8,250
Buffer Tank	2,800
WSHP	8,250
HSHP	16,500
Thermal Tank	2,800
RSC panel	2,100
Solar Collector Array	21,000

With this information, the capital cost of each system was calculated and compared. With the installation cost calculated, the benefit must also be considered for each system. In this case, there is potential for environmental and economic benefit. To analyze the benefit of each system fully, the operational cost and energy consumption over each system's lifespan

must also be considered. Furthermore, maintenance was also considered as a cost in this analysis.

According to [60], an annual maintenance plan for a boiler system costs from \$200 - \$500. From this, the median value of \$350 was taken as the annual maintenance cost of a boiler system. The average cost of an annual maintenance plan for a heat pump is slightly cheaper, ranging from \$120 - \$360 according to [61]. Here, the median value of \$240 was assumed as the annual heat pump maintenance cost. For the solar collector array and thermal tank, maintenance costs range from .5% to 1% of the initial project cost, according to [62]. In this analysis, it was assumed that .75% of the initial cost of these systems represents the annual maintenance cost. This assumption was further applied to the RSC system in this analysis. Then, the maintenance costs for each system are shown in Table 6.2.

Table 6.2: Annual Maintenance Costs

Annual Maintenance	Cost (\$)
Boiler	350
ASHP	240
WSHP	240
HSHP	240
Solar Collector Array	319.4925
Thermal Tank	72.315
RSC Panel	30.75

The various capital costs of each system were compared in order of increasing cost. The capital costs for each tested system are shown in Table 6.3, Table 6.4, Table 6.5, Table 6.6, and Table 6.7.

Table 6.3: Boiler and LG AC Unit System Capital Costs

Equipment	Cost (\$)
Boiler	2,432
Burner	651
Pump	595
LG AC Unit	469
Installation	Cost (\$)
Boiler	2,200
<b>Total</b>	<b>6,347</b>

Table 6.4: Single ASHP System Capital Costs

Equipment	Cost (\$)
Boiler	2,432
Burner	651
Pump	595
ASHP	7,747
80-gallon buffer tank	2,578
Pump	595
HP Valves/Fittings	400
Installation	Cost (\$)
Boiler	2,200
ASHP	8,250
Buffer Tank	2,800
<b>Total</b>	<b>28,248</b>

Table 6.5: Dual ASHP System Capital Costs

<b>Equipment</b>	<b>Cost (\$)</b>
Boiler	2,432
Burner	651
Pump	595
(x2) ASHPs	15,494
80-gallon buffer tank	2,578
(x2) Pumps	1,190
(x2) HP Valves/Fittings	800
<b>Installation</b>	<b>Cost (\$)</b>
Boiler	2,200
(x2) ASHP	16,500
Buffer Tank	2,800
<b>Total</b>	<b>45,240</b>

Table 6.6: WSHP System Capital Costs

<b>Equipment</b>	<b>Cost (\$)</b>
Boiler	2,432
Burner	651
Pump	595
WSHP	24,265
HP Valves/Fittings	400
Pump	595
Thermal Tank	1,242
Solar Collector Array	21,599
RSC panel	2,000
Tank to RSC parts	2,800
Tank to Solar Array Parts	2,800
<b>Installation</b>	<b>Cost (\$)</b>
Boiler	2,200
WSHP	8,250
Thermal Tank	2,800
RSC panel	2,100
Solar Collector Array	21,000
<b>Total</b>	<b>95,729</b>

Table 6.7: HSHP System Capital Costs

Equipment	Cost (\$)
Boiler	2,432
Burner	651
Pump	595
ASHP	7,747
80-gallon buffer tank	2,578
WSHP	24,265
(x2) HP Valves/Fittings	400
(x2) Pump	595
Thermal Tank	1,242
Solar Collector Array	21,599
RSC panel	2,000
Tank to RSC parts	2,800
Tank to Solar Array Parts	2,800
Installation	Cost (\$)
Boiler	2,200
HSHP	16,500
Buffer Tank	2,800
Thermal Tank	2,800
RSC panel	2,100
Solar Collector Array	21,000
<b>Total</b>	<b>117,104</b>

With the capital and O&M costs defined for each system, the social benefit associated with the reduction of heating oil consumption was calculated.

No. 2 heating oil was used previously in this thesis due to its readily available cost data. Although there is only a small difference of 1.6% in energy density between #1 and #2 type heating oil, there is a significant difference in the amount of sulfate in each [4]. This major

difference in sulfate content directly affects the amount of estimated  $PM_{2.5}$  emissions from each type of fuel, resulting in 48.6% less  $PM_{2.5}$  emitted with No. 1 versus No. 2 heating oil [4]. For this reason, No. 2 heating oil has been banned in the Fairbanks  $PM_{2.5}$  non-attainment area [3], and has been replaced with #1 heating oil. To account for the modern-day use of No. 1 heating oil in the FNSB non-attainment area, the effective  $PM_{2.5}$  emissions from #1 heating oil were used in this section of the analysis. According to the Alaska Department of Environmental Conservation, the emissions of  $PM_{2.5}$  from No. 1 heating oil is predicted at .00234lb/MMBtu [4]. From these values, the effective  $PM_{2.5}$  emissions from heating oil burning was found to be .000146kg/gal.

Quantifying the benefit of emissions reductions requires an estimation of the social cost of each concerning pollutant. The social cost of pollution aims to estimate the monetary damages to the human population and the environment. The social cost of  $PM_{2.5}$  emissions in the US is estimated from \$88,000 - \$130,000 per ton of  $PM_{2.5}$ , according to [63]. This analysis assumed the lower end value of \$88,000/ton or \$97/kg, which has typically been used to calculate the social cost of  $PM_{2.5}$  emissions in Fairbanks [64]. Furthermore, the social cost of  $CO_2$  emissions is estimated as \$210/metric ton or \$.21/kg from [65]. In this analysis, the associated social cost of manufacturing emissions was not considered.

### 6.3 Results

With the costs and benefits calculated, each system was quantitatively compared. In this section, three separate categories each contributed to the overall benefit-cost analysis. This analysis considered the capital costs including equipment and installation, the operation and maintenance costs including fuel and electricity, and the social benefit from the reduction of heating oil combustion emissions. In this section these categories were separately compared for each tested system and were also evaluated together for an overall project benefit-cost analysis over the assumed 15-year lifespan of each system. The annual costs of each system are shown in Table 6.8.

Table 6.8: Annual Cost Comparison of Systems

Annual Cost (\$)	Boiler & LG	ASHP and	2 ASHPs and	WSHP and	HSHP and
	AC Unit	Boiler	Boiler	Boiler	Boiler
Operations	2,252.69	2,131.54	2,066.83	1,845.41	1821.92
Maintenance	350.00	590.00	830.00	1,012.56	1,252.56
Social Cost of CO2	1,053.70	927.69	855.73	819.62	777.64
Social Cost of PM2.5	6.53	4.70	3.61	4.50	3.71

With the annual costs compared separately, the individual cost categories were grouped as shown in Table 6.9 to provide a total project viability comparison.

Table 6.9: 15-Year Project Cost Comparison of Systems

15-year project Costs (\$)	Boiler & LG AC Unit	ASHP and Boiler	2 ASHPs and Boiler	WSHP and Boiler	HSHP and Boiler
Capital	6347.03	28,248.03	45,240.03	95,729.03	117,104.03
O&M	39,040.35	40,823.10	43,452.45	42,869.51	46,117.16
Social	15,903.49	13,985.89	12,890	12,361.70	11,720.24
<b>Total</b>	<b>61,290.87</b>	<b>83,057.02</b>	<b>101,582.50</b>	<b>150,960.20</b>	<b>174,941.40</b>

#### 6.4 Discussion

The benefit-cost analysis gave a simple projection for the total project costs of each HVAC system, considering the capital, social, and O&M costs. This analysis was not intended to provide a rigorous cost projection for a specific installation, but rather to quantitatively compare each system. For this reason, a few simplifications were made to this analysis. Differing from a typical financial analysis, neither the time value of money nor loan interest payments were considered. This methodology provided a simple approximate cost projection for the tested systems, without considering increases in operating costs over time. The relative increases as compared to the baseline system are shown in Table 6.10.

Table 6.10: Relative Cost Compared to a Standard Boiler and Portable AC unit System

% Increased from baseline	ASHP and Boiler	2 ASHPs and Boiler	WSHP and Boiler	HSHP and Boiler
Capital Costs	345.06%	612.78%	1408.25%	1745.02%
Operations Costs	- 5.37%	- 8.25%	- 18.08%	- 19.12%
Maintenance Costs	68.57%	137.14%	189.30%	257.87%
Social Costs	- 12.06%	- 18.95%	- 22.27%	- 26.30%
<b>Total Costs</b>	<b>35.51%</b>	<b>65.74%</b>	<b>146.30%</b>	<b>186.43%</b>

As previously noted in the system configuration study of chapter 5, each tested system costs less than the standard boiler system to operate. With large reductions in heating oil consumption, the social costs of each tested system are significantly lower than the standard system. However, the capital costs skyrocket as new components are added. Although the standard boiler system is expensive to operate and highly emissive, its capital costs are small in comparison to even the simplest ASHP system. Furthermore, increasing HVAC system complexity requires more extensive maintenance. The maintenance costs increased so heavily that they completely negated any savings from the increased operating efficiency. As seen from the Table 6.10, the net O&M costs increase steadily with system complexity. For the typical homeowner, these massive capital and maintenance costs completely outweigh the social benefit and operational cost savings. While the tested systems are all capable of operating at a lower cost, they are far from economically viable in a residential setting in Fairbanks.

As heat pump technology improves, the operational efficiencies of these systems will also improve, and the capital costs will decrease relative to a homeowner's purchasing power. Over time, the barrier will become lower for these renewable systems, while the social costs and emissions of heating oil are likely to grow. Another potential for overcoming the massive capital costs of these renewable HVAC systems are government clean energy assistance programs, such as the FNSB Air Quality Division Change Out Program. This program offers up to \$14,000 to residents in the FNSB  $PM_{2.5}$  non-attainment area who are interested in improving

their heating systems [66]. Currently, the focus of this program is to reduce emissions from wood, pellet and coal by helping with replacement or removal. Additionally, the program helps with conversion or replacement of oil heaters with natural gas heaters. While the systems tested in this thesis are not viable even with this assistance, some components of these systems may be more viable than others. Currently, the FNSB change out program offers up to \$14,000 to assist with replacement of wood, pellet, or coal hydronic heaters with heat pumps [66]. This assistance significantly offsets the high capital cost of a heat pump system. Although it is not currently offered, direct installation of solar thermal collectors for hot water generation has been shown to significantly offset the price of water heating in Fairbanks [67]. This type of installation is commercially available in Fairbanks through private contractors such as [67] who estimate installed costs of solar heating systems starting at around \$10,000. Additional government assistance could make this technology widely accessible for Fairbanks residents, greatly reducing the consumption of heating oil in the FNSB non-attainment area [67].

## Chapter 7: Conclusion

In this thesis, a Python model was developed to simulate the performance of a variety of HVAC systems in a Fairbanks home over a one-year period. This model utilized location specific weather data from TMY3 [31], as well as historic pricing for heating oil and electricity in Fairbanks from the State of Alaska [35] and GVEA [34]. This model was iteratively developed to represent a Fairbanks home with a deadband temperature range of 66°F – 73°F, with a setpoint of 70°F. Variable load distribution controls were implemented which allowed the HVAC system to run for up to 4 hours at a time, limiting the maximum load to 20kW. Furthermore, each HVAC system was selected and sized for optimal performance and low capital cost based on the Fairbanks ASHRAE design temperatures and the maximum heating loads experienced throughout the year. The product data for each of the chosen commercially available HVAC systems was implemented in the model for accuracy, and conservative assumptions were taken outside of the provided values. Each of these realistic HVAC systems were quantitatively compared separately for their heating and air conditioning performance. An emphasis was placed on heating performance evaluation since heating accounts for 92.6% of the total yearly HVAC load in Fairbanks. Finally, the capital, operations and maintenance, and social costs of each system were compared annually and over a 15-year period. This benefit-cost analysis allowed for a true evaluation of the economic viability of each system compared to a heating oil boiler and portable air conditioner, which is typical in Fairbanks homes.

The proposed HSHP system was found to have an operational cost savings of 19.12% for combined cooling and heating as compared to a typical HVAC system composed of a boiler and portable AC unit. The HSHP also reduced the heating oil consumption by 43.1%, resulting in a 26.30% increase in social benefit, specifically from reduced  $CO_2$  and  $PM_{2.5}$  emissions. However, the HSHP system was also found to be the most cost prohibitive, with capital and maintenance costs increasing 1745.02% and 257.87% from the baseline system, respectively.

Other systems were tested including single ASHP, dual ASHP, and WSHP integrated with a thermal storage tank, radiative sky cooling loop, and solar evacuated tube heating array. Each

of these systems achieved operational cost savings and social benefits, but with a disproportionately large increase in capital and maintenance costs from the standard system.

The single ASHP was the most affordable in terms of capital and maintenance cost compared to the standard system but achieved menial savings in operation of only 5.37%. The single ASHP managed to reduce the consumption of heating oil by 28.02% but produced a less impressive social benefit increase of 12.06% due to its relatively low  $CO_2$  emissions savings. The dual ASHP, which effectively provided double the heating capacity, managed to decrease operational costs by 8.25%, decrease heating oil consumption by 44.72%, and increase social benefit by 18.95%. Although the dual ASHP system gave the greatest reduction in heating oil consumption, it heated with an average COP of only 1.95, leading to excessive electricity consumption and associated  $CO_2$  emissions, which resulted in a disproportionately low increase social benefit. Furthermore, both the single and dual ASHP provided air conditioning at an average COP of 2.88, which was poor in comparison to the WSHP and HSHPs COP of 5.82. Even the baseline LG portable AC unit provided a COP of 2.12 at a fraction of the ASHPs capital cost.

The WSHP system reduced the consumption of heating oil by 31.13%, operational costs by 18.08%, and showed a social benefit increase of 22.27% as compared to the standard system. Unfortunately, both the WSHP and HSHP systems were integrated with a thermal storage tank, RSC panel, and solar heating array, which led to extremely high capital and maintenance costs that negated any operational cost savings. The capital investment, maintenance costs, and shear bulk of materials required for both the WSHP and HSHP systems were far too extreme for residential applications in Fairbanks. The WSHP and HSHP systems showed a total project cost increase of 146.30% and 186.43% over 15 years, compared to the standard boiler system. The difference in operational cost savings from the WSHP to the HSHP was found to be minimal and was greatly outweighed by the additional capital and maintenance cost associated with the additional complexity of the HSHP system.

None of the tested systems were found to be economically viable in Fairbanks annually or over a 15-year period. However, each system proved to be effective in reducing operational

costs, heating oil consumption, and  $CO_2$  and  $PM_{2.5}$  emissions. While this study demonstrated a real-world application of the developed model in Fairbanks, the primary contribution of this thesis lies in the versatility and adaptability of the developed Python model for simulating various HVAC systems across different locations. The model's structure enables users to seamlessly input new location-specific data, such as TMY3 weather and energy costs, to conduct a one-year HVAC simulation anywhere such data is available. Although this thesis focuses on a representative Fairbanks home, the model allows for easy modification of building geometry and material properties, providing flexibility in analyzing different structures. Likewise, the HVAC system parameters can be customized, enabling users to input performance specifications for existing commercial equipment or explore emerging technologies in diverse settings. This flexibility makes the model suitable for both residential and commercial applications, supporting cost analysis and advancing research and development in HVAC system optimization.

## **7.1 Limitations and Model Improvements**

Throughout the development of this thesis, several assumptions and limitations were noted which can be improved upon in future studies. This section summarizes these assumptions and limitations for improvement in new applications.

In chapters 2 and 3 of this thesis, a new air source heat pump technology from Samuel et al. [43] was modeled. When chapter 4 was written, this new technology was not yet commercially available, and there was no available product data for heating capacity. Since that time, both the heat pump and its product data have become publicly available, and show promising results for high efficiency space heating in cold climates [43]. While the ASHP from [44] was designed for cold climate operation, it yields a lower COP and heating capacity than the heat pump from [43] at extreme temperatures. In future Fairbanks studies, this new heat pump technology from Samuel et al. should be again considered in analysis.

One of the major improvements made in this thesis from previous studies was the use of SMARTS [33] to generate spectral solar irradiance from TMY3 broadband irradiance data [31]. However, the spectral atmospheric emissivity in this study was calculated using AM1.5

transmissivity, which uses a “clear sky” assumption. As with solar irradiance, the spectral atmospheric emissivity also depends on many meteorological parameters such as precipitable water, which vary greatly throughout the day and year. In a future study which focuses on RSC assisted air conditioning, an approach should be taken to account for variable weather conditions from TMY3 when calculating the spectral atmospheric emissivity. This approach will allow for a more accurate calculation of what radiation is allowed to pass through the atmosphere from the RSC panel, and what radiation is absorbed and reradiated by the atmosphere.

In this thesis, a national average was used to estimate the  $CO_2$  emissions resulting from electricity generation, taken from [46]. While this provided a useful estimate applicable to a wide range of locations, the emissions from electricity depend completely on the methods of generation, which vary greatly across different grids. In many rural Alaskan communities, power generation relies heavily on fossil fuels such as diesel. In these cases, electrification of space heating may not provide a significant reduction in  $CO_2$  emissions. Even in Fairbanks, the electric grid is powered largely by diesel, along with some renewable energy generation. In other regions of Alaska and the United States, there is a higher percentage of natural gas contributing to power generation, which burns significantly cleaner than diesel and has lower resulting emissions. Furthermore, the results of the model are highly sensitive to the value used to calculate the  $CO_2$  emissions from electricity consumption. Future studies should calculate a location specific estimation of the  $CO_2$  emissions from electricity consumption, accounting for the types of generation which power the grid in that area.

For simplicity, a 200W pump was selected for use with each heating and cooling loop in this thesis, and the circulation of the RSC and solar collector loops was not accounted for in calculations. Pumps should be sized and selected specifically according to the required flow conditions. In this thesis, one of the solar collector arrays consisted of 20 collectors, which would likely require a much larger pump, or multiple heating loops/pumps. In future studies, the electricity consumption for circulating pumps should be considered during the system selection process, where pumps should be sized appropriately for each loop application. This

will provide a more rigorous calculation of the electricity consumed during the circulation of each heating and cooling loop.

In this thesis, values for installation and maintenance of HVAC systems were estimated from location specific construction estimation tools [58], [59], [59], [60], [57], [58], [61]. While these estimates provided a useful approximation for capital and maintenance costs in the Fairbanks area, pricing for HVAC installations varies with installation conditions, material costs, contractor availability, and even time of year. For this reason, future studies should use estimates directly from a certified contractor taken at the time of the study.

The benefit-cost analysis provides a simplified comparison of the various costs and benefits associated with each tested system. In this analysis, the costs of electricity, fuel, and maintenance are not adjusted for inflation over time. The time value of money is not considered in this simple analysis, nor is the interest rate associated with any potentially required loans. In future studies focused on economic viability, a more robust financial analysis should be carried out to fully consider the value of the tested systems over their lifespan.

In the system optimization study of chapter 4, a technique was employed to choose the optimal component sizes for the renewable energy systems, balancing optimized performance with low capital cost. There are several improvements which could be made upon this approach in future studies. When optimizing these component sizes for low operational cost, a single-variable optimization technique was used to search for a local minimum. Here, only one component size was varied, and the lowest operational cost was searched for. This process was only executed once. In future studies, a multivariable optimization technique could be used to search for a global minimum, corresponding to the lowest possible cost of all component configurations. An iterative approach could also be taken to improve upon the single-variable optimization technique. Furthermore, a statistical approach was not taken when balancing low operating costs with low capital costs. Instead, a reasonable commercially available component size was chosen graphically. An improved study might weigh the operational benefits over the lifespan of the component with the capital cost, taking the time value of money into consideration to select an optimal component size.

In its current state, the model developed throughout this thesis takes the form of a Python script. To use the model, a user must manually adjust the code to make changes, run the model, and perform post-processing. These tasks are non-trivial and require a user to carefully study the model structure. To make this model easily applicable to more locations and different HVAC components, a user interface should be developed for ease of operation. This interface would prompt a user to upload the required data and provide location specific parameters such as latitude, and  $CO_2$  emissions from electricity generation in the area. With these improvements in place, the model can be used to provide a powerful analysis of HVAC system operation across a wide range of applications.

### Nomenclature

Symbol	Value	Brief Description of the Constant	Units	Source
$ACH$	.35	Air changes per hour	$h^{-1}$	[40]
$A_{floor}$	218.42	Surface area of floor	$m^2$	C. Hnilicka
$A_{roof}$	277.20	Surface area of roof	$m^2$	C. Hnilicka
$A_{RSC}$	10	Area of the RSC panel	$m^2$	Assumed
$A_{sc}$	10	Area of the solar collector	$m^2$	Assumed
$A_{walls}$	204.11	Surface area of walls	$m^2$	C. Hnilicka
$A_{windows}$	19.60	Total window area	$m^2$	C. Hnilicka
$B(\lambda)$	Varies	Blackbody spectral emissive power by Planck's law	$\frac{W}{m^2 \cdot \mu m}$	[42]

Symbol	Value	Brief Description of the Constant	Units	Source
$C_B$	22925.34	Heat capacity of building	$\frac{Wh}{K}$	Calculated
$C_{cladding}$	Varies	Heat capacity of sheet metal roofing and siding	$\frac{Wh}{K}$	Calculated
$C_{drywall}$	Varies	Heat capacity of gypsum drywall	$\frac{Wh}{K}$	Calculated
$C_{floor}$	Varies	Heat capacity of floor	$\frac{Wh}{K}$	Calculated
$C_{framing}$	Varies	Heat capacity of framing	$\frac{Wh}{K}$	Calculated
$C_{insulation}$	Varies	Heat capacity of insulation	$\frac{Wh}{K}$	Calculated
$C_{plywood}$	Varies	Heat capacity of plywood	$\frac{Wh}{K}$	Calculated
$C_{windows}$	Varies	Heat capacity of windows	$\frac{Wh}{K}$	Calculated

Symbol	Value	Brief Description of the Constant	Units	Source
$C_1$	$3.74 \times 10^8$	First constant for Planck's law	$W \cdot m^2$	[39]
$C_2$	$1.44 \times 10^9$	Second constant for Planck's law	$\mu m \cdot K$	[39]
$CEER$	7.22	Combined Energy Efficiency Ratio	$\frac{BTU}{h} \cdot W^{-1}$	[56]
$COP_{ASHP}$	Varies	Coefficient of performance of the ASHP	Dimensionless	Calculated
$COP_{WSHP}$	Varies	Coefficient of performance of the WSHP	Dimensionless	Calculated
$CO2_{ASHP}$	Varies	$CO_2$ emissions from ASHP	$kg$	Calculated
$CO2_{boiler}$	Varies	$CO_2$ emissions from boiler	$kg$	Calculated
$CO2_{electricity}$	.00039	Emissions associated with distributed electricity	$\frac{kg}{Wh}$	[46]

Symbol	Value	Brief Description of the Constant	Units	Source
$CO2_{oil}$	10.21	$CO_2$ combustion emissions of No. 2 heating oil	$\frac{kg}{gal}$	[45]
$CO2_{WSHP}$	Varies	$CO_2$ emissions from WSHP	$kg$	Calculated
$c_{cladding}$	.49	Specific heat of steel sheet metal siding and roofing	$\frac{kJ}{kg \cdot K}$	[68]
$c_{concrete}$	.653	Specific heat of concrete	$\frac{kJ}{kg \cdot K}$	[39]
$c_{glass}$	.8	Specific heat of glass	$\frac{kJ}{kg \cdot K}$	[39]
$c_{gypsum}$	1.09	Specific heat of gypsum	$\frac{kJ}{kg \cdot K}$	[39]
$c_{insulation}$	2.1	Specific heat of wood fiber insulation	$\frac{kJ}{kg \cdot K}$	[69]
$c_{plywood}$	1.21	Specific heat of Douglas fir plywood	$\frac{kJ}{kg \cdot K}$	[39]

Symbol	Value	Brief Description of the Constant	Units	Source
$c_{wood}$	1.38	Specific heat of soft wood	$\frac{kJ}{kg \cdot K}$	[39]
$cp_{air}$	1005	Specific heat capacity of dry air at constant pressure	$\frac{J}{kg \cdot K}$	[39]
$cp_{glycol}$	3559	Heat capacity of glycol mixture at constant pressure	$\frac{J}{kg \cdot K}$	[70]
$cp_{water}$	4186	Heat capacity of water at ambient temperature and at constant pressure	$\frac{J}{kg \cdot K}$	[39]
$cp_{water vapor}$	1840	Heat capacity of water averaged over -40°F to 70°F at constant pressure	$\frac{J}{kg \cdot K}$	[39]
$DHI$	Varies	Diffuse horizontal irradiance	$\frac{W}{m^2}$	[31]
$DNI$	Varies	Direct normal irradiance	$\frac{W}{m^2}$	[31]
$day$	1 – 365	Day of the year	$day$	Calculated

Symbol	Value	Brief Description of the Constant	Units	Source
$d\lambda$	.01	Incremental change in wavelength used for integration	$\mu m$	Assumed
$d\theta$	$\frac{\pi}{32}$	Incremental change in polar angle used for integration	radians	Assumed
$E_{WSHP}$	Varies	Electricity consumed by the WSHP	kWh	Calculated
$E_{ASHP}$	Varies	Electricity consumed by the ASHP	kWh	Calculated
$E_{boiler}$	Varies	Electricity consumed by the boiler	kWh	Calculated
$E_{pump}$	.2	Pump operational power consumption	kWh	[44]
$EER$	Varies	Energy Efficiency Ratio	$\frac{BTU}{h} \cdot W^{-1}$	Calculated
$F_{boiler}$	Varies	Fuel consumed by boiler	gal	Calculated

Symbol	Value	Brief Description of the Constant	Units	Source
$FR$	.77	Solar collector heat removal factor	<i>Dimensionless</i>	Assumed
$GHI$	Varies	Global horizontal irradiance	$\frac{W}{m^2}$	[31]
$HI$	Varies	Solar irradiance incident on a horizontal surface	$\frac{W}{m^2}$	Calculated
$HVF$	Varies	View factor of the sun on a horizontal surface	<i>Dimensionless</i>	Calculated
$h$	Varies	Variable convection coefficient	$\frac{W}{m^2 \cdot K}$	[8]
$h_{dry}$	Varies	Specific enthalpy of dry air	$\frac{J}{kg}$	Calculated
$h_{in}$	Varies	Specific enthalpy of the inside air	$\frac{J}{kg}$	Calculated
$h_{out}$	Varies	Specific enthalpy of the ambient air	$\frac{J}{kg}$	Calculated

Symbol	Value	Brief Description of the Constant	Units	Source
$h_{set}$	Varies	Specific enthalpy of moist air at setpoint temperature	$\frac{J}{kg}$	Calculated
$h_{vapor}$	Varies	Specific enthalpy of water vapor in air	$\frac{J}{kg}$	Calculated
$hour$	1 – 24	Hour of the day	$h$	Calculated
$LHV_{oil}$	$44349.9 \times 10^3$	Lower Heating Value of No. 2 Heating Oil	$\frac{J}{kg}$	[71]
$m_{air}$	Varies	Mass of moist air inside home	$kg$	Calculated
$m_{glycol}$	Varies	Total mass of glycol solution	$kg$	Calculated
$\dot{m}_{air}$	Varies	Mass flow rate of air	$\frac{kg}{s}$	Calculated
$P_{air}$	Varies	Ambient air pressure	$Pa$	[31]

Symbol	Value	Brief Description of the Constant	Units	Source
$P_{atm}$	101325	Atmospheric pressure	Pa	[39]
$P_{sat\ vapor}$	Varies	Saturation pressure of water vapor in air	Pa	Calculated
$P_{vapor}$	Varies	Partial pressure of water vapor in air	Pa	Calculated
$q_{floor}$	Varies	Rate of heat loss through floor	W	Calculated
$q_{Loss}$	Varies	Net rate of heat loss from home	W	Calculated
$q_{net}$	Varies	Net rate of heat transfer into the thermal tank	W	Calculated
$q_{roof}$	Varies	Rate of heat loss through roof	W	Calculated
$q_{RSC}$	Varies	Net rate of heat transfer absorbed by RSC panel	W	Calculated

Symbol	Value	Brief Description of the Constant	Units	Source
$q_{walls}$	Varies	Rate of heat loss through walls	W	Calculated
$q_{windows}$	Varies	Rate of heat loss through windows	W	Calculated
$q_{WSHP\ Cond}$	Varies	Rate of heat transfer out of tank into the WSHP's condenser	W	Calculated
$q_{ventilation}$	Varies	Rate of heat loss through ventilation	W	Calculated
$q_{latent}^*$	$2500.9 \times 10^3$	Specific latent heat of vaporization of water	$\frac{J}{kg}$	[39]
$Q_{Load}$	Varies	Heat energy required to bring home back to setpoint	Wh	Calculated
$Q_{Loss}$	Varies	Heat energy lost from the home in a one-hour heating cycle	Wh	Calculated
$Q_{net}$	Varies	Net heat energy transferred into the tank in a one-hour heating and cooling cycle	Wh	Calculated

Symbol	Value	Brief Description of the Constant	Units	Source
$q_{sensible}^*$	Varies	Specific sensible heat	$\frac{J}{kg}$	Calculated
$q''_{atm}$	Varies	Rate of heat flux absorbed by RSC panel from atmospheric radiation	$\frac{W}{m^2}$	Calculated
$q''_{conv}$	Varies	Rate of heat flux absorbed by RSC panel from convection	$\frac{W}{m^2}$	Calculated
$q''_{space}$	Varies	Rate of heat flux lost by RSC panel to deep space	$\frac{W}{m^2}$	Calculated
$q''_{sun}$	Varies	Rate of heat flux absorbed by RSC panel from the sun	$\frac{W}{m^2}$	Calculated
$R_{air}$	286.9	Gas constant for dry air	$\frac{J}{kg \cdot K}$	[72]
$R_{floor}$	50.5	Insulation R-value for floor	$\frac{m^2 \cdot K}{W}$	C. Hnilicka
$R_{roof}$	75.3	Insulation R-value for roof	$\frac{m^2 \cdot K}{W}$	C. Hnilicka

Symbol	Value	Brief Description of the Constant	Units	Source
$R_{walls}$	38.976	Insulation R-value for walls	$\frac{m^2 \cdot K}{W}$	C. Hnilicka
$R_{vapor}$	461.5	Gas constant for water vapor	$\frac{J}{kg \cdot K}$	[72]
$S$	.5	Exterior wall shading factor	Dimensionless	Assumed
$SSI$	Varies	Spectral solar irradiance (GHI)	$\frac{W}{m^2 \cdot \mu m}$	[33]
$ST$	.09375	Scaling factor for wood framing stud spacing	Dimensionless	Assumed
$T_{amb}$	Varies	Ambient air temperature	K	[31]
$T_{set}$	294.25	Setpoint temperature	K	Assumed
$T_{sol-air walls}$	Varies	Effective temperature on exterior wall surface	K	Calculated

Symbol	Value	Brief Description of the Constant	Units	Source
$T_{sol-air\ roof}$	Varies	Effective temperature on exterior roof surface	K	Calculated
$T_{tank}$	Varies	Initial temperature of the tank	K	Calculated
$TB_{water}$	373.15	Boiling point of water	K	[39]
$TI$	Varies	Solar irradiance incident on a tilted surface	$\frac{W}{m^2}$	Calculated
$TVF$	Varies	View factor of the sun on a tilted surface	Dimensionless	Calculated
$t_{floor}$	.15	Thickness of concrete slab	m	Assumed
$t_{gypsum}$	.012	Thickness of gypsum drywall	m	Assumed
$t_{glass}$	.005	Thickness of glass windows	m	Assumed

Symbol	Value	Brief Description of the Constant	Units	Source
$t_{wood}$	.28575	Thickness of soft wood framing	$m$	Assumed
$t_{insulation}$	.28575	Thickness of wood fiber batt insulation	$m$	Assumed
$t_{plywood}$	.0127	Thickness of Douglas fir plywood sheathing	$m$	Assumed
$t_{cladding}$	.00061	Thickness of steel sheet metal siding and roofing	$m$	Assumed
$U_{sc}$	15.7	Solar collector overall heat loss coefficient	$\frac{W}{m^2 \cdot K}$	Assumed
$U_{windows}$	.22	U-value for windows	$\frac{W}{m^2 \cdot K}$	C. Hnilicka
$V_{tank}$	Varies	Volume of the tank	$m^3$	Assumed
<i>Vent Rate</i>	Varies	Home's air ventilation rate	$\frac{m^3}{h}$	Calculated

Symbol	Value	Brief Description of the Constant	Units	Source
$VI$	Varies	Solar irradiance incident on a vertical surface	$\frac{W}{m^2}$	Calculated
$VVF$	Varies	View factor of the sun on a vertical surface	<i>Dimensionless</i>	Calculated
$WC$	.6	Window curtain shading factor	<i>Dimensionless</i>	Assumed
$\alpha_{house}$	.91	Absorptivity of building	<i>Dimensionless</i>	[73]
$\alpha_{sc}$	.9	Collector absorptance	<i>Dimensionless</i>	Assumed
$\beta$	Varies	Tilt angle of the solar evacuated tube heater	radians	Calculated
$\Delta H_{air}$	Varies	Change in enthalpy of the inside air	Wh	Calculated
$\Delta H_{building}$	Varies	Change in enthalpy of the building	Wh	Calculated

Symbol	Value	Brief Description of the Constant	Units	Source
$\Delta H_{sys}$	Varies	Change in enthalpy of the system	Wh	Calculated
$\delta_{day}$	Varies	Daily initial solar declination angle	radians	Calculated
$\delta_{hour}$	Varies	Solar declination hour angle	radians	Calculated
$\varepsilon_{atm}(\lambda, \theta)$	Varies	Spectral emissivity of the atmosphere	Dimensionless	Calculated
$\varepsilon_{house}$	.91	Emissivity of building	Dimensionless	[74]
$\varepsilon_{RSC}(\lambda)$	Varies	Spectral emissivity of RSC panel	Dimensionless	[12]
$\eta_{boiler}$	Varies	Boiler efficiency	Dimensionless	[52]
$\theta$	0 to $\frac{\pi}{2}$ with a resolution of $\frac{\pi}{32}$	Polar angle	radians	Assumed

Symbol	Value	Brief Description of the Constant	Units	Source
$\theta_Z$	Varies	Zenith angle	radians	Calculated
$\lambda$	.3 to 15 with a resolution of .01	Wavelength	$\mu\text{m}$	Assumed
$v_{wind}$	Varies	Wind speed	$\frac{\text{m}}{\text{s}}$	[31]
$\rho_{air}$	Varies	Ambient air density	$\frac{\text{kg}}{\text{m}^3}$	Calculated
$\rho_{cladding}$	7851	Density of steel sheet metal siding and roofing	$\frac{\text{kg}}{\text{m}^3}$	[75]
$\rho_{concrete}$	2300	Density of concrete	$\frac{\text{kg}}{\text{m}^3}$	[39]
$\rho_{glass}$	2230	Density of glass	$\frac{\text{kg}}{\text{m}^3}$	[39]
$\rho_{glycol}$	1055	Density of 50/50 Propylene Glycol mixture	$\frac{\text{kg}}{\text{m}^3}$	[70]

Symbol	Value	Brief Description of the Constant	Units	Source
$\rho_{gypsum}$	800	Density of gypsum	$\frac{kg}{m^3}$	[39]
$\rho_{insulation}$	50	Density of wood fiber insulation	$\frac{kg}{m^3}$	[69]
$\rho_{oil}$	875	Density of No. 2 heating oil at 15°C	$\frac{kg}{m^3}$	[71]
$\rho_{plywood}$	545	Density of Douglas fir plywood	$\frac{kg}{m^3}$	[75]
$\rho_{water}$	997	Density of water	$\frac{kg}{m^3}$	[39]
$\rho_{wood}$	513	Density of soft wood	$\frac{kg}{m^3}$	[39]
$\tau_{atm(\lambda)}$	Varies	Spectral atmospheric transmissivity	Dimensionless	[8]
$\tau_{sc}$	.9	Collector glass transmittance	Dimensionless	Assumed

Symbol	Value	Brief Description of the Constant	Units	Source
$\tau_{windows}$	.7	Transmittance of windows	<i>Dimensionless</i>	C. Hnilicka
$\varphi$	Varies	Latitude of Fairbanks	radians	[31]
$\omega$	Varies	Absolute humidity	<i>Dimensionless</i>	Calculated
$\$_{ASHP}$	Varies	Cost to run the ASHP	US Dollar (\$)	Calculated
$\$_{boiler}$	Varies	Cost to run the boiler	US Dollar (\$)	Calculated
$\$_{electricity}$	Varies	Electricity price	$\frac{\$}{kWh}$	[34]
$\$_{heating oil}$	Varies	Heating oil price	$\frac{\$}{gal}$	[35]
$\$_{WSHP}$	Varies	Cost to run the WSHP	US Dollar (\$)	Calculated

## References

- [1] A. Moon *et al.*, “Primary Sulfate Is the Dominant Source of Particulate Sulfate during Winter in Fairbanks, Alaska,” *ACS EST Air*, vol. 1, no. 3, pp. 139–149, Mar. 2024, doi: 10.1021/acsestair.3c00023.
- [2] “Air-Quality-Comprehensive-Plan-PDF.pdf.” Accessed: Feb. 19, 2025. [Online]. Available: <https://www.fnsb.gov/DocumentCenter/View/1209/Air-Quality-Comprehensive-Plan-PDF>
- [3] A. N.-P. & M. Sources, “Fairbanks Nonattainment Area Fuel Switch Requirement.” Accessed: Feb. 19, 2025. [Online]. Available: <https://dec.alaska.gov/air/anpms/communities/fbks-pm2-5-fuel-switch-requirement/>
- [4] Alaska Department of Energy Conservation, “STF-12.” 2019. Accessed: Feb. 19, 2025. [Online]. Available: <https://dec.alaska.gov/media/16210/iiid707-control-strategies-public-notice-draft.pdf>
- [5] O. US EPA, “Health and Environmental Effects of Particulate Matter (PM).” Accessed: Feb. 19, 2025. [Online]. Available: <https://www.epa.gov/pm-pollution/health-and-environmental-effects-particulate-matter-pm>
- [6] Rod Boyce, “Study finds home heating fuel is direct source of sulfate in Fairbanks winter air | Geophysical Institute,” UAF Geophysical Institute. Accessed: Feb. 19, 2025. [Online]. Available: <https://www.gi.alaska.edu/news/study-finds-home-heating-fuel-direct-source-sulfate-fairbanks-winter-air>
- [7] A. L. Association, “Fairbanks Ranks as Most-Polluted City in the Nation.” Accessed: Feb. 19, 2025. [Online]. Available: <https://www.lung.org/media/press-releases/fairbanks-ranks-as>
- [8] R. J. Magrath, “Radiative Emitter Assisted Space Cooling in Alaska,” M.S., University of Alaska Fairbanks, United States -- Alaska, 2024. Accessed: Feb. 20, 2025. [Online]. Available: <https://www.proquest.com/docview/3051826133/abstract/EEFC66EF34914442PQ/1>
- [9] A. P. Raman, M. A. Anoma, L. Zhu, E. Rephaeli, and S. Fan, “Passive radiative cooling below ambient air temperature under direct sunlight,” *Nature*, vol. 515, no. 7528, pp. 540–544, Nov. 2014, doi: 10.1038/nature13883.
- [10] D. Zhao *et al.*, “Radiative sky cooling: Fundamental principles, materials, and applications,” *Appl. Phys. Rev.*, vol. 6, no. 2, p. 021306, Jun. 2019, doi: 10.1063/1.5087281.

- [11] P. Poredoš *et al.*, “Radiative sky cooling thermal concentration with cooling power exceeding one kW per square meter,” *Energy Environ. Sci.*, vol. 17, no. 6, pp. 2336–2355, Mar. 2024, doi: 10.1039/D3EE03214K.
- [12] S. Yoon *et al.*, “Performance analysis of a hybrid HVAC system consisting of a solar thermal collector and a radiative cooling panel,” *Energy Build.*, vol. 241, p. 110921, Jun. 2021, doi: 10.1016/j.enbuild.2021.110921.
- [13] D. Singh, S. P. Singh, M. Agnihotri, K. Palley, and A. K. Singh, “An Experimental and Economic Study of room heating through Solar Evacuated Tube Collector,” *Int. J. Res. Advent Technol.*, vol. 7, no. 1, pp. 516–519, Feb. 2019, doi: 10.32622/ijrat.71201998.
- [14] Ashutosh Sharma, “(PDF) Performance Investigation of Evacuated Tube Solar Heating System: A Review,” ResearchGate. Accessed: Feb. 20, 2025. [Online]. Available: [https://www.researchgate.net/publication/329337053\\_Performance\\_Investigation\\_of\\_Evacuated\\_Tube\\_Solar\\_Heating\\_System\\_A\\_Review](https://www.researchgate.net/publication/329337053_Performance_Investigation_of_Evacuated_Tube_Solar_Heating_System_A_Review)
- [15] SunMaxx Solar, “ThermoPower™ 20 Tube Evacuated Tube Collector,” SunMaxx Solar. Accessed: Feb. 20, 2025. [Online]. Available: <https://www.sunmaxxsolar.com/product/20-evacuated-tube-collector/>
- [16] I. Budihardjo and G. L. Morrison, “Performance of water-in-glass evacuated tube solar water heaters,” *Sol. Energy*, vol. 83, no. 1, pp. 49–56, Jan. 2009, doi: 10.1016/j.solener.2008.06.010.
- [17] H. Hassan, S. Abo-Elfadl, and M. F. El-Dosoky, “An experimental investigation of the performance of new design of solar air heater (tubular),” *Renew. Energy*, vol. 151, pp. 1055–1066, May 2020, doi: 10.1016/j.renene.2019.11.112.
- [18] X. Li *et al.*, “Combination principle of hybrid sources and three typical types of hybrid source heat pumps for year-round efficient operation,” *Energy*, vol. 193, p. 116772, Feb. 2020, doi: 10.1016/j.energy.2019.116772.
- [19] D. Wu, B. Hu, and R. Z. Wang, “Performance simulation and exergy analysis of a hybrid source heat pump system with low GWP refrigerants,” *Renew. Energy*, vol. 116, pp. 775–785, Feb. 2018, doi: 10.1016/j.renene.2017.10.024.
- [20] S. Zhang, S. Liu, J. Wang, Y. Li, and Z. Yu, “Analysis of a solar-assisted heat pump system with hybrid energy storage for space heating,” *Appl. Therm. Eng.*, vol. 231, p. 120884, Aug. 2023, doi: 10.1016/j.applthermaleng.2023.120884.
- [21] R. A. Jordan, J. T. Yamasaki, V. Silveira Júnior, and E. C. B. Dória, “HYBRID SOLAR HEAT PUMP SYSTEM FOR WATER HEATING,” *Eng. Agríc.*, vol. 39, no. 4, pp. 419–425, Aug. 2019, doi: 10.1590/1809-4430-eng.agric.v39n4p419-425/2019.

- [22] M. Haller and E. Frank, “On the Potential of Using Heat From Solar Thermal Collectors for Heat Pump Evaporators,” in *Proceedings of the ISES Solar World Congress 2011*, Kassel, Germany: International Solar Energy Society, 2011, pp. 1–10. doi: 10.18086/swc.2011.26.06.
- [23] G. Mohammed, A. Saleh, and A. H. Khalifa, “A comprehensive review of the hybrid heating systems consisting of heat pumps and solar collectors for hot water and space heating application,” *Eng. Technol. J.*, vol. 0, no. 0, pp. 1–17, Jul. 2024, doi: 10.30684/etj.2024.146976.1696.
- [24] L. Wang *et al.*, “Experimental performance analysis of a dual source heat pump integrated with thermal energy storage,” in *Proceedings of the IGSHPA Research Track 2022*, International Ground Source Heat Pump Association, 2022. doi: 10.22488/okstate.22.000036.
- [25] A. de Gracia and L. F. Cabeza, “Phase change materials and thermal energy storage for buildings,” *Energy Build.*, vol. 103, pp. 414–419, Sep. 2015, doi: 10.1016/j.enbuild.2015.06.007.
- [26] D. Zhao *et al.*, “Radiative sky cooling: Fundamental principles, materials, and applications,” *Appl. Phys. Rev.*, vol. 6, no. 2, p. 021306, Jun. 2019, doi: 10.1063/1.5087281.
- [27] F. Jerald, “Enhancing Energy Efficiency in HVAC Systems through Intelligent Control Strategies,” *Adv. Nonlinear Var. Inequalities*, vol. 28, no. 1s, pp. 57–74, Nov. 2024, doi: 10.52783/anvi.v28.2187.
- [28] S. I. Noubissie Tientcheu, S. P. Chowdhury, and T. O. Olwal, “Intelligent Energy Management Strategy for Automated Office Buildings,” *Energies*, vol. 12, no. 22, p. 4326, Nov. 2019, doi: 10.3390/en12224326.
- [29] C. Gomez-Otero, R. Martinez, and J. Caffarel, “ClimApp: A novel approach of an intelligent HVAC control system,” in *7th Iberian Conference on Information Systems and Technologies (CISTI 2012)*, Jun. 2012, pp. 1–6. Accessed: Feb. 20, 2025. [Online]. Available: <https://ieeexplore.ieee.org/document/6263228>
- [30] Y. Peng, A. Rysanek, Z. Nagy, and A. Schlueter, “Case Study Review: Prediction Techniques in Intelligent HVAC Control Systems,” p. 8 p., Oct. 2016, doi: 10.3929/ETHZ-B-000130722.
- [31] S. Wilcox and W. Marion, “Users Manual for TMY3 Data Sets,” *Tech. Rep.*, 2008. [Online]. Available: <https://www.nrel.gov/docs/fy08osti/43156.pdf>
- [32] “‘Alaska’s Changing Environment’ — a new report.” Accessed: Feb. 20, 2025. [Online]. Available: <https://www.uaf.edu/news/alaskas-changing-environment-new-report.php>

- [33] “SMARTS: Simple Model of the Atmospheric Radiative Transfer of Sunshine.” Accessed: Feb. 20, 2025. [Online]. Available: <https://www.nrel.gov/grid/solar-resource/smarts.html>
- [34] GVEA, “Historic Residential Rates.” Accessed: Feb. 20, 2025. [Online]. Available: <https://www.gvea.com/wp-content/uploads/Historic-Residential-Rates-2009-Present-1.pdf>
- [35] “State of Alaska Geoportal.” Accessed: Feb. 20, 2025. [Online]. Available: <https://gis.data.alaska.gov/datasets/e08c3faedf7842b382f415511402d9d1/explore?location=56.914959,75.816571,2.97>
- [36] “NumPy.” Accessed: Feb. 20, 2025. [Online]. Available: <https://numpy.org/>
- [37] *Transactions of the American Society of Mechanical Engineers 1946: Vol 68.* American Society of Mechanical Engineers, 1946. Accessed: Feb. 20, 2025. [Online]. Available: [http://archive.org/details/sim\\_american-society-of-mechanical-engineers-transactions\\_1946\\_68](http://archive.org/details/sim_american-society-of-mechanical-engineers-transactions_1946_68)
- [38] “Moist Air - Density vs. Water Content and Temperature.” Accessed: Feb. 20, 2025. [Online]. Available: [https://www.engineeringtoolbox.com/density-air-d\\_680.html](https://www.engineeringtoolbox.com/density-air-d_680.html)
- [39] Y. A. Çengel, M. A. Boles, and M. Kanoglu, *Thermodynamics: an engineering approach*, Ninth edition. New York, NY: McGraw-Hill Education, 2019.
- [40] “Addendum n to ANSI/ASHRAE Standard 62-2001, Ventilation for Acceptable Indoor Air Quality”. [Online]. Available: [https://www.ashrae.org/File%20Library/Technical%20Resources/Standards%20and%20Guidelines/Standards%20Addenda/62-2001/62-2001\\_Addendum-n.pdf](https://www.ashrae.org/File%20Library/Technical%20Resources/Standards%20and%20Guidelines/Standards%20Addenda/62-2001/62-2001_Addendum-n.pdf)
- [41] “Integration (scipy.integrate) — SciPy v1.15.2 Manual.” Accessed: Feb. 21, 2025. [Online]. Available: <https://docs.scipy.org/doc/scipy/tutorial/integrate.html>
- [42] T. L. Bergman and F. P. Incropera, Eds., *Fundamentals of heat and mass transfer*, 7th ed. Hoboken, NJ: Wiley, 2011.
- [43] Nick Samuel, “Analysis of cold climate performance of residential heat pump: Field test in Fairbanks, Alaska,” *ASHRAE Winter Conf.*, vol. OR-25-C153, Feb. 2025.
- [44] “Arctic Heat Pump EVI - V4.6 - 2024.” Arctic Heat Pumps, 2025. [Online]. Available: [https://www.arcticheatpumps.com/?gad\\_source=1&gclid=CjwKCAiAlPu9BhAjEiwA5NDSA44PhE2Vos70XMV37iZyekcz43NYqFKbhpWc2m0azk8HqlwBUvWUhhoCzH8QAvD\\_BwE](https://www.arcticheatpumps.com/?gad_source=1&gclid=CjwKCAiAlPu9BhAjEiwA5NDSA44PhE2Vos70XMV37iZyekcz43NYqFKbhpWc2m0azk8HqlwBUvWUhhoCzH8QAvD_BwE)
- [45] “Emission Factors for Greenhouse Gas Inventories,” 2011. [Online]. Available: [https://www.epa.gov/sites/default/files/2015-07/documents/emission-factors\\_2014.pdf](https://www.epa.gov/sites/default/files/2015-07/documents/emission-factors_2014.pdf)

- [46] “Frequently Asked Questions (FAQs) - U.S. Energy Information Administration (EIA).” Accessed: Feb. 21, 2025. [Online]. Available: <https://www.eia.gov/tools/faqs/faq.php>
- [47] T. Duszynski, “Home Energy Rating Certificate.” Alaska Housing Finance Corporation, Aug. 05, 2024.
- [48] “Reference Air Mass 1.5 Spectra.” Accessed: Feb. 21, 2025. [Online]. Available: <https://www.nrel.gov/grid/solar-resource/spectra-am1.5.html>
- [49] “Design Temperature Limit Reference Guide (2015 Ed) - ENERGY STAR Certified Homes\_Rev10.pdf.” Accessed: Feb. 23, 2025. [Online]. Available: [https://www.energystar.gov/sites/default/files/asset/document/Design%20Temperature%20Limit%20Reference%20Guide%20%282015%20Ed%29%20-%20ENERGY%20STAR%20Certified%20Homes\\_Rev10.pdf](https://www.energystar.gov/sites/default/files/asset/document/Design%20Temperature%20Limit%20Reference%20Guide%20%282015%20Ed%29%20-%20ENERGY%20STAR%20Certified%20Homes_Rev10.pdf)
- [50] www.supplyhouse.com, “386-701-012 - Weil-McLain 386-701-012 - WGO-2 - 75,000 BTU Output Cast Iron Gold Oil Boiler - Series 4,” SupplyHouse.com. Accessed: Feb. 23, 2025. [Online]. Available: <https://www.supplyhouse.com/Weil-McLain-386-701-012-WGO-2-75000-BTU-Output-Cast-Iron-Gold-Oil-Boiler-Series-4>
- [51] www.supplyhouse.com, “386-700-392 - Weil-McLain 386-700-392 - GO-2 Beckett Oil Burner, for WGO-2, 386-700-392,” SupplyHouse.com. Accessed: Feb. 23, 2025. [Online]. Available: <https://www.supplyhouse.com/Weil-McLain-386-700-392-GO-2-Beckett-Oil-Burner-for-WGO-2-7211000-p>
- [52] “Weil-McLain-386-701-012-Brochure.pdf.” Accessed: Feb. 23, 2025. [Online]. Available: [https://s3.amazonaws.com/s3.supplyhouse.com/product\\_files/Weil-McLain-386-701-012-Brochure.pdf](https://s3.amazonaws.com/s3.supplyhouse.com/product_files/Weil-McLain-386-701-012-Brochure.pdf)
- [53] “Greensource SI Series Model CE Residential Geothermal Heat Pump Engineering Submittal Sheet.” Bosch. Accessed Feb 12, 2025. [Online]. [https://www.bosch-homecomfort.com/us/media/country\\_pool/documents/engineering-submittal-sheets/water-to-air-water-source-heat-pumps/btc761808101m\\_bosch\\_ce\\_ess\\_09.2023.pdf](https://www.bosch-homecomfort.com/us/media/country_pool/documents/engineering-submittal-sheets/water-to-air-water-source-heat-pumps/btc761808101m_bosch_ce_ess_09.2023.pdf)
- [54] “Efficiently Heat Your Home with Evacuated Tube Solar Collectors from SunMaxx.” Accessed: Feb. 23, 2025. [Online]. Available: <https://www.sunmaxxsolar.com/product/30-evacuated-tube-collector/>
- [55] “2000 Gallon Fresh Water Storage Tank ... IN STOCK,” All About Tanks. Accessed: Feb. 23, 2025. [Online]. Available: <https://allabouttanks.com/products/2000-gallon-vertical-tank2>
- [56] “8,000 BTU Portable Air Conditioner - LP0821GSSM,” LG USA. Accessed: Feb. 23, 2025. [Online]. Available: <https://www.lg.com/us/air-conditioners/lg-lp0821gssm-portable-air-conditioner>

- [57] “2025 Solar Water Heater Cost & Installation Prices,” HomeGuide. Accessed: Feb. 23, 2025. [Online]. Available: <https://homeguide.com/costs/solar-water-heater-cost>
- [58] “Heat Pump Cost in Fairbanks, Alaska.” Accessed: Feb. 23, 2025. [Online]. Available: <https://www.homeblue.com/heat-pump/fairbanks-ak-heat-pump-cost.htm>
- [59] “2025 New Boiler Installation & Replacement Costs,” HomeGuide. Accessed: Feb. 23, 2025. [Online]. Available: <https://homeguide.com/costs/boiler-replacement-cost>
- [60] “2025 Boiler Service Cost — Repairs, Inspection, & Annual Charges,” HomeGuide. Accessed: Feb. 23, 2025. [Online]. Available: <https://homeguide.com/costs/boiler-service-cost>
- [61] “How Much Does Heat Pump Maintenance or Repair Cost? (2025),” HomeGuide. Accessed: Feb. 23, 2025. [Online]. Available: <https://homeguide.com/costs/heat-pump-maintenance-or-repair-cost>
- [62] “Estimating the Cost and Energy Efficiency of a Solar Water Heater,” Energy.gov. Accessed: Feb. 23, 2025. [Online]. Available: <https://www.energy.gov/energysaver/estimating-cost-and-energy-efficiency-solar-water-heater>
- [63] J. Heo, P. J. Adams, and H. O. Gao, “Public Health Costs of Primary PM<sub>2.5</sub> and Inorganic PM<sub>2.5</sub> Precursor Emissions in the United States,” *Environ. Sci. Technol.*, vol. 50, no. 11, pp. 6061–6070, Jun. 2016, doi: 10.1021/acs.est.5b06125.
- [64] K. Reese, “Renewable Energy Policies in Fairbanks, Alaska: Benefit-Cost Analysis of a Carbon Tax and a Renewable Portfolio Standard for Golden Valley Electric Association”. Accessed Feb 20, 2025. [Online]. Available: <https://scholarworks.alaska.edu/bitstream/handle/11122/15568/RenewableEnergyPoliciesinFairbanksAlaska.pdf?sequence=1&isAllowed=y>
- [65] “EPA Report on the Social Cost of Greenhouse Gases: Estimates Incorporating Recent Scientific Advances”. November 2023. [Online]. Available: [https://www.epa.gov/system/files/documents/2023-12/epa\\_scghg\\_2023\\_report\\_final.pdf](https://www.epa.gov/system/files/documents/2023-12/epa_scghg_2023_report_final.pdf)
- [66] “Air Quality Division – Change Out Program.” Accessed: Feb. 23, 2025. [Online]. Available: <https://aq.fnsb.gov/changeout/>
- [67] “Solar Heat Alaska.” Accessed: Feb. 23, 2025. [Online]. Available: <https://solarheatalaska.com/economics.php>
- [68] “Solids - Specific Heats.” Accessed: Feb. 23, 2025. [Online]. Available: [https://www.engineeringtoolbox.com/specific-heat-solids-d\\_154.html](https://www.engineeringtoolbox.com/specific-heat-solids-d_154.html)

- [69] “Insulation materials and their thermal properties.” Accessed: Feb. 23, 2025. [Online]. Available: <http://www.greenspec.co.uk/building-design/insulation-materials-thermal-properties/>
- [70] “Propylene Glycol based Heat-Transfer Fluids.” Accessed: Feb. 23, 2025. [Online]. Available: [https://www.engineeringtoolbox.com/propylene-glycol-d\\_363.html](https://www.engineeringtoolbox.com/propylene-glycol-d_363.html)
- [71] “The Engineering Toolbox.” [Online]. Available: [https://www.engineeringtoolbox.com/fuel-oil-combustion-values-d\\_509.html](https://www.engineeringtoolbox.com/fuel-oil-combustion-values-d_509.html)
- [72] “Gases - Specific Heats and Individual Gas Constants.” Accessed: Feb. 25, 2025. [Online]. Available: [https://www.engineeringtoolbox.com/specific-heat-capacity-gases-d\\_159.html](https://www.engineeringtoolbox.com/specific-heat-capacity-gases-d_159.html)
- [73] “Infrared Emissivity Table.” Accessed: Feb. 25, 2025. [Online]. Available: <https://www.thermoworks.com/emissivity-table/>
- [74] W. B. Rose, “Measured Summer Values of Sheathing and Shingle Temperatures for Residential Attics and Cathedral Ceilings”.
- [75] “Solids - Densities.” Accessed: Feb. 25, 2025. [Online]. Available: [https://www.engineeringtoolbox.com/density-solids-d\\_1265.html](https://www.engineeringtoolbox.com/density-solids-d_1265.html)